Diss. ETH No 13694

Modulation Techniques for the Application of FTIR/DRIFT Spectroscopy in Heterogeneous Catalysis

A dissertation submitted to the
SWISS FEDERAL INSTITUTE OF TECHNOLOGY ZÜRICH

for the degree of
Doctor of Technical Sciences

Presented by

Enrico Eugenio Ortelli
dipl. Chem.-Ing. ETH

born the 3rd December 1971
citizen of Meride (TI)

accepted on the recommendation of

Prof. Dr. Alexander Wokaun, *examiner*
Prof. Dr. Alfons Baiker, *co-examiner*

Zürich 2000

This is page 2 !

This page was left intentionally blank !

In ricordo dei cari nonni

Zora, Romeo ed Enrico Eugenio.

This is page 4 !

This page was left intentionally blank !

Acknowledgements

I would like to thank my advisor, Professor Dr. A. Wokaun, for stimulating discussions, the continuous help and support during the time of my thesis. Without him, this work would not have been possible.

I am also grateful to Professor Dr. A. Baiker for being my co-referee, and for making available many of the catalyst samples investigated in this study.

I would like to thank Dr. J. Kritzenberger and Dr. J. Weigel-Meier for introducing me to IR spectroscopy, and Dr. A. Bill for his assistance in the first FTIR experiments.

I would also like to thank Dr. J. Wambach for his friendly advice in the wide field of heterogeneous catalysis.

I am grateful to Dr. D. Franzke, Dr. Th. Kunz, Dr. Ch. Hahn and Dr. T. Lippert for stimulating discussions about science.

Particular thanks go to Dr. O. Haas, Dr. E. Newson, E. Uenala, F. Geiger, M. Kraus and K. Geissler for their support and to P. Binkert, R. Hugi and Ch. Marmy for help with all the mechanical and electronic problems.

Very special thank goes to my girlfriend, Marina, for her patience, continuing support, love and confidence.

Finally, I would like to thank my parents for their understanding and support.

This is page 6 !

This page was left intentionally blank !

Ringraziamenti

Desidero ringraziare il mio referente, Professor Dr. A. Wokaun, per le stimolanti discussioni, il continuo aiuto e supporto durante tutto il mio dottorato. Senza di Lui questo lavoro non sarebbe mai stato possibile.

Un grazie anche al Professor Dr. A. Baiker per vestire i panni del coreferente, e per aver fornito gran parte dei catalizzatori utilizzati in questo studio.

Un ringraziamento anche al Dr. J. Kritzenberger e alla Dr.ssa J. Weigel-Meier per avermi introdotto alla spettroscopia IR, nonchè al Dr. A. Bill per il suo aiuto durante la prima parte degli esperimenti.

Desidero anche ringraziare il Dr. J. Wambach per i suoi sempre amichevoli consigli sul vasto campo della catalisi eterogenea.

Un grazie anche al Dr. D. Franzke, Dr. Th. Kunz, Dr.ssa Ch. Hahn e Dr. T. Lippert per le stimolanti discussioni nel campo scientifico.

Un grazie particolare al Dr. O. Haas, Dr. E. Newson, E. Uenala, F. Geiger, M. Kraus e K. Geissler per il loro sostegno; e a P. Binkert, R. Hugi e Ch. Marmy per il sempre pronto aiuto nel risolvere i vari problemi sia di ordine meccanico che elettronico.

Un ringraziamento veramente speciale va alla mia ragazza, Marina, per la sua pazienza, il continuo supporto, l'amore e la fiducia sempre presenti.

In ultimo, vorrei ringraziare i miei genitori per la comprensione e il supporto dimostratomi.

This is page 8 !

This page was left intentionally blank !

Table of contest

Acknowledgements 5

Ringraziamenti 7

Table of contest 9

Summary 15

Riassunto 17

Zusammenfassung 19

1. Introduction 21

1.1 Infrared spectroscopy 21
1.1.1 Definitions 21
1.1.2 Brief history of IR spectroscopy 23

1.2 Fourier transform IR spectroscopy 24
1.2.1 Introduction of the Fourier transform in the IR spectroscopy 24
1.2.2 Michelson interferometer and Fourier transform 26

1.3 Diffuse reflectance 27
1.3.1 Definitions 27
1.3.2 Specular reflectance 28
1.3.3 Diffuse reflectance 29
1.3.4 Parameters affecting the DRIFT spectrum 30
1.3.5 Gas phase species in DRIFT spectroscopy 31

1.4 DRIFT in heterogeneous catalysis 32
1.4.1 Introduction of DRIFT in heterogeneous catalysis 32
1.4.2 Use of DRIFT in heterogeneous catalysis 33

1.5 Scope of this thesis 33

2. Experimental 35

2.1 The experimental setup ____ *35*

2.2 The control program ____ *36*
2.2.1 The programming language: LabVIEW ... 36
2.2.2 The control program ... 37
2.2.3 Management of the mass flow controllers (*measure FCs*) ... 39
2.2.4 Management of the temperature controllers (*measure TCs*) ... 41
2.2.5 The triggering of the spectrometer (*trigger IFS*) ... 42

2.3 The gas dosing systems ____ *44*
2.3.1 The Preparative Unit ... 44
2.3.2 The Modulation Unit ... 46

2.4 DRIFT: optical accessories and methodic ____ *48*
2.4.1 Controlled Environmental Chamber ... 48
2.4.2 Environmental Chamber ... 49
2.4.3 Representation of DRIFT spectra ... 50
2.4.4 Sample preparation ... 51

2.5 The micro reactor / gas cell system ____ *51*

2.6 The FTIR spectrometer ____ *53*
2.6.1 The instrument ... 53
2.6.2 The macro ... 53

2.7 Catalytic tests ____ *55*

2.8 Compounds ____ *56*

3. Reactants modulation ____ **57**

3.1 Introduction ____ *57*

3.2 Approach to the problem ____ *59*

3.3 Modulation of the reactants ____ *60*
3.3.1 Mathematical background ... 60
3.3.2 Modelling the setup ... 62
3.3.3 Experimental procedure ... 63
3.3.4 Experimental parameters ... 65
3.3.4.1 Determination of t_{delay} 65
3.3.4.2 Delay element of 1st Order (PT_1) 66
3.3.4.3 Delay element of 2nd Order (PT_2) 68
3.3.5 Recording techniques ... 72
3.3.6 Recording parameters ... 73

3.4 Useful simple models ____ *74*
3.4.1 A few definitions in heterogeneous catalysis ... 74
3.4.2 Heterogeneous reactions in the used setup ... 75
3.4.2.1 Adsorption/desorption equilibrium 76

3.4.2.2 Series reactions 77
3.4.2.3 Parallel reactions 78
3.4.2.4 Series-parallel reactions 79

3.5 Conclusions 82

4. Reaction pathway investigation 85

4.1 Introduction 85

4.2 Experimental 86

4.3 Results 89
4.3.1 Models 89
4.3.1.1 Model 1: Parallel reactions 89
4.3.1.2 Model 2: Series reactions 90
4.3.1.3 Model 3: Series-parallel reactions 90
4.3.2 Experimental results 91
4.3.2.1 Modulation of CO_2 91
4.3.2.2 Modulation of H_2 93

4.4 Discussion 94

4.5 Conclusions 95

5. Reaction rate constants investigation 97

5.1 Introduction 97

5.2 Experimental 98

5.3 Results and discussion 102
5.3.1 Interaction of CO with the catalyst 103
5.3.1.1 Model 103
5.3.1.2 Experimental results 104
5.3.2 Interaction of CO_2 with the catalyst 107
5.3.2.1 Model 107
5.3.2.2 Experimental results 109
5.3.3 Effect of CO in the CO oxidation reaction 111
5.3.3.1 Model 111
5.3.3.2 Experimental results 114
5.3.4 Effect of O_2 in the CO oxidation reaction 119
5.3.4.1 Model 119
5.3.4.2 Experimental results 120

5.4 Error sources 123
5.4.1 Signal-to-Noise Ratio (SNR) 123
5.4.2 Phase resolution 123
5.4.3 Optical path of the DRIFT cell 124

5.4.4 Reflectivity of the sample 124
5.4.5 Changes in the concentration 124
5.4.6 Experimental errors 125
5.4.7 Dead time 126
5.4.8 Selection of the model 127
5.4.9 Error propagation 127

5.5 Conclusions *128*
5.5.1 Reaction order of CO 128
5.5.2 Influence of the CO_2 adsorption on the oxidation reaction 128
5.5.3 Energy scheme of the reaction 129
5.5.4 CO-CO_2 equilibrium 130
5.5.5 Modulation technique 131

6. Methanol synthesis pathway over Cu/ZrO_2 catalysts **133**

6.1 Introduction *133*

6.2 Experimental and procedures *135*
6.2.1 Catalyst 135
6.2.2 Infrared spectroscopy 135
6.2.3 Experimental setup 136
6.2.4 Catalyst preparation 136
6.2.5 Experimental procedures 136
6.2.5.1 ^{13}C-paraformaldehyde and ^{12}C-formic acid adsorption followed by reduction *136*
6.2.5.2 ^{13}C-formic acid and ^{12}C-paraformaldehyde adsorption followed by reduction *137*

6.3 Results and discussion *137*
6.3.1 Frequencies of labelled substances 137
6.3.2 Adsorption of $H_2{}^{13}CO$ and $H^{12}COOH$ 139
6.3.3 Hydrogenation of surface species 141
6.3.4 Adsorption of $H^{13}COOH$ and $H_2{}^{12}CO$ 142
6.3.5 Hydrogenation of surface species 144

6.4 Conclusions *145*
6.4.1 Water gas shift reaction 146
6.4.2 Methanol formation 146

7. Investigation of a complex system **149**

7.1 Introduction *149*

7.2 Experimental *152*

7.3 Results and discussion *156*
7.3.1 CO_2 adsorption on the reduced catalyst 157

7.3.1.1 Model 157
7.3.1.2 Experimental results 159
7.3.2 CO adsorption on the reduced catalyst....161
7.3.2.1 Model 161
7.3.2.2 Experimental results 163
7.3.3 CO_2 hydrogenation reaction....166
7.3.3.1 Model 166
7.3.3.2 Experimental results 168
7.3.4 CO hydrogenation reaction....171
7.3.4.1 Model 171
7.3.4.2 Experimental results 173

7.4 Conclusions ***175***
7.4.1 Methanol synthesis via hydrogenation of CO....175
7.4.2 Methanol synthesis via hydrogenation of CO_2....177
7.4.3 Tentative energy scheme....178
7.4.4 Modulation technique....180

8. Conclusions **181**

8.1 Introduction ***181***

8.2 Advantages of the method ***181***
8.2.1 Simplicity....181
8.2.2 Flexibility....182
8.2.3 Speed....182
8.2.4 Economic....183

8.3 The boundaries of the method ***183***
8.3.1 The detection setup....184
8.3.2 The analysis of the data....184
8.3.3 The modulation setup....185
8.3.4 The catalytic system....185

8.4 Outlook ***186***
8.4.1 Better detection....186
8.4.2 Faster measurements....187
8.4.3 Improved experiments....187
8.4.4 Additional investigations....188

8.5 Final remarks ***188***

Curriculum vitae **189**

Bibliography **193**

This is page 14 !

This page was left intentionally blank !

Summary

In this work a new experimental method based on FTIR and DRIFT spectroscopy has been presented. The method is applicable to both qualitative and quantitative measurements in heterogeneous catalysis. The basis of the modulation theory, its advantages, limitations, possible improvements, and several examples are discussed. The necessary setup consists of the same components as used in standard studies of heterogeneously catalysed reactions, and includes mainly commercial parts.

The method is based on the idea that, from the analysis of the transformation of an input perturbation signal into a response signal, information about the investigated system can be obtained. Sinusoidal modulation of the reactant concentrations is chosen as the perturbation, which allows one to monitor the concomitant changes in the concentrations of different intermediates and products along the reaction pathway.

For quantitative measurements, the use of sinusoidal shaping of the modulation has the advantage that calibration curves (FTIR spectroscopy) and *ad hoc* mathematical models for the variation of the reflectivity of the used catalyst (DRIFT spectroscopy) are unnecessary. Several parameters are collected at the same time during a single measurement. The accumulated data provide information about the different characteristics of the investigated system, from which other kinetic and thermodynamic parameters can be derived.

The four essential components of a modulation experiment are the catalytic system, the modulation setup, the detection system, and the data analysis algorithms. These components are closely related to each other, and each characterised by a set of operating parameters. To achieve the optimum working conditions, all possible

parameters must be considered and tested. Extended test experiments have been carried out for this purpose.

The following reactions have been studied.

1. *Reaction pathway investigation.* As a test reaction, the methanol synthesis from $CO/CO_2/H_2$ over a commercial $Cu/ZnO/Al_2O_3$ catalyst was used. The investigation was performed using FTIR spectroscopy and possible reaction pathways were discussed in terms of standard chemical reaction engineering models. The modulation data were found to be represented by a set of series and parallel reactions.

2. *Reaction rate constants investigation.* The CO oxidation over a $Pd_{25}Zr_{75}$ based catalyst was studied in detail using DRIFT spectroscopy. Reaction rate constants as well as the rate limiting step were determined. The repetition of the experiments at different temperatures allowed the calculation of the activation energies of different reaction steps, as well as modelling the conversion in the corresponding catalytic tests.

3. *Investigation of a complex system.* The application of the modulation concept to study *in situ* (DRIFT) the reaction pathway and the reaction rate constants of a complex, solid-state catalysed reaction system is described. The methanol synthesis over a $Cu_{46}Zr_{54}$ based catalyst starting from H_2/CO and H_2/CO_2 was chosen as test reaction. Reaction rate constants as well as activation energies of the different reaction steps were determined.

Riassunto

In questo lavoro viene presentato un nuovo metodo sperimentale applicato alla spettroscopia FTIR e DRIFT, sia per ricerche quantitative che qualitative nel campo della catalisi eterogenea. Le basi del metodo, i vantaggi, i limiti, le possibili migliorie come pure diversi esempi di applicazione vengono riportati e discussi. Le infrastrutture e le apparecchiature necessarie per eseguire gli esperimenti sono le medesime che si usano per condurre normali ricerche in catalisi eterogenea.

Il metodo è basato sulla semplice idea che ogni azione induce una reazione, pertanto analizzando come reagisce un sistema che viene perturbato da un segnale definito, si possono ottenere informazioni sul sistema stesso. Modulando sinusoidalmente la concentrazione dei reattandi si ottiene un'oscillazione indotta nelle concentrazioni dei diversi composti intermedi così come dei prodotti.

L'uso di curve sinusoidali elimina la necessità di creare delle curve di calibrazione (spettroscopia FTIR) come pure l'elaborazione di modelli matematici *ad hoc* che tengano conto delle variazioni della reflettività del catalizzatore usato (spettroscopia DRIFT). Durante la medesima misurazione, diversi parametri sono raccolti allo stesso momento. Questi forniscono, da un lato, informazioni sulle differenti caratteristiche del sistema, dall'altro sono usati per ricavare dati riguardanti i processi cinetici come pure le caratteristiche termodinamiche del sistema stesso.

I quattro gruppi di elementi che limitano il sistema sono: il sistema di detezione, l'analisi dei dati, il dosaggio dei gas e il sistema catalitico. Dato che questi s'influenzano l'un l'altro, per ottenere le condizioni ideali di sperimentazione è necessario considerare tutti i possibili parametri. L'esecuzione di esperimenti per testare l'influsso dei vari parametri può diventare un processo lungo e impegnativo.

Gli esempi di applicazione presentati sono i seguenti.

1. *Classificazione del meccanismo di reazione.* Come reazione è stata scelta la sintesi del metanolo partendo da $CO/CO_2/H_2$ su un catalizzatore commerciale $Cu/ZnO/Al_2O_3$. La spettroscopia FTIR viene utilizzata per ottenere delle informazioni sui possibili meccanismi di reazione. I dati raccolti sono discussi basandosi sui modelli standard usati nel campo del genio chimico. Nel caso considerato viene dimostrata l'esistenza di reazioni in parallelo e in serie.

2. *Studio sulle costanti di reazione.* L'ossidazione del CO su un catalizzatore $Pd_{25}Zr_{75}$ viene analizzata in dettaglio usando la spettroscopia DRIFT. I dati raccolti vengono usati per determinare le velocità di reazione dalle quali si ottiene poi la reazione limitante. La ripetizione dell'esperimento a diverse temperature fornisce la possibilità di stimare l'energia di attivazione delle differenti reazioni presenti nonchè la conversione.

3. *Studio di un sistema catalitico complesso.* Il concetto di modulazione viene applicato ad un sistema complesso quale la sintesi del metanolo su un catalizzatore $Cu_{46}Zr_{54}$ partendo da $CO/CO_2/H_2$. Il sistema viene analizzato *in situ* (DRIFT) al fine di ottenere informazioni sui meccanismi di reazione e sulle velocità di reazione, queste sono poi usate per stimare l'energia di attivazione delle differenti reazioni.

Zusammenfassung

In dieser Arbeit wird eine neue experimentelle Methode präsentiert, die auf FTIR- und DRIFT-Spektroskopie basiert. Die Methode kann benutzt werden, um qualitative sowie quantitative Untersuchungen in der heterogenen Katalyse durchzuführen. Die Theorie der Modulationstechnik, Vorteile, Begrenzungen, mögliche Verbesserungen sowie Anwendungsbeispiele werden vorgestellt. Der notwendige Aufbau besteht aus ähnlichen Komponenten, wie sie bei Standarduntersuchungen in der heterogenen Katalyse eingesetzt werden.

Die Methode basiert auf der einfachen Idee, dass aus der Analyse der Umwandlung eines Störsignal in ein Antwortsignal Informationen über das untersuchte System erhalten werden können. Als Störsignal wird die sinusförmige Modulation der Konzentration eines der Edukte benutzt, so dass die dadurch verursachte Änderung der verschiedenen Zwischen- und Endprodukte beobachtet werden kann.

Der Einsatz von sinusförmiger Modulation eignet sich besonders für quantitative Analysen, da man auf Eichkurven (FTIR Spektroskopie) oder *ad hoc* entwickelte mathematische Modelle (DRIFT Spektroskopie), welche die optischen Eigenschaften des untersuchten Katalysators voraussetzen, verzichten kann. Weiterhin werden gleichzeitig mehrere Kenngrössen erhalten. Aus den Daten werden Informationen über die verschiedenen Eigenschaften des untersuchten System gewonnen, aus denen weitere kinetische und thermodynamische Parameter abgeleitet werden.

Die vier wesentlichen Komponenten des Experimentes sind die Beaufschlagung des katalytischen Systems, die Vorbereitung und Modulation der Feedgas-Konzentration, das Detektions-system und die Analyse der Daten. Diese beeinflussen sich gegenseitig, weswegen alle möglichen Parameter betrachtet werden sollen, um ideale

Reaktionsbedingungen zu finden. Zu diesem Zweck wurden eingehende Testmessungen durchgeführt.

Die folgenden Reaktionen wurden untersucht.

1. *Klassifizierung des Reaktionsmechanismus.* Als Test-Reaktion wurde die Methanol Synthese aus $CO/CO_2/H_2$ über einen kommerziellen $Cu/ZnO/Al_2O_3$ Katalystor benutzt. FTIR-Spektroskopie wurde angewendet, um Informationen über mögliche Reaktionsmechanismen zu erhalten. Die Resultate wurden im Rahmen von Standard-Modellen der chemischen Reaktionstechnik diskutiert und lieferten im vorliegenden Fall Evidenz für das simultane Ablaufen von seriellen und parallelen Reaktionen.

2. *Bestimmung von Reaktionsgeschwindigkeitskonstanten.* Die CO-Oxidation über einem $Pd_{25}Zr_{75}$-basierten Katalysator wurde mit DRIFT-Spektroskopie im Detail studiert. Die Reaktionsgeschwindigkeitskonstanten und der geschwindigkeits-limitierende Schritt konnte ermittelt werden. Durch Experimente bei verschieden Temperaturen wurden die Aktivierungsenergien der verschiedenen Schritte bestimmt und der Umsatz in den entsprechenden katalytischen Experimenten modelliert.

3. *Untersuchung eines komplexeren katalytische Systems.* Das Modulationskonzept wurde zur Untersuchung des Reaktionsmechanismus der Methanolsynthese aus H_2/CO und H_2/CO_2 über einen $Cu_{46}Zr_{54}$ Katalysator verwendet. Die Reaktionsgeschwindig-keitskonstanten und die Aktivierungsenergien der verschiedenen Reaktionsschritte wurden bestimmt.

1. Introduction

1.1 Infrared spectroscopy

1.1.1 Definitions

Infrared spectroscopy (from Latin *spectrum = the appearance* and from Greek *skopein = to view*) is defined as the use of instrumentation in measuring a physical property of matter, and the relating of the obtained data to the chemical composition. The measured physical property of the matter is the ability of absorption, transmission or reflection of infrared radiation. The analysis of the radiation gives information about the identity, the quantity, the structure, and the environment of molecules as well as ions.

Not all forms of matter are capable of producing an infrared spectrum (i. e. metals do not). To give rise to the absorption bands appearing in the spectrum the infrared radiation has to interact with vibrational (and rotational) excitations of the molecule. In contrast to pure rotational (microwave) spectroscopy, a permanent dipole moment is not required in vibrational spectroscopy. However, only those vibrations involving a dipole momentum that changes its intensity (dM) during the bond excursion (dq) are infrared active.

$$\frac{dM}{dq} \stackrel{!}{\neq} 0 \qquad (1.1)$$

Example: methane (CH_4) has $M = 0$ but several vibrations with $dM/dq \neq 0$.

Vibrations may involve the modification of bond lengths -*stretching*- or of the bond angles -*deformation*-, or relative torsional motions of molecular moieties. The intensity of the infrared radiation (IR_{Band}) is proportional to the square of the change of the dipole momentum as function of the interatomic distance (dr) [1].

$$IR_{Band} \propto \left(\frac{dM}{dr} \right)^2 \tag{1.2}$$

The electromagnetic spectrum is divided into several regions (see Figure 1-1). Each energy window is used for different purposes, and gives a different type of information. These divisions are arbitrary, and the boundaries are not well defined, because there exist overlaps among these windows. The region of the electromagnetic spectrum corresponding to energy of vibrational (and rotational) transitions is called *Infrared* (IR).

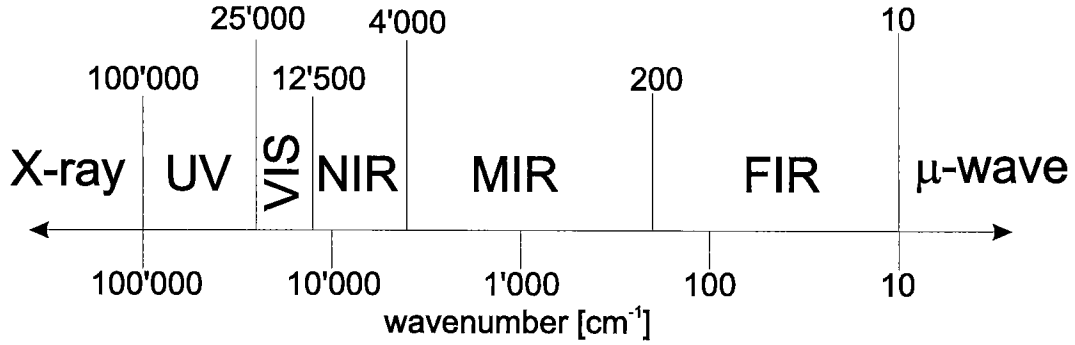

Figure 1-1: Schematic representation of the electromagnetic spectrum. The IR region (12'500 ÷ 10 cm^{-1}) is divided in Near-IR, Middle-IR, and Far-IR (according to [2]).

The *Mid-IR* (MIR) is the region where the lowest vibrational energy changes (fundamental excitations) of most molecules occur. Therefore, it represents the most interesting region for the vibrational-rotational spectroscopy. The relationship between Energy E [J] and wavenumber $\tilde{\upsilon}$ [cm^{-1}] is defined as follows:

$$E = h\,c\,100\,\tilde{\upsilon} \tag{1.3}$$

where c is the speed of the light and h the Planck's constant ($6.626 \cdot 10^{-34}$ J s). The wavenumber $\tilde{\upsilon}$ as a function of the wavelength λ [m] is given by the following equation.

$$\tilde{\upsilon} = \frac{1}{100\,\lambda} \tag{1.4}$$

1.1.2 Brief history of IR spectroscopy

The basis for the development of the spectroscopy was originated several billion of years ago with the creation of the light (*And God said: 'Let there be light'.* - Genesis 1;3) and its composition (*I set my bow in the clouds, and it shall be a sign,* - Genesis 9;13).

Several centuries ago humans recognised that light is necessary for colours to exist (Aristotele, 400 BC), and, after two millennia, that it can be divided into a spectrum (Newton, *Principia*, 1666). In 1678 Huygens proposed the wave theory of light. This was validated in 1802 by Thomas Young, who obtained the spectrum of light by diffraction using a crude transmission grating. In 1860 J. C. Maxwell developed the mathematical equations describing the light as an electromagnetic wave.

In 1800 F. W. Herschel noted that different amounts of heat passed through distinct coloured glasses. He hence deduced that heat is similar to light. In 1900 William Coblentz collected the first IR spectra of organic compounds. In 1949 John White and Max Listen developed the double-beam optical zero adjustment IR spectrometer. With the commercialisation of this system the chemical infrared spectroscopy came into widespread use. These dispersive instruments proved the tremendous importance of infrared analysis which soon became the characterisation workhorse in chemical laboratories.

The mathematical equation describing the attenuation of a wave passing through a sample was found in 1760 by Johann Lambert. His starting point were the experiments of Pierre Bouger (1729), who noticed the attenuation of light as it passed through successive thicknesses of glass. In 1852 August Beer showed the logarithmic relation of the Bouguer-Lambert Law. The Bouger-Lambert-Beer Equation (see Equation 1.5) describes the attenuation *dI* of a radiation having a wavelength λ through a sample with a concentration *c* and natural extinction coefficient $\varepsilon_n(\lambda)$ as function of the sample thickness *dl*.

$$\frac{dI}{dl} = -I\ c\ \varepsilon_n(\lambda) \tag{1.5}$$

1.2 Fourier transform IR spectroscopy

1.2.1 Introduction of the Fourier transform in the IR spectroscopy

To pursue his studies on the speed of light in 1891, A. A. Michelson developed a device able to produce an interference pattern from a beam of light: the interferometer [3]. He was able to obtain plausible spectra from the observed interferograms, by using an iterative series of reverse Fourier transforms and fitting sequences. Manual by calculated spectra were elaborated and manipulated to obtain the best representation of the collected raw data.

The *Fourier Transform* (FT) [4,5] is a complex mathematical computation used to convert the time-domain into frequency-domain, or the spatial-domain into spatial-frequency (wavenumber). It is named after its French discoverer the mathematician and physicist, Baron Jean Baptiste Joseph Fourier.

In 1949 the astrophysicist Peter Fellgett used an interferometer, similar to those of Michelson, to measure light from celestial bodies and produced the first *Fourier Transform Infrared* (FTIR) spectrum. By using an interferometer, all source wavelengths are measured simultaneously, whereas in a dispersive spectrometer they are measured successively. Thus, a complete spectrum can be collected very rapidly and multiple scans can be averaged in the same time needed for a single scan of a dispersive spectrometer [6]. This improvement was called *Multiplex* or *Fellgett advantage*.

During the same period Jacquinot observed that, for the same resolution, the energy throughput in an FTIR interferometer could be higher than in a dispersive spectrometer, where it was restricted by the slits [7]. This discovery was called *Throughput* or *Jacquinot advantage*.

Using a FTIR spectrometer it was possible to achieve the same signal-to-noise ratio as from a dispersive instrument, but in a much shorter time. The Fourier transformation of the interferograms required large and expensive computers as well as up to 12 hours to convert an interferogram into a spectrum. Thus, only a restricted number of advanced research groups used FTIR. The application of this technique was limited to study problems which could not be solved by dispersive techniques.

In 1964 Cooley-Tukey developed an algorithm, which quickly performs a FT: the *Fast Fourier Transform* (FFT) [8]. The introduction of microprocessors (1972), and the subsequent digital handling of spectral data (Gary Horlick, 1972) was pivotal in the commercialisation of FTIR spectrometers. Nevertheless, the first FTIR spectrometers were large and expensive and found exclusively in few well-to-do research labs.

A further improvement occurred in 1966. HeNe lasers were introduced as an internal reference for each scan to derive the wavenumber scale of the interferometer [9]. The wavelength of the HeNe laser is known accurately and is very stable. The calibration of FTIR instruments resulted in a higher accuracy and long term stability than that of dispersive instruments. This improvement was called *Frequency* or *Connes advantage*.

In 1988 the Joint Committee on Atomic and Molecular Physical Data created a standard language (JCAMP-DX) [10] allowing, theoretically, the exchange of data between the different types of IR spectroscopy softwares.

Gradually, technology reduced the costs, increased the availability, and enhanced the capacities and accuracy of the systems. Today FTIR spectroscopy is one of the most widely used techniques available for all fields of analytical chemistry. It is suitable for qualitative as well as quantitative analyses, and serves both research and routine studies carried out in application and process-control laboratories. More details about FTIR spectroscopy can be found in the literature [11,12].

1.2.2 Michelson interferometer and Fourier transform

The heart of the FT spectrometer is the interferometer. This is a device that encodes the light from the infrared source. The Michelson interferometer (see Figure 1-2) consists of a fixed-position mirror (A), a beamsplitter (B), and a moving mirror (C).

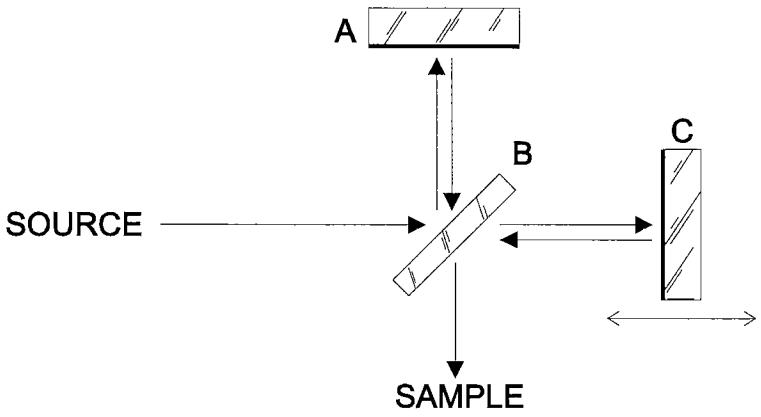

Figure 1-2: Scheme of a Michelson interferometer with the fixed mirror (A), the beamsplitter (B), and the moving mirror (C).

Infrared energy is transmitted from the source to the beamsplitter, where approximately half of the beam intensity is reflected towards the fixed-position mirror and the other

half transmitted towards the moving mirror. The returning beam from each mirror comes back to the beamsplitter where the two beams are recombined. There they interfere constructively or destructively, depending on the magnitude of the phase shift between each other. This light is then directed towards the sample compartment.

From the sample, the infrared radiation reaches the detector where the remaining light is measured and an interferogram is produced. The interferogram is a spatial-domain (x [m]) representation of the interference patterns created in the interferometer. The spectrum is a spatial-frequency-domain ($\tilde{\upsilon}$) representation of the same data. The Fourier transform is used to decode the interferogram ($f(x)$) into a single-beam spectrum ($F(\tilde{\upsilon})$).

$$F(\tilde{\upsilon}) = \int_{-\infty}^{\infty} f(x)\, e^{-i \cdot 2\pi 100\, \tilde{\upsilon}\, x} dx \tag{1.6}$$

After subtraction of the background signal the obtained spectrum can be represented in three modes: transmittance, absorbance, or diffuse reflectance.

1.3 Diffuse reflectance

1.3.1 Definitions

An infrared beam directed onto a sample (see Figure 1-3) can either be specular reflected from the surface, or penetrate it. The radiation penetrating the surface can be absorbed or reflected.

The overall intensity of the specularly reflected beam is determined by the refractive index of the solid, and the derived FTIR spectrum contains mainly features of the gas phase above the sample. In contrast, from the diffusely reflected radiation information

about the constituents of the solid (and adsorbates) can be obtained. The combined use of special detectors and of FT systems allows to overrule the problem of the low levels of diffusely scattered light and radiation loss by specular reflectance. At the same time a very high sensitivity, down to ppm levels, is ensured.

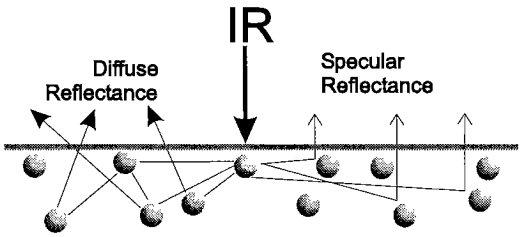

Figure 1-3: An infrared beam is directed on the surface of a sample, specular and diffuse reflected rays are displayed.

Diffuse reflectance permits the rapid analysis of many types of solid samples including powders, fibres, rough surfaces and coatings. The preparation of the sample is normally rapid and simple. The use of special sampling kits allows to extend the analysis to large intractable samples. *Diffuse Reflectance Infrared Fourier Transform Spectroscopy* (DRIFTS) is nowadays a widespread method in several fields of analytical chemistry.

1.3.2 Specular reflectance

Specular reflectance is the simple reflection of a beam on the surface of a particle acting as a mirror. The angle of incidence and the angle of reflection are the same. Rays that undergo multiple reflections generate the specular diffuse reflectance. The specular reflectance for an incident beam normal to the surface is described by the Fresnel Equation:

$$R_{Specular}(\lambda) = \frac{I}{I_0} = \frac{(n-1)^2 + n^2\kappa^2}{(n+1)^2 + n^2\kappa^2} \tag{1.7}$$

$R_{Specular}(\lambda)$ is the reflectivity of an incident ray. I is the intensity of the reflected beam and I_0 is the intensity of the incident beam. n is the refractive index of the sample and κ the absorption index of the matter. The absorption index is defined through Lambert's Law:

$$I = I_0 \exp\left(-\frac{4\pi n\kappa l}{\lambda_0}\right) \tag{1.8}$$

where λ_0 denotes the wavelength of the radiation in vacuum, and l the layer thickness. It is simple to observe that for a non-absorbing material ($\kappa \approx 0$) the specular reflectance $R_{Specular}(\lambda)$ is small except for very high values of n, whereas for strongly absorbing substances ($\kappa >> 0$) $R_{Specular}(\lambda)$ approaches unity, indicating a quasi total reflection of the light beam.

1.3.3 Diffuse reflectance

Diffuse reflectance is the interaction and reflection of a beam by the surface of a particle. The interpretation of diffuse reflectance is based on the theory developed by Kubelka and Munk [13,14,15] and extended by Kortüm [16,17], and Kortüm *et al.* [18] about the scattering of light in samples diluted in non-absorbing matrices. This model considers that parallel layers of particles are randomly illuminated (isotropically) with monochromatic radiation, and particles with dimensions smaller than the thickness of the layer can absorb and/or scatter the radiation.

The obtained equation is only valid for samples of infinite thickness, i. e. samples for which an increase in the depth does not appreciably change the spectrum. For infrared radiation a layer of 1 - 3 mm of finely grinded powder can be considered as infinite thickness. The diffuse reflectance R_∞ for a diluted sample of infinite thickness is given by the Kubelka-Munk (K-M) Equation:

$$f(R_\infty) = \frac{(1-R_\infty)^2}{2R_\infty} = 2.303\frac{a\,C}{s} \qquad (1.9)$$

where C is the concentration of the sample, a the absorptivity and s the scattering coefficient. In practice it is not always possible to measure R_∞. Therefore, the relative diffuse reflectance R/R_0 is used instead, where R is the reflectance of the sample and R_0 the reflectance of the reference material.

1.3.4 Parameters affecting the DRIFT spectrum

From the theoretical point of view, it is possible to obtain spectra from samples ranging from highly diluted to neat. In practice, the quality and the result of an analysis depend on several parameters, the modification of which can largely affect the collected data. Refractive index, scattering coefficient, and used diluents are the most important parameters.

Any change of the sample refractive index [19,20,21] can significantly alter the obtained spectrum, e. g. it may cause peak inversions, spectra which can be misinterpreted or not even interpreted at all. Such problems can be caused by increasing coverage of adsorbed substances [22,23]. In this case, i. e. highly concentrated samples with a high refractive index, a dramatic increase in the specular contribution to the spectral data is observed.

To minimize this effect an adequate dilution of the sample in a non-absorbing matrix or the use of special designed accessories [24,25,26], for a reduction of the specular reflectance, is necessary.

Since the scattering coefficient depends on both particle size and degree of sample packing [27,28], the linearity of the Kubelka-Munk Function can only be assured if particle size and packing method are strictly controlled [29,30,31,32]. The particle size is very important in diffuse reflectance measurements of powders [33,34,35,36]. Too

large particles result in the alteration of band width and intensity. Uniformly fine-grinded samples can reduce or solve this problem.

To avoid any artefacts, the used reference or dilution matrix should not absorb radiation at the same wavelengths as the sample. If an analytic compound is mixed with a non-absorbing diluent it is necessary that the sample is as homogeneous as possible [37]. An inhomogeneous distribution of the matter may affect the relative peaks intensities [22,38].

If all of the previously discussed conditions are taken into account, quantitative accurate measurements can be obtained [39,40,41]. Sometimes these conditions can not be completely fulfilled. To overcome this difficulty, special *ad hoc* models based onto the K-M theory have been developed [39,42,43,44,45,46,47,48].

Such models are based on reference measurements and calibration curves used to develop the theory and the necessary mathematical equations. The validity of the models is usually limited to the used samples and applied measurement conditions. Modifications of these parameters frequently result in radical changes of the collected spectra. Hence, the specialised model would no longer be valid.

1.3.5 Gas phase species in DRIFT spectroscopy

Another important feature of DRIFT spectroscopy is the possibility to observe adsorbed as well as gas phase species at the same time. Therefore, it is possible to correlate the gas phase composition with the observed surface compounds. Indications about gas phase species are collected by both specular and diffusely reflected radiation. To perform a quantitative measurement the refractive index of the sample should be nearly constant. However, if the gas phase species react with the sample, this condition can not always be accomplished.

In gas phase analysis the optical path within the cell is very important, because it is directly related to the quality of the obtained spectrum. The path inside a DRIFT cell does usually not exceed 10 mm, which is very short compared to the ten or more meters of a gas cell. Hence, in DRIFT cells the effects of the change of the refractive index are enhanced by the reduced optical path. The consequences are a limited sensitivity and a large uncertainty towards gas phase species. Therefore, quantitative measurements of the gas phase are difficult to obtain.

1.4 DRIFT in heterogeneous catalysis

1.4.1 Introduction of DRIFT in heterogeneous catalysis

Heterogeneous catalysis is one of the numerous applications of IR spectroscopy. Catalysis is by definition a kinetic phenomenon, yet it is noteworthy that vibrational spectroscopy has been used to follow the transient response of kinetically significant intermediates on heterogeneous catalysts [49,50,51,52]. One of the fundamental approaches of vibrational spectroscopy applied to surface species is the transmission-absorption infrared spectroscopy, which has a history dating back to 1911 [53]. This technique offers an adequate sensitivity for weakly infrared absorbing surface species.

The main disadvantage of transmission is the necessity to press self supporting disks of catalyst material, which must have three properties. They have to be transparent to the IR beam, allow the throughput of the reaction gases as well as contain enough matter to permit the observation of the surface species. Compressed catalyst disks have poor porosity compared to the original powder. This characteristic can limit the usefulness of transmission for *in situ* studies of surface reaction kinetics as a consequence of diffusion control of reaction rates.

The use of diluent powders is not a simple solution at all. The chosen material should be completely inert towards all the components of the investigated reactions to avoid any artefacts. The preparation of the disks is often a difficult, tedious trial and error process.

All these troubles can be partially eliminated with the use of the *Diffuse Reflectance Infrared Fourier Transform* (DRIFT) spectroscopy [22,54,55,56]. This technology has several advantages. The catalysts can be investigated *in situ*. The sample preparation is unspecific and very simple, because the substance can be placed directly in the sample holder. No dilution is normally necessary, because highly opaque, weakly absorbing and non-reflecting materials can be analysed too. Therefore, DRIFT spectroscopy is nowadays a very powerful tool to perform investigations in many fields of heterogeneous catalysis.

1.4.2 Use of DRIFT in heterogeneous catalysis

DRIFT spectroscopy is, at the present, essentially applied for semiquantitative and qualitative investigations. Quantitative measurements are usually not plausible, because the reaction of the gas phase components with the sample induces a modification of the refractive index of the used material. Therefore, small alterations of the reaction conditions can induce large variations of the amount of reflected radiation. Even the development and the application of special mathematical models, which consider these deviations, is not simple, because a large number of parameters have to be considered and monitored.

1.5 Scope of this thesis

Aim of the present investigation is an extension of the applicability of the FTIR/DRIFT spectroscopy in the field of the heterogeneous catalysis. The purpose is to develop an

analytical method, which is able to obtain qualitative and quantitative information at the same time, i. e. reaction pathway and rate constants. The method should be insensitive towards the used setup and the applied reaction conditions. It has to be simple, quick, flexible, precise and economic.

2. Experimental

2.1 The experimental setup

The laboratory setup was modularly built to achieve the maximal flexibility. The different components can be assembled to attain the necessary requisites to perform the desired investigations. In Figure 2-1 the setup is outlined.

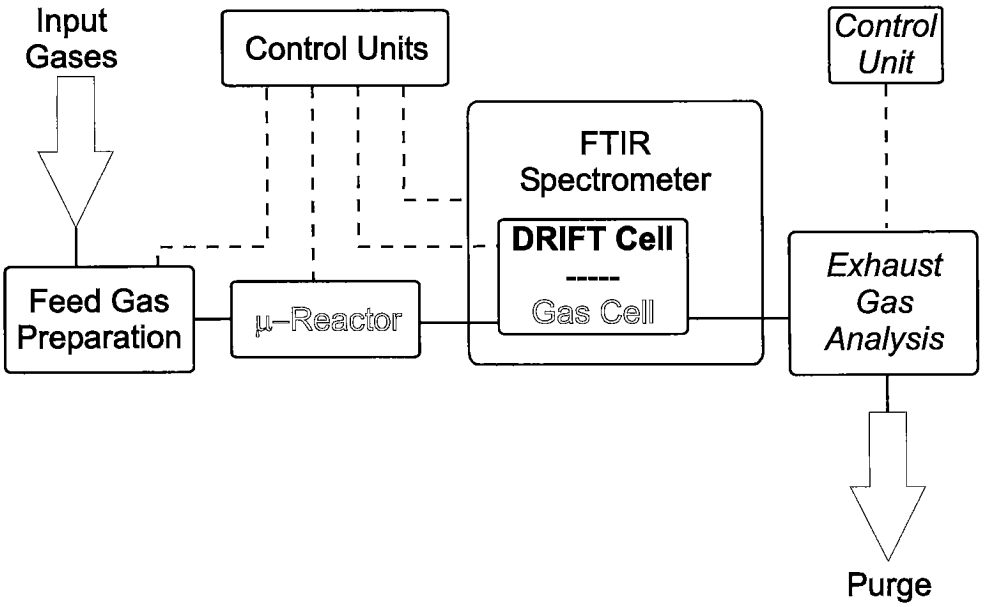

Figure 2-1: Schematic representation of the laboratory setup. Main components are the *Control Units*, the *Feed Gas Preparation*, the reaction/analytical unit (*DRIFT Cell*, or *μ-Reactor* and *Gas Cell*) with the *FTIR Spectrometer*, and the independent *Exhaust Gas Analysis*.

The first component of the setup is the *Feed Gas Preparation*. It consists of two different gas dosing systems (*Preparative Unit* and *Modulation Unit*) that can be utilised either separately or together. The second element is the reaction/analytical unit, where the investigated process can be monitored either *in situ* by using a *DRIFT cell* (bold font in Figure 2-1), or *ex situ* by using a *plug-flow micro reactor* (μ-reactor) and a *Gas Cell* (outlined font in Figure 2-1). The DRIFT, respectively the gas cell is placed in the *Infrared Fourier Transform Spectrometer* (IFS). In the last part, an independent analytical unit for the analysis of the exhausted gases during test and steady state measurements was attached (italic font in Figure 2-1).

The whole setup is controlled using four independent electronic units. The gas dosing system *Preparative Unit*, the FTIR spectrometer, and the supplementary analytical unit have their own independent control system. A homemade electronic system connected to a PC is used to manage the second gas dosing system (*Modulation Unit*), the four temperature regulators as well as trigger source for the IFS. A dedicated *LabVIEW* based program on the PC is used as user interface.

2.2 The control program

2.2.1 The programming language: LabVIEW

LabVIEW (Ver. 3.1, National Instruments Corporation) is a program development application, like other commercial *C++* or *Pascal* development languages. However, it is different from those applications in one important feature: other programming systems use text-based languages to create lines of code, while *LabVIEW* uses graphical symbols to create block flow diagrams [57].

LabVIEW uses the concept of modular programming. An application is divided into a series of dedicated tasks, which can be further divided until a complicated application becomes a series of simple subtasks. The final recombination of all subtasks represents the program.

2.2.2 The control program

Main tasks of the control program are the management and the co-ordination of temperature and flow controllers as well as the triggering of the spectrometer. The use of special dedicated subtasks as well as the division of the program into a main loop and some secondary loops allow to achieve high precision and flexibility. In Figure 2-2 the flow diagram of the control program is outlined.

After the initialisation of the communication protocols and of the variables the main loop is started. The first step is to check if the *End* procedure has to be executed and the program terminated. The second step is the choice of the operating mode: *Survey* or *Multimeasure*. In the *Survey* mode the setpoints and the commands for the different instruments are entered by the operator. In the *Multimeasure* mode they are managed by the program using the information contained in a dedicated database.

The next step is the selection of the working procedure: *Dynamic* or *Steady State*. In the *Steady State* procedure the subtasks for the management of the flow controllers (*measure FCs*), temperature controllers (*measure TCs*) as well as the triggering of the FTIR spectrometer (*trigger IFS*) are successively executed. Subsequently the main loop restarts. The *Dynamic State* procedure is a loop with a built in loop and some subtasks that are executed in a defined sequence in order to maximize the repetition frequency of the secondary loop. The temperature can be controlled within an accuracy of $\pm$ 1 K. Because the subtask *measure TCs* is up to 15 times slower than *measure FCs* subtask, the temperature is not monitored at each cycle of the secondary loop to save time and obtain higher frequencies.

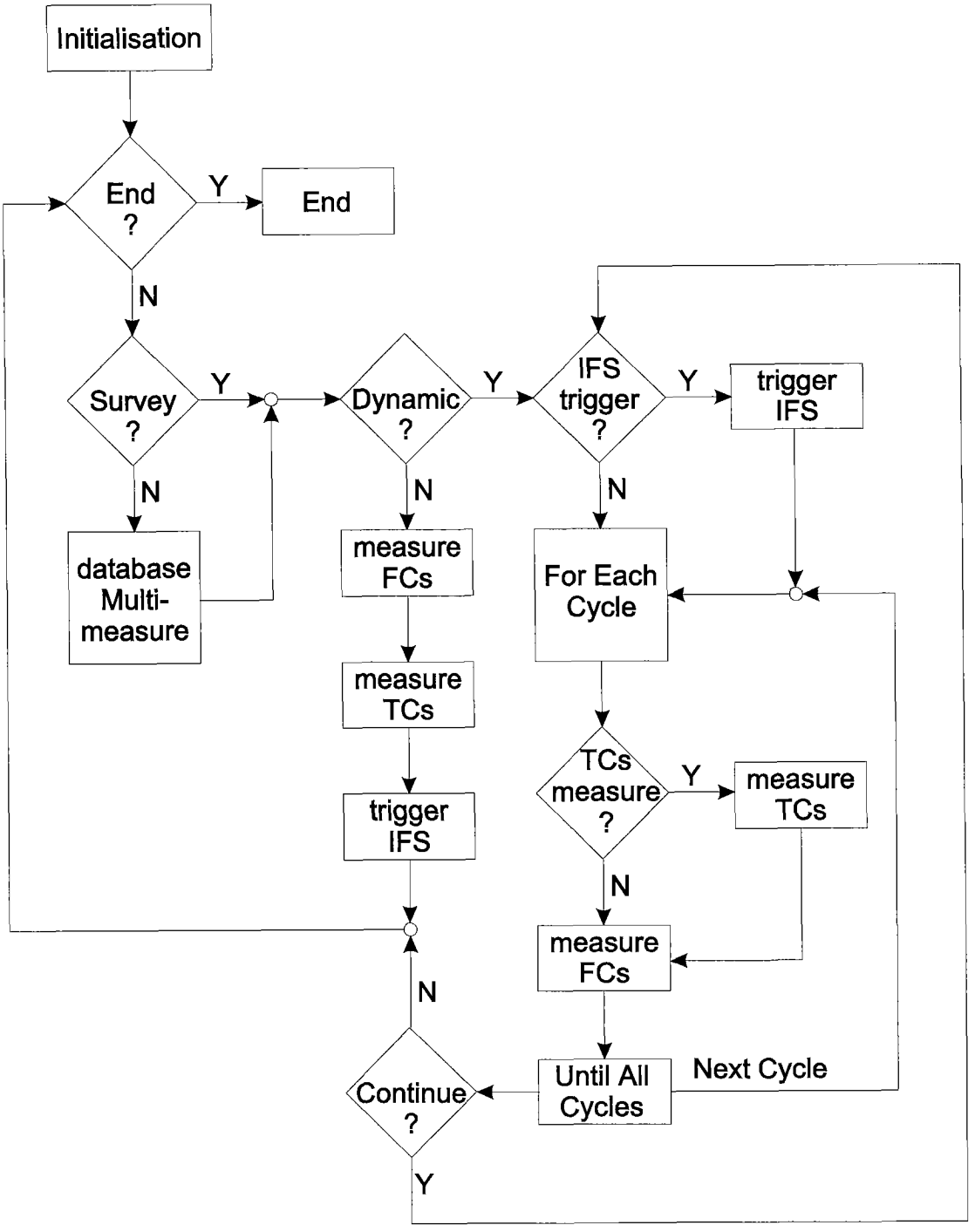

Figure 2-2: Flow diagram of the control program. Main components are the main loop, with the *Steady State* and the *Dynamic State* loops, as well as the subtasks *measure FCs*, *measure TCs* and *trigger IFS*.

The *Dynamic State* loop checks first if the routine to send the trigger signal to the FTIR spectrometer (*trigger IFS*) has to be executed. The secondary loop is then started and repeated for a specified number of accumulations. Each cycle start checking if the temperatures have to be measured, and if so, the routine *measure TCs* is then executed. Then the subtask *measure FCs* is executed and the cycle ends. When the secondary loop is terminated the *Dynamic State* loop ends too. The program can then either restart another *Dynamic State* loop or the main loop. To avoid possible conflicts between commands simple Errors-Controls are implemented [58].

2.2.3 Management of the mass flow controllers (*measure FCs*)

The four *mass flow controllers* and the *liquid flow controller* (FCs) of the *Modulation Unit* have to be managed with high precision and flexibility. The programmed subtask has to adjust the setpoints and to monitor the output.

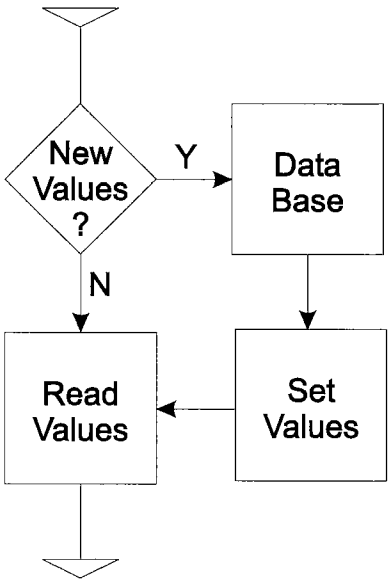

Figure 2-3: Flow diagram of the subtask dedicated for the management of the *flow controllers* (FCs). Further details are given in the text.

The programmed subtask has to adjust the setpoints and monitor the output. The flows have to be changed either sinusoidally or stepwise, and the total flow has to stay constant. The regulation of a single FC for the use of fluids which differ from the calibration fluid has to be simple. A quick data transmission is essentially to minimize the reaction time and to maximize the frequency of the applied sinusoidal patterns. The flow diagram of the subtask is shown in Figure 2-3.

The communication between PC and FCs occurs via two high-performance acquisition boards, *AT-A0-6* and *AT-MIO-16XE-50* (both National Instruments), for analogue output and digital input/output. Two connector blocks, *CB-50* and *SCB-68* (both National Instruments), are used as physical interfaces between the control PC and the electronic unit. The advantage of the use of this setup is the parallel control of all FCs.

To speed up the execution of the subtask a simple method, based on the multiplication of two matrices, was applied. In this way the whole subtask can be accomplished in a single run, and iteration frequencies up to 90 Hz are reached. The database-matrix carries the correction parameters to convert setpoints and output values from calibration fluids to applied fluids and *vice versa* [59,60]. The values-matrix is used to store setpoints and output values. The first step of the sub task looks for new setpoints and conversion values. Old parameters of the two matrices are replaced by the new data. The new setpoints are converted using the database-matrix, and sent to the FCs. If no changes are necessary this step is skipped. The output values are collected, transformed using the database-matrix, and the results are stored in the values-matrix. Then the subtask ends.

The control of the total flow is obtained by using a flow controller to compensate any variations of the volume caused by variation of the reactive components. Each fluid flow is adjusted using a polynomial 3^{rd} degree calibration function [59,60,61]. The achieved maximal deviation is $\pm$ 0.3 %.

2.2.4 Management of the temperature controllers (*measure TCs*)

The required specifications for the management of the four *temperature controllers* (TCs) are similar to those of the FCs. Flexibility, precision and quick transmission are major topics. The setup consists of four TCs of three different types, which have their own command structures and configurations [62,63,64]. The user interface has to eliminate all these differences and to allow the management of any temperature controller in the same, simple manner. The subtask has to adjust the setpoints, monitor the output values, control the execution of the temperature ramps as well as manage the tuning modes. The selection of the necessary thermocouples has to be automatically accomplished. To avoid collisions or conflicts between the commands extended Errors-Handling-Procedures were implemented.

The communication with the TCs occurs via a serial port RS 422 using a transmission rate of 9600 Baud. The serial port does not allow to manage all values at the same time. Therefore, the different steps of the programmed subtask are repeated for each temperature controller. In Figure 2-4 the flow diagram of the subtask is shown.

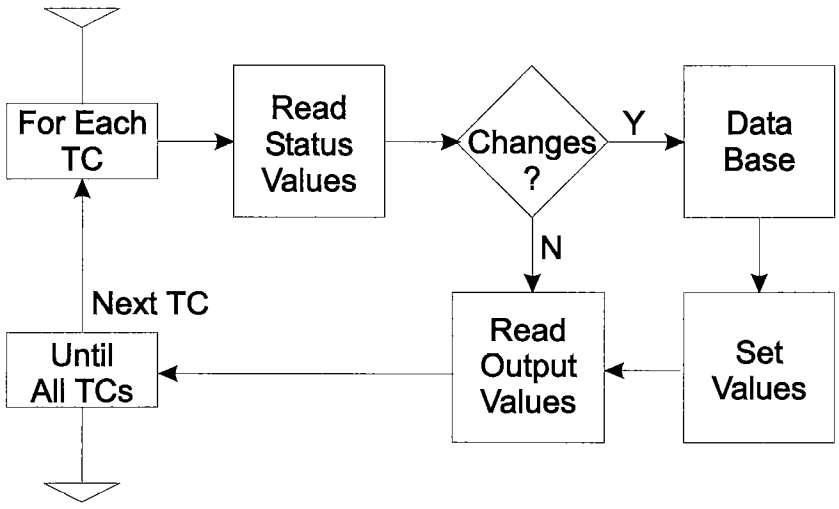

Figure 2-4: Flow diagram of the subtask dedicated for the management of the temperature controllers (TCs). Further details are given in the text.

In this case a programming technique based on two matrices is also used. A database-matrix contains setting values and status flags. A values-matrix is used for the setpoints and output values. In the first step the program collects information about the actual status of the TC. In the second, the occurred changes and the new values are combined and elaborated, the database-matrix is updated, the new setpoints converted and the necessary commands are sent to the TC. The steps are skipped if no changes are indicated. In the last step the output values are collected, using the database-matrix, converted and stored in the values-matrix. Then the whole task is repeated for another TC. As in the FCs subtask only the necessary operations are performed.

The selection of the thermocouple is obtained by sending the necessary command sequences and putting the TC off-line for several seconds. Temperature ramp programs and tune modes of the TCs are activated by starting the dedicated request procedures. The use of self and adaptive tune programs results in a maximum temperature deviation of ± 1 K. The achieved mean iteration time is 175 ms for each TC.

2.2.5 The triggering of the spectrometer (*trigger IFS*)

The triggering of the FTIR spectrometer (see section 2.6) is used to set the starting points for time resolved measurements. Therefore, the management of the data communications with the FTIR spectrometer is very important. A simple data protocol is essential to permit a fast transmission and therefore a minimal time delay between send of the start signal (*-trigger now-)* and start of the measurement. The subtask *trigger IFS* has to monitor the actual status of the IFS and of the running measurement but also to coordinate the start of new measurements by setting the trigger flag.

A high-performance acquisition board *AT-MIO-16XE-50* for analogue output and digital input/output and a connector block *CB-50* (both National Instruments) are used as communication interface between the control PC and IFS. The advantage of this setup is

the simultaneous control of the spectrometer in- and output. In Figure 2-5 the flow diagram of the subtask is shown.

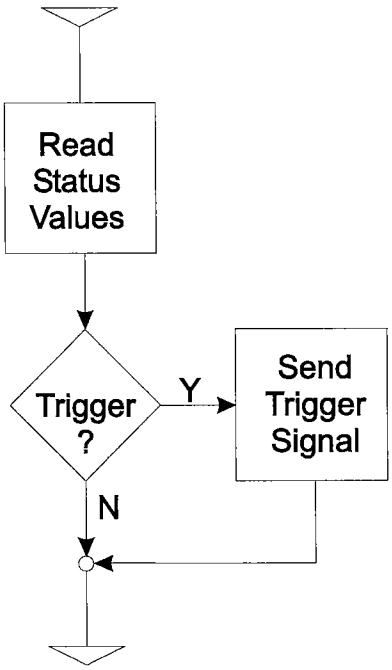

Figure 2-5: Flow diagram of the subtask dedicated for the communication with the IFS and to set the trigger flag. Further details are given in the text.

A simple subtask performs all necessary operations in one run. The communication protocol is reduced to the minimum and consists of only three flags. In the first step the actual status of the FTIR spectrometer and of the running measurement are monitored by reading the two flags: *-IFS ready to measure-* and *-new set of measurements ready to start-*. In the second step the situation is evaluated and the program decides if a trigger signal has to be sent by setting the flag *-trigger now-*. Then the subtask ends. In the worst case the time delay does not exceed 20 ms.

The time delay can be obtained in a two-steps experiment. In the first step a special designed macro collects a set of spectra. The measurement of each spectrum is started by an incoming trigger signal. The trigger signals are managed by a control program

which can send an impulse every 10 ms. The time at which the spectrum is collected is automatically stored by the FTIR spectrometer. The first starting time is subtracted from the last one, then this value is divided by the number of collected spectra. The mean time necessary for the *collection of a spectrum - wait for trigger signal - interpretation of the signal - start next measurement* is obtained.

In a second step a macro collects a set of spectra without waiting for trigger signals. Identical to the first step the mean value between starting times is calculated. In this case the mean time for *collection of a spectrum - start the next measurement* is obtained. The difference between the first and the second mean time is the value for *wait for trigger signal - interpretation of the signal*. This interval corresponds to the time delay between the start signal (*-trigger now-)* and start of the measurement.

2.3 The gas dosing systems

2.3.1 The Preparative Unit

The gas dosing system *Preparative Unit* is designed either to prepare special gas mixtures for the other gas dosing system (*Modulation Unit*) or to directly introduce the gases into the reaction chamber. All components, tubes, manometers, fittings and valves (Swagelok Co.) are made from stainless steel. In Figure 2-6 the scheme of the *Preparative Unit* is outlined.

The setup can be divided into two parts. In the first part (see Figure 2-6 on the left) up to four gas flows can be introduced independently and mixed successively. The flows are regulated by four mass flow controllers (MFC 5850E, Brooks Instrument B.V.) which are controlled via a dedicated independent electronic unit *WMR 04* (Westphal Mess- u. Regeltechnik GmbH).

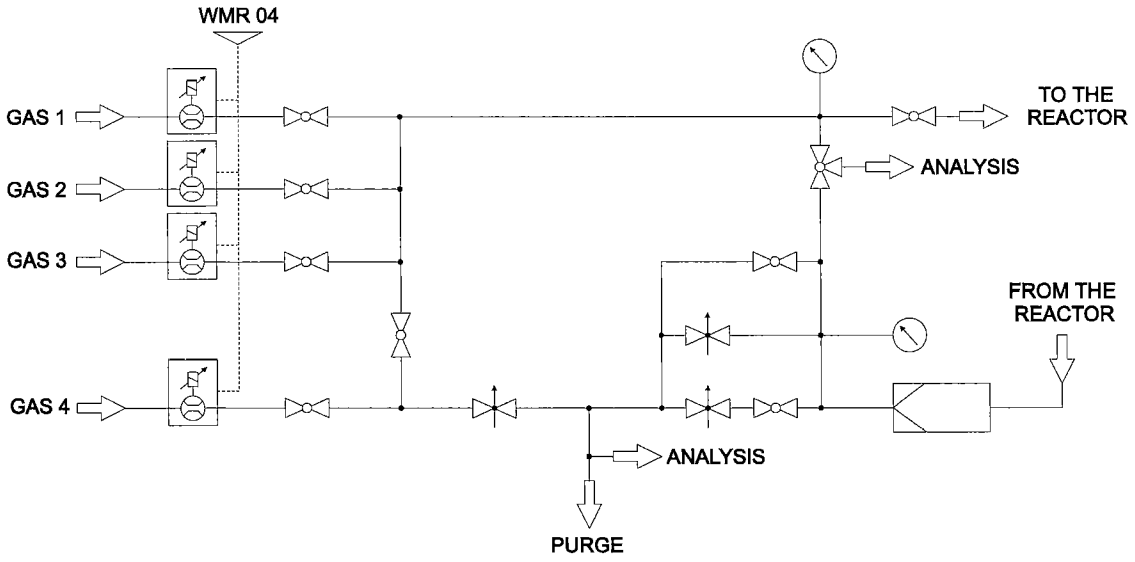

Figure 2-6: Schematic representation of the *Preparative Unit.* Main parts are the preparation (left) and the pressure regulation (bottom right).

In the second part (see Figure 2-6 bottom right) a manometer, *ON/OFF* valves and needle valves with different *Flow Coefficient* (C_V) are used to regulate the desired pressure within the reaction chamber.

The three lines are parallel mounted. In the middle line a needle valve with a small C_V (0.004) is used to control the gas flow down to 10 $ml_N\ min^{-1}$. The lower line consists of a needle valve with a higher C_V (0.03) and an *ON/OFF* valve. This is used to control the pressure at higher gas flows. The upper line is equipped with an *ON/OFF* valve. In this way it is possible to bypass the two other lines without changing the settings of the needle valves. This is useful for flushing samples prior, during or after other experiments. This special designed setup is very sensitive to pressure control. The desired pressure value is quickly reached, and is held without detectable changes over a long period. Two exits are used to connect additional analytical units.

A supplementary unit (see Figure 2-7) can be placed between the gas dosing system and the reactor. It consists of a heatable sample loop with two injection ports that can be used to introduce either evaporated liquids or sublimated solids into the reaction

chamber. This unit consists of two parallel lines. When a substance is introduced in one loop, the gas flow is directed to the other line.

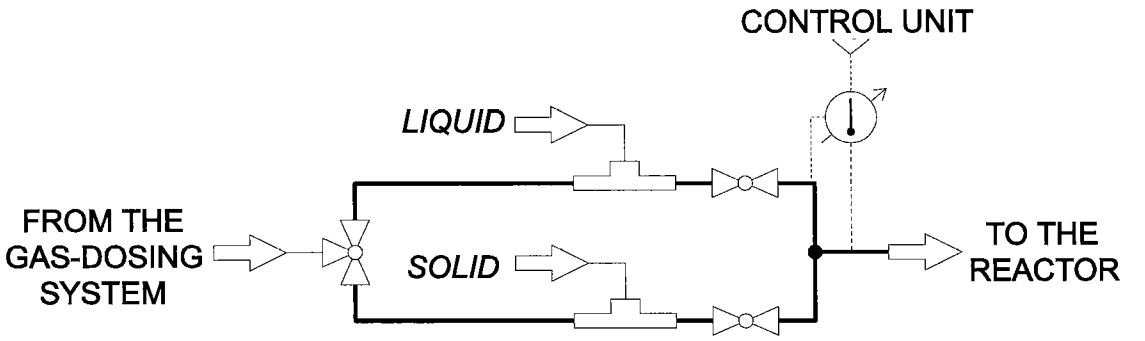

Figure 2-7: Schematic view of the supplementary unit of the *Preparative Unit*. Main components are the heatable sample loop and the two injection ports.

Then the gas flow is switched to the line containing the evaporated or sublimated compound. The loop can be heated up to 473 K using a heating tape (Hillesheim GmbH), while the temperature is controlled by a digital temperature regulator (model 94C, Eurotherm Regler GmbH). The thermocouple (Type K, ∅ 1 mm) is placed at the gas exit.

2.3.2 The Modulation Unit

The second gas dosing system *Modulation Unit* is designed to independently introduce up to four gases and one liquid into the reaction chamber. All components, tubes, manometers, fittings and valves (Swagelok Co.) are made from stainless steel. The diameter of the tubes was chosen in order to obtain a minimal dead volume. The gas flows are regulated to the desired values using mass flow controllers (MFC F-201C-FA-31, Bronkhorst Hi-Tec).

In spite of the reduced dead volume the mixing of the gases remains very difficult. To ensure homogeneous gas mixtures down to the ppb range three gas mixing chambers (GMC 1-3-3, Bronkhorst Hi-Tec) are successively assembled after the mass flow controllers.

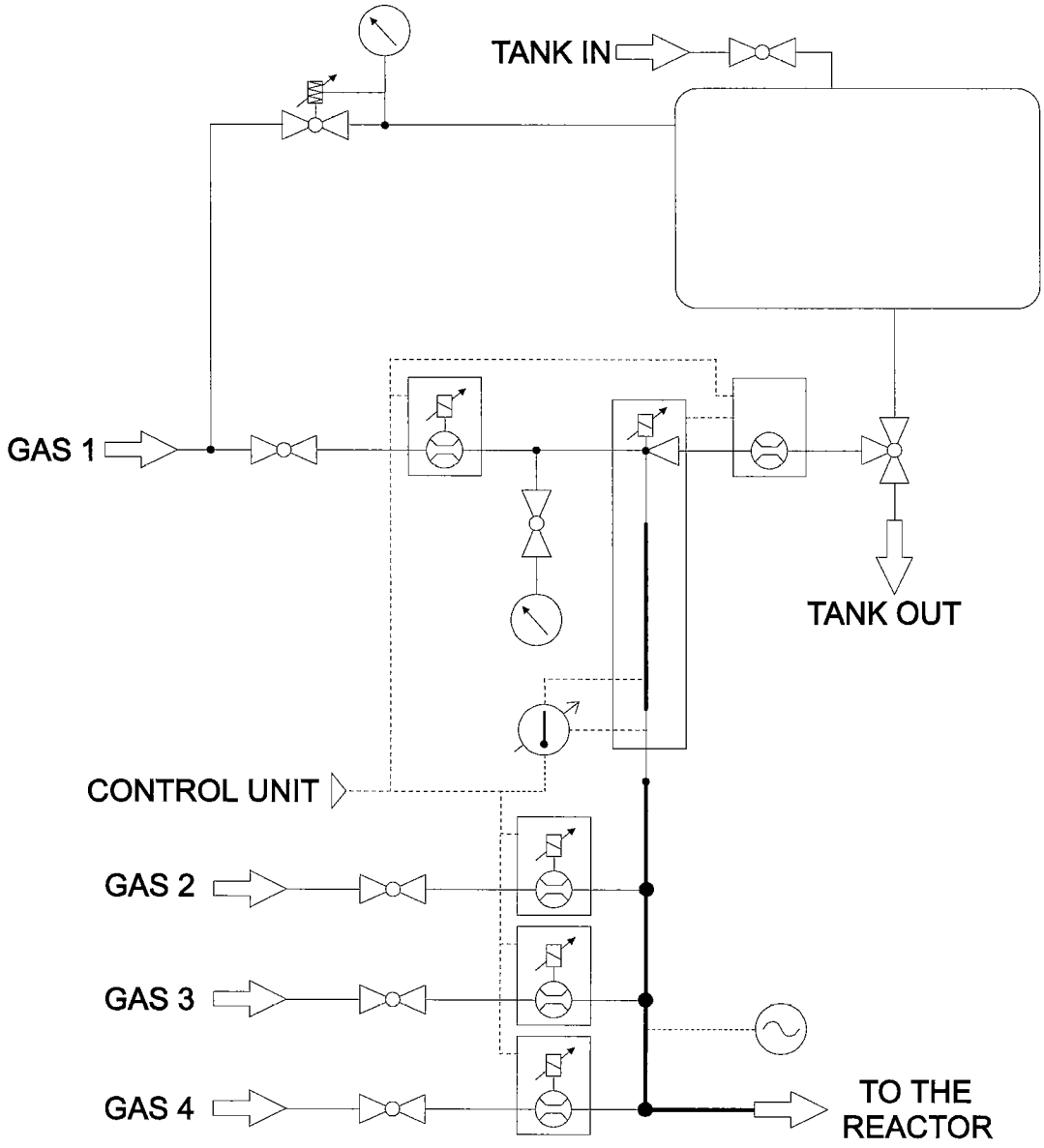

Figure 2-8: Schematic representation of the *Modulation Unit*. Main parts are the gas dosing system (bottom) and the liquid evaporator (middle).

To avoid possible condensation in the system the mixing chambers are heated by a semiconductor-based heating tape HBRT40 (Hillesheim GmbH) allowing a maximum temperature of 393 K.

The liquid is placed in a 0.2 l high pressure stainless steel tank, its flow is monitored via a liquid flow controller (LF L1-FA-11-0, Bronkhorst Hi-Tec) and regulated by an electromagnetic needle valve at the top of the evaporation unit. Then the liquid is introduced into the controlled evaporator mixer (CEM W-102-131-P, Bronkhorst Hi-Tec).

A digital temperature regulator (model 94C Eurotherm Regler GmbH) is used to control the temperature in the evaporation unit. The thermocouple (Type Pt100) is placed at the gas exit. The mass flow controllers, the liquid flow controller and the temperature controller are managed through a dedicated homemade electronic system connected to the control PC using the *LabVIEW* based program.

2.4 DRIFT: optical accessories and methodic

Two different environmental chambers are used, which allow to emulate process conditions.

2.4.1 Controlled Environmental Chamber

The *Controlled Environmental Chamber* (Model 0030-102, Spectra-Tech) is suitable for experiments requiring temperatures up to 1173 K and pressures among 10^{-4} Pa and 0.7 MPa. The chamber hood is fitted with two NaCl windows (transparent from 48'000 to 650 cm^{-1}) (Korth Kristalle GmbH).

The sample holder has a volume of about 0.1 ml, and the reaction gases flow over the sample. The heater element is part of the sample holder. The thermocouple (Type K, ∅ 0.5 mm) is placed directly below the sample holder surface. The temperature is controlled using a digital temperature regulator (model 94C Eurotherm Regler GmbH). A water cooling canal is contained, below the steel dome, in the top part of the cell support, to protect the gaskets from high temperatures. A gas-tight attachment of the steel dome over the cell support is obtained by viton O-rings. A schematic view of the DRIFT cell can be found elsewhere [65].

The environmental chamber is placed in the *COLLECTOR*™ (Diffuse Reflectance Accessory 0030-0XX, Spectra-Tech). Its characteristic is the measurement in *on-axis* geometry that provides a high energy throughput. Some modifications of the original design were carried out in order to obtain a quick and better fixation of the whole unit in the measurement chamber of the FTIR spectrometer. Further details about the accessory can be found elsewhere [66].

Test measurements have shown that, under the applied conditions, the specular reflectance effect is normally very weak or not present at all. No pronounced artefacts could be detected.

2.4.2 Environmental Chamber

The *Environmental Chamber* (HT-HP EC 19933, Graseby-Specac) is suitable for experiments requiring temperatures up to 773 K and pressures between 10^{-4} Pa and 3.3 MPa. The chamber hood is fitted with a ZnSe window (transparent from 20'000 to 455 cm^{-1}).

A volume of about 0.1 ml of material can be loaded into the sample holder. The original design was modified in order to allow the reaction gases to pass through the sample. A mesh, placed at the bottom of the sample holder where the gases enter, acts as support

for the loaded compound and distributes the gas flow uniformly through the whole sample. The heater element is part of the sample holder. The thermocouple (Type Pt100, ∅ 1.0 mm) is placed directly below the sample holder surface. The temperature is controlled using a digital temperature regulator (model 847, Eurotherm Regler GmbH).

A water-cooling body is placed between the cell support and the dome, to protect the gaskets from the high temperatures. A gas-tight attachment of the steel dome over the cell support is obtained by viton O-rings. A schematic view of the DRIFT cell can be found elsewhere [67].

Test measurements, using two thermocouples (Type K, ∅ 0.33 mm, Philips A.G.), placed on the surface and the bottom of the catalyst bed in the sample holder, have shown that the thermal gradient is below 1.5 K ± 0.5 K.

The environmental chamber was placed in the *SELECTOR* (Diffuse Reflectance Accessory 19900, Graseby-Specac). The measurements in *off-axis* geometry ensure the minimization of unwanted specular reflectance. A scheme of this accessory can be found elsewhere [68].

2.4.3 Representation of DRIFT spectra

The DRIFT spectra are usually displayed in Kubelka-Munk units. Catalysts of greyish-black colour absorb strongly throughout the MIR region, and their reflectance during the reaction (R) is higher than those of freshly pretreated catalysts which are used as reference (R_0). These properties violate one of the basic assumptions of the Kubelka-Munk theory, i. e. the presence of a non- or weakly absorbing substrate [13,14,15]. Therefore, in this work the spectra will be presented as relative reflectance units (R/R_0).

Several authors use multiplication of the background spectrum by a factor of 20 [69] in the K-M equation or the logarithm of the inverse of the reflectance [70,71] instead of the

K-M model. However, these procedures are not suitable when desorption or reactive consumption of surface species must be considered. Therefore, the use of relative reflectance units, which are directly related to the experiment, is more appropriate.

The dilution of the sample with a non-absorbing substance is not possible in heterogeneous catalysis. Alkali halides (KCl, KBr, ...) are chemically not inert under the applied conditions and react either with the catalyst or with the reaction gases. Other diluents (e. g. metal oxides, ...) can perturb the reaction via secondary reactions or induce the migration of adsorbed species, i. e. spillover, between the different sample components.

2.4.4 Sample preparation

As mentioned in the previous chapter, DRIFT spectra are greatly influenced by sample packing [29,30,31]. The duration and the pressure applied to the sample are critical in affecting the scattering coefficients. To ensure the reproducibility of the experiments, the catalyst is pressed, for 0.5 to 1 minute, with a constant pressure of 1 MPa into the sample holder of the environmental chamber with a home made sample packing device [72]. Test experiments performed with this packing system have shown reproducibility of the spectra with a small standard deviation [73].

2.5 The micro reactor / gas cell system

The setup consists of a *plug flow micro reactor* (μ-reactor) placed in a vertically mounted furnace and a gas cell. This system is suitable for experiments requiring temperatures up to 973 K and pressures among 0.1 and 4 MPa. A scheme of the setup is outlined in Figure 2-9.

The homemade fixed bed μ-reactor (Asea Brown Boveri A.G.) has a variable volume, and up to 3 ml of sample can be loaded. Its special design allows to hold the catalyst bed in the isothermal zone of the *ad hoc* developed furnace (MTF 10/38/130, Carbolite), which has a temperature uniformity of ± 2.5 K over 30 mm.

Two thermocouples (Type K, ∅ 0.33 mm) are used for precise temperature measurements in the catalyst bed. An additional thermocouple (Type K, ∅ 1.5 mm) is applied to control the temperature of the heating jacket. The temperature is controlled using a digital temperature regulator (model 904A, Eurotherm Regler GmbH). Test experiments have shown, that in the worst case the temperature gradients do not exceed 2.5 K along the catalyst bed.

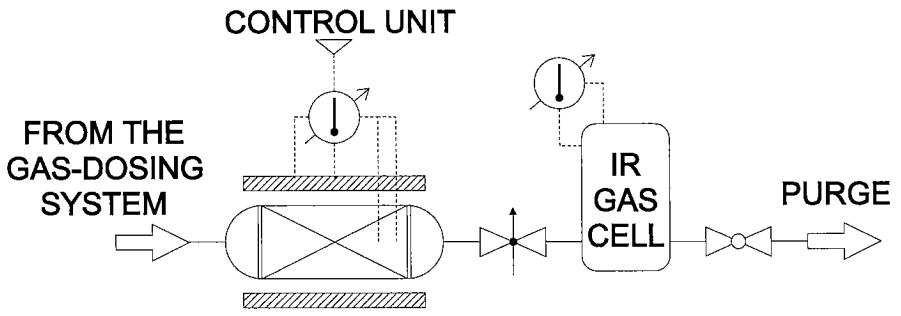

Figure 2-9: The μ-reactor/gas cell setup. Main components are the reactor, the furnace and the gas cell.

A stainless steel needle valve placed between the reactor and the gas cell is used to regulate the pressure in the μ-reactor. The leaving gases are then analysed using a special developed *Ultra-Mini-Long-Path* gas cell (G-1-3.2-PA-BA-PG, Graseby-Specac) having an optical path length of 3.2 m and a total volume of 120 ml. The cell was heated to 333 K using a heating jacket with an independent digital temperature controller (Omron) to avoid any condensation on mirrors and walls.

2.6 The FTIR spectrometer

2.6.1 The instrument

The *Infrared Fourier Transform Spectrometer* (IFS) is a IFS 55/S EQUINOX (Bruker GmbH) equipped with a liquid nitrogen-cooled *Mercury-Cadmium-Telluride* (MCT) detector (sensitivity from 12'000 to 600 cm^{-1}). A *silicon carbide* (SiC) *globar* (emission from 7'500 to 100 cm^{-1}) is used as infrared radiation source. The beamsplitter is a germanium-coated KBr crystal (transparent from 7'500 to 370cm^{-1}).

The spectra are recorded with a resolution of 4 cm^{-1} and a scan velocity between 80 kHz and 160 kHz. The accumulation of scans per spectrum depends on the *Signal-to-Noise Ratio* (SNR) as well as on the necessary time resolution. Therefore, up to 512 interferograms were accumulated for time-dependent spectra and up to 1024 interferograms for background spectra.

Spectra were usually collected by manual initialisation. During some experiments, in which spectra have to be recorded successively, the manual collection of the spectra would be very tedious. Therefore, a dedicated macro capable of coordinating and managing the collection of series of spectra was used.

2.6.2 The macro

The dedicated macro was programmed using OPUS-macros language of the OPUS/IR (Ver. 3.0, Bruker GmbH) IFS control software [74].

he macro consists of an initialisation step, in which the necessary data are entered by the operator, and of a main loop, which is repeated for different temperatures. To minimize the number of heating and cooling cycles, sets of spectra are recorded for different

parameters at a chosen temperature. Then the same sequence is repeated at a new temperature.

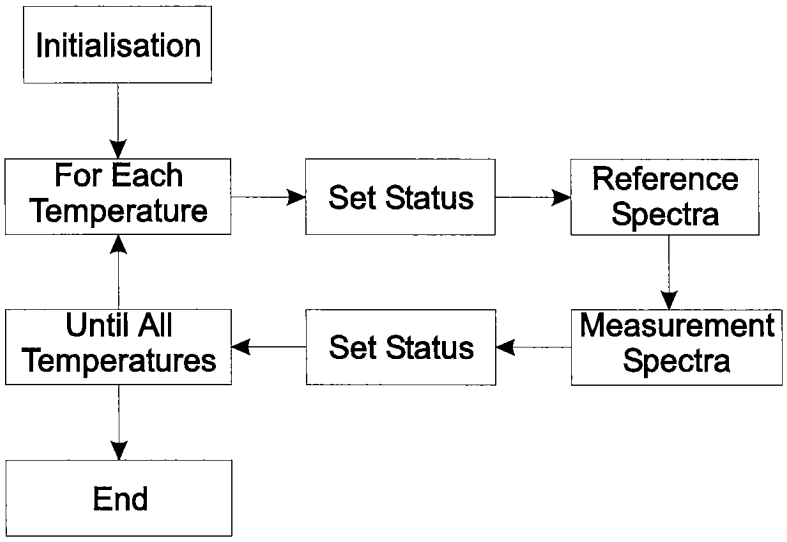

Figure 2-10: Flow diagram of the macro used to perform multiple measurements during experiments. Further details are given in the text.

The first step of the loop is the setting of flags. Two flags *-IFS ready to measure-* and *-new set of measurements ready to start-* are used to indicate the status of the IFS and the measurement. The first flag indicates when new spectra can be collected. The second flag is used to control the start of a new set of measurements at a new temperature. Two similar submacros are started subsequently: one for the accumulation of reference spectra, the other for the collection of measurement spectra. The flags are then reset and the loop can be restarted for a new temperature.

Both submacros have the same flow diagram, but differ for the number of collected interferograms per sample and background spectra. The task of these submacros is to coordinate the collection of spectra. In Figure 2-11 the flow diagram of the submacros is shown.

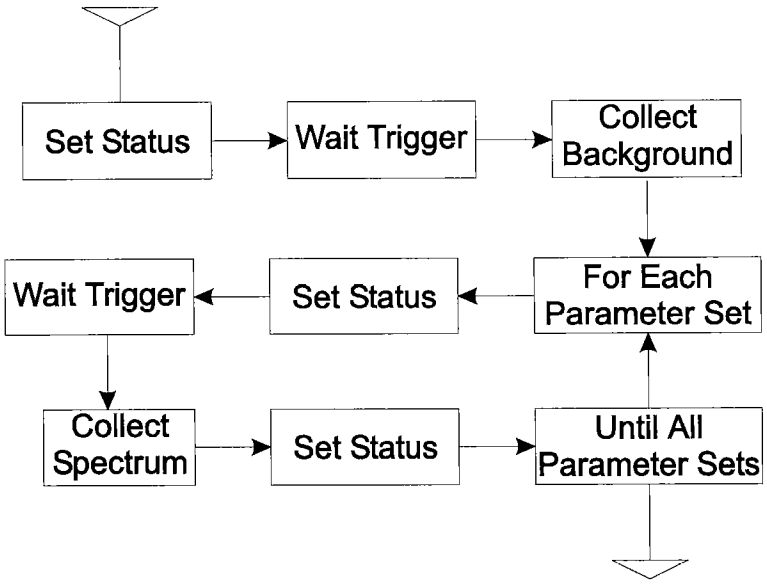

Figure 2-11: Flow diagram of the macro used for the automatic control of the spectrometer. Further details are given in the text.

The first steps of the submacros are the setting of the flag and waiting for the trigger signal. The collection of the background spectrum follows. Then the loop starts and is repeated for each set of parameters. The tasks in the loop are quite simple: set the flag, wait for the trigger signal, collect the spectrum and reset the flag. At the end the loop can be restarted for a new set of parameters.

2.7 Catalytic tests

Catalytic tests were only carried out in steady state condition using the same reaction parameters as applied for the dynamic experiments. The additional analytical setup was connected to the output of the DRIFT cell. Two different independent analytical setup were used.

A *Quadrupole Mass Spectrometer* (QMS) MD-100 (VG-Gas) was used to analyse complex gas mixtures. Compounds up to 100 amu can be monitored. The error was

estimated to be ± 2 % of the measured value. A Siemens IR CO/CO_2 analyser was used to measure carbon monoxide and carbon dioxide. The error of the apparatus was ± 5 % of the measured value.

2.8 Compounds

Nitrogen, that was used as carrier gas, as well as carbon monoxide, carbon dioxide, hydrogen and oxygen were used without further purification. All gases were commercially available (Sauerstoff Lenzburg A.G.) in 5.0 quality (purity >99.999 %).

Formic acid, methanol and paraformaldehyde (both Fluka purum ≥ 98%) were used as reference substances; labelled formic acid and paraformaldehyde (both > 99%, ^{13}C; chemical purity ≥ 98%) were obtained from Cambridge Isotope Laboratories.

The $Pd_{25}Zr_{75}$ catalyst for the CO oxidation was prepared by the melt spinning technique [75]. The $Cu_{46}Zr_{54}$ catalyst for the CO_2/CO hydrogenation to methanol was prepared by coprecipitation of the corresponding metal nitrates, at constant pH and temperature, as described elsewhere [76,77]. Both catalysts were prepared in the group of Prof. Dr. A. Baiker at the Swiss Federal Institute of Technology, ETH Zürich, Switzerland. We thank him for making available these samples.

The $Cu/ZnO/Al_2O_3$ catalyst for the CO/CO_2 hydrogenation to methanol was provided by *Haldor Topsøe A/S*.

3. Reactants modulation

3.1 Introduction

The characterisation of catalytic reactions is important for the production of new catalysts, and for the optimisation of industrial catalytic processes [78,79,80]. The primary goal of the characterisation is to provide a basis for understanding the activity and selectivity of the investigated system. The secondary goal is to obtain all necessary information in order to develop better catalysts and find the best working conditions.

From a systems theory point of view, investigated catalytic processes can be considered as unknown systems with their own internal rules. The investigation of unknown systems and the determination of the governing rules is one of the main tasks of the *Control System Theory* [81,82,83] and of the *Signal Processing Theory* [84,85,86]. The investigation is based on the application of theoretical concepts to the experimental result.

In the *theoretical analysis* existing information is used to create complete models and to evaluate possible modifications allowing high flexibility. The developed model can be rapidly and simply adapted to describe similar systems. The disadvantage is the impossibility to know *a priori* if the obtained model will be appropriate.

The *experimental analysis* uses experimentally obtained data to develop a model. A simple model is normally enough to describe the raw data, but no new knowledge about the investigated system can be acquired. Best results are obtained by modifying a theoretical model to match the experimental data.

A similar procedure is used in the modulation analytical concept in heterogeneous catalysis, to be described below, in order to obtain information about reaction pathways and reaction rate constants of a catalytic system. In this new concept theoretical knowledge is used to create models, which are modified to match the experimental data. Models that adequately represent the reality are obtained using the classical method of fitting the experimental data to the control system models.

An external perturbation applied to the system induces time-dependent selective modifications of the different components. The temporal evolution of the signals is monitored over large spectral intervals. Then the collected data are elaborated and fitted to the applied model. Information about the processes occurring in the system are thus obtained.

In the 2D correlation techniques, extensively applied in NMR [87,88,89,90] and IR [91,92,93,94,95] spectroscopy, two different perturbations were used to obtain additional information about the investigated system.

In the field of heterogeneous catalysis several methods based on a similar idea were used, e. g. *Transient Response Methods*, *Temperature Programmed Desorption* and *Temperature Programmed Reaction* [96,97,98]. Theoretical studies of the application of *Frequency Response* techniques to catalytic systems were presented by several authors [99,100,101,102]. More recently, practical applications of these techniques were used in the investigation of adsorption kinetics of gases [103,104] and catalytic systems [105,106,107].

3.2 Approach to the problem

In our approach the equilibrium of a system is perturbed by a test signal. The choice of this test signal is very important, because it influences directly the output signals. These have to be monitored and should not be influenced by the setup.

For heterogeneously catalysed reactions studied by DRIFT spectroscopy, the choice of the test signal is not very simple. As explained in the first chapter, small variations of the sample refractive index induce large changes in the measured values. Therefore, test signals, e. g. ramps or step up/step down, where information about the system are obtained from the form and intensity of the output signals, are not often applicable.

The problem of the refractive index can be solved by using repetitive test signals, e. g. sinusoidal waves. In such a case the system influences form, intensity and position of the output signals. The output signal is also sinusoidal, and maxima respectively minima in the concentrations unambiguously correspond to maxima and minima in the measured values. Information about the investigated system can hence be obtained from the position, or phase lag, of the output signals.

In gas phase FTIR spectroscopy, the use of sinusoidal functions as test signals allows the elimination of calibration curves.

Heterogeneous catalytic systems can be perturbed by varying different parameters, i. e. temperature, total pressure and reactant concentrations in the feed gas. Modulation of the temperature induces the parallel modification of all reaction components. In this case it is very difficult to observe selective changes of single components. Due to the superposition of the system answers, the information can not be easily extracted.

Modulation of the total pressure or of a single component, participating in different steps of the process, allows the reduction of the responses superposition, and therefore conclusions can be drawn. On the other hand, the modulation of a component that reacts

in the first step of the process allows to follow the selective modification of the different components along the reaction path. Information is collected about the individual reaction steps present in the investigated system.

3.3 Modulation of the reactants

3.3.1 Mathematical background

Any heterogeneous catalytic system can be described as a dynamic system that transforms, via an operator T, an input signal $x_{in}(t)$ into an output signal $x_{out}(t)$.

$$x_{out}(t) = T\left[x_{in}(t)\right] \tag{3.1}$$

These systems are continuous, and can therefore be modelled using sets of differential equations up to n^{th} order. In the control system theory, differential equations of n^{th} order are described using *delay elements of n^{th} order with proportional behaviour* (PT_n).

$$\sum_{i=0}^{n} a_i \frac{d^i}{dt^i} x_{out}(t) = x_{in}(t) \tag{3.2}$$

This equation can be simply solved using the *Fourier Transformation* (see also Equation 1.6).

$$F(\omega) = \int_{-\infty}^{\infty} f(t)\, e^{-i\,\omega t} dt \tag{3.3}$$

The solution corresponds to the *Frequency Response $G(i\omega)$ of the Admittance Function $G(s)$*. The advantages of a similar transformation are multiple, e. g. no complicated calculations in the time domain and transformations into the frequency domain are necessary, because $G(i\omega)$ is in the frequency domain. Another advantage is the

possibility to linearly combine simple $G(i\omega)$ functions to create the $G_{Total}(i\omega)$ of the complete model. The obtained equations are the solutions of the set of differential equations which describe the investigated system. The third advantage is the possibility to use $G(i\omega)$ to convert a given input signal $x_{in}(\omega)$ directly into the corresponding output signal $x_{out}(\omega)$.

$$x_{out}(\omega) = G(i\omega) \cdot x_{in}(\omega) \tag{3.4}$$

$x_{out}(\omega)$ and $x_{in}(\omega)$ represent the input and output signals $x_{in}(t)$ and $x_{out}(t)$ in the frequency domain. The solution of the differential equations can be achieved by using the *Laplace Transformation*. In this case, the obtained solution is an *Admittance Function* $G(s)$ containing the complex variable $s = \sigma + i\omega$. In the special case, when $\sigma = 0$ the solution corresponds to the *Frequency Response* $G(i\omega)$ *of the Admittance Function* $G(s)$.

$G(i\omega)$ can be divided into a real $\Re(\omega)$ and an imaginary part $\Im(\omega)$ expressed as function of the frequency ω.

$$G(i\omega) = \Re(\omega) + i\,\Im(\omega) \tag{3.5}$$

It is possible to calculate the *Amplitude Response* $A(\omega)$ and the *Phase Response* $\varphi(\omega)$ from the imaginary and real parts. $A(\omega)$ is used to obtain the ratio between the amplitude of the output signal and the amplitude of the input signal as a function of the frequency. $\varphi(\omega)$ represents the retardation of the output signal referred to the input signal as function of the applied frequency. $|x_{in}|$ is the amplitude and $\varphi\,(x_{in})$ the initial retardation of the input signal $x_{in}(\omega)$.

$$A(\omega) = \sqrt{\Re(\omega)^2 + \Im(\omega)^2} = \frac{|x_{out}(\omega)|}{|x_{in}|} \tag{3.6}$$

$$\varphi(\omega) = \arctan\frac{\Im(\omega)}{\Re(\omega)} = \varphi(x_{in}) - \varphi(x_{out}(\omega)) \tag{3.7}$$

All the delay elements with proportional behaviour, e. g. PT_1 up to PT_n, present lowpass properties. Low frequencies are transmitted better, while high frequencies are strongly weakened. This behaviour is described by the concept of *bandwidth*, which is the frequency ω_b where the intensity of the amplitude, relative to its value at $\omega = 0$, is reduced by 3 dB. This corresponds to an attenuation of the measured signal to about $[1\text{-}2^{-0.5}]$ ($\approx 30\%$). The maximal value of the amplitude is attained at the *Resonance Frequency* ω_r, which is calculated by setting the derivative of the amplitude response $A(\omega)$ equal to 0.

3.3.2 Modelling the setup

Before starting the practical experiments, a basic model appropriate to the applied reaction conditions and setup is developed.

The system μ-reactor/gas cell is divided into two parts. The first part consists of the reactor, in which the gases pass through the catalyst. The use of large gas flows, compared to the reactor volume, justifies the assumption that no concentration gradients are present in the catalyst bed, neither by with respect to gas nor surface species. Therefore, the reactor can be considered as a *Continuous Stirred Tank Reactor* (CSTR) with a residence time τ. The residence time is defined as the ratio between the volume of the vessel and the total flow. Note that the use of large flows induces τ to approach zero.

The second part is the gas cell where the output gases are analysed. The cell has a reduced volume, which is used to monitor the present gases. The collected signals are mean values for the whole cell. Therefore, it was modelled as a continuous stirred tank with a residence time $\tau_{IR\text{-}cell}$.

The DRIFT cell presents another situation. The geometry offers the possibility to monitor surface and gas phase composition. The use of a thin catalyst bed and a small total flow allows the assumption that the gas phase and surface species are always in

equilibrium. Therefore, it is possible to assume that the content is well mixed and that the outgoing gases have the same composition as the fluid within the reactor. Consequently, the system was modelled as a CSTR with a residence time τ.

The use of a practical residence time, instead of the exactly calculated value has the advantage that no conversion of the flows and estimation of the effective volume is necessary. The evolution of τ as function of the temperature T (see Equation 3.9) was approximated with the Ideal Gas Law (see Equation 3.8).

$$p\,\dot{V} = \dot{n}\,R\,T \tag{3.8}$$

$$\tau(T) = \frac{k_\tau}{T} \tag{3.9}$$

To ensure a constant total flow, each change in the flow of a component was compensated by an equivalent inverse change in the carrier gas flow. For all reaction rate constants, the Arrhenius equation was used. The pre-exponential factor k_0 was assumed to be temperature independent.

$$k(T) = k_0\, e^{-\frac{\Delta E_A}{R\,T}} \tag{3.10}$$

3.3.3 Experimental procedure

As explained above, information about the investigated system can be obtained by the analysis of the retardation. Modulated test signals using well defined frequencies ω are introduced in the system, and simultaneously time resolved measurements are started. The collected spectra, which cover some modulation period, are integrated and the peak area of each component is plotted as function of time. Then a sinus function is fitted and the relative retardation, which is measured between the generated input and the output

signals, is obtained. The absolute retardation is calculated by subtracting the time delay to the relative retardation (see Figure 3-1).

$$\varphi_{absolute}(\omega) = \varphi_{relative}(\omega) - t_{delay}\ \omega \tag{3.11}$$

The time delay t_{delay} is the time necessary for the gas flow to cover the distance between the feed gas preparation and the measuring cell. $\varphi_{absolute}(\omega)$ represents the actual retardation between output signal (dotted line in Figure 3-1) and input signal (solid line in Figure 3-1) in the measuring cell. To observe each single reaction step separately, the $\varphi_{absolute}(\omega)$ of the previous component is subtracted from the $\varphi_{absolute}(\omega)$ of the generated component. Thus, the effective retardation between the two components can be calculated.

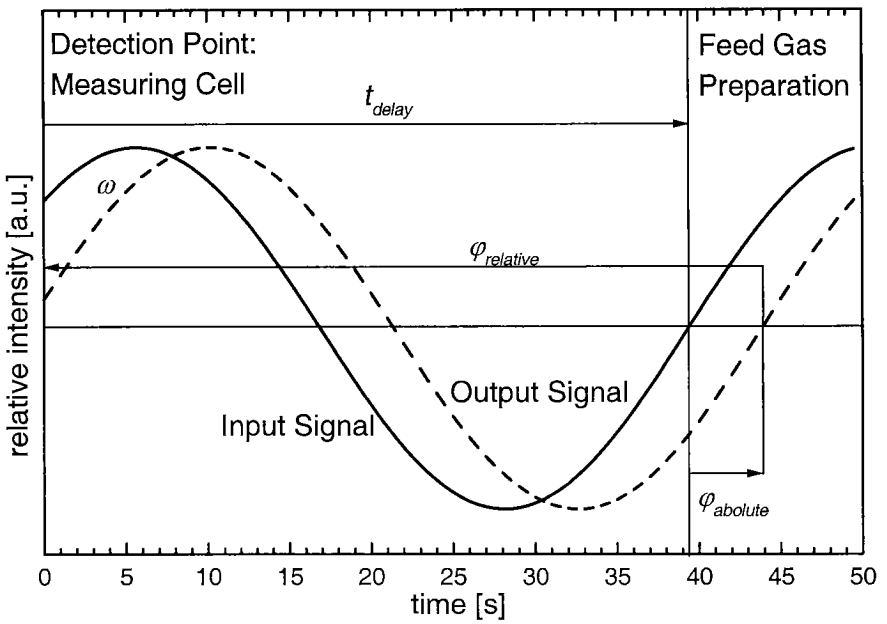

Figure 3-1: Input and output signal (solid, respectively dotted line) with the corresponding $\varphi_{absolute}(\omega)$ and $\varphi_{relative}(\omega)$. t_{delay} is the time necessary for the gas flow to reach the measuring point.

The interpretation of the evolution of the phase retardation as function of the applied frequencies is useful to obtain information about the reaction pathway and possible

intermediates. To estimate the reaction rate constants, the tangent of the retardation is plotted as function of the modulation frequency. The reaction parameters are obtained by fitting this curve with the appropriate mathematical function. Using these parameters, selectivity and conversion can be estimated. Repetition of the experiment at various temperatures is used to determine the associated activation energies (Arrhenius plots) and to create an energy scheme.

3.3.4 Experimental parameters

In order to determine the appropriate parameters for modulation experiments, some test with the stepwise changes of the reactant concentration (step up/step down) are performed. The amplitude has to be as wide as possible to induce a better signal propagation, but should not be too strong to avoid saturation of the detector or of the catalyst surface, which would cause a loss of signal propagation.

Possible interesting frequency regions can be obtained from the concentration changes of the different compounds. Preliminary information about an appropriate theoretical model for the investigated process can also be acquired. Simple models, consisting of differential equations of first and second order, are presented in the next paragraphs.

Similar tests were also performed to estimate the delay time, t_{delay}.

3.3.4.1 Determination of t_{delay}

The time delay is determinated by stepwise changing the concentration of one compound.

Experiments are performed as follow. The reactant concentration is changed stepwise, and the time resolved measurement is simultaneously started. The peak areas of the test component in the spectra are integrated and plotted as function of time. Then the curve

is fitted in the first part with a straight line and the second with an exponential decay of 1st order. t_{delay} is determined by the intersection of the two fits (see Figure 3-2).

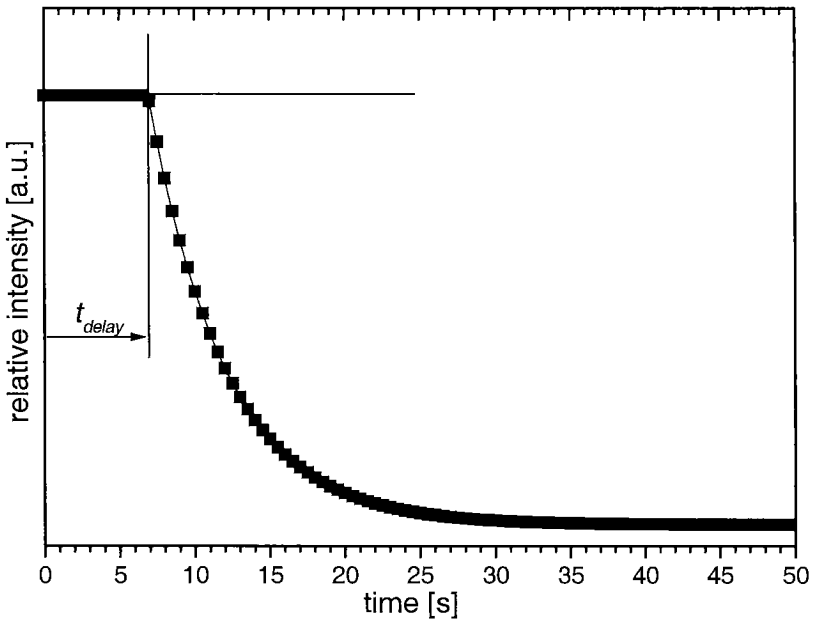

Figure 3-2: Peak area evolution of the test signal (dotted line) as a function of time. The t_{delay} is estimated by fitting the first part of the curve with a straight line and the second part with an exponential decay of 1st order.

3.3.4.2 Delay element of 1st Order (PT_1)

Differential equations of 1st order are described in the control system theory using a delay element of 1st order with proportional behaviour (PT_1).

$$T_1 \cdot \dot{x}_{out}(t) + x_{out}(t) = K \cdot x_{in}(t) \tag{3.12}$$

Equation 3.12 is solved using the Fourier transformation. The frequency response function $G(i\omega)$ is:

$$G(i\omega) = \frac{K}{1 + i\omega T_1} \tag{3.13}$$

From Equation 3.13 amplitude and phase response are simply derived:

$$A(\omega) = \frac{K}{\sqrt{1+\omega^2 T_1^2}} \tag{3.14}$$

$$\varphi(\omega) = -\arctan\left(\omega T_1\right) \tag{3.15}$$

Only the amplitude response $A(\omega)$ depends on the intensity K of the used test signal, while $\varphi(\omega)$ is independent. $A(\omega)$ decreases with increasing frequency. At $\omega = 0$, which corresponds to the resonance frequency ω_r (see paragraph 3.3.1), the amplitude ratio is at its maximum and approaches zero at $\omega \approx \infty$. The phase response $\varphi(\omega)$ presents an inverse behaviour. At $\omega = 0$ the retardation is 0, and approaches $-\pi/2$ at $\omega \approx \infty$. Therefore, a decrease of the frequency allows a better detection of the signal and a better discrimination of the retardation, and *vice versa*.

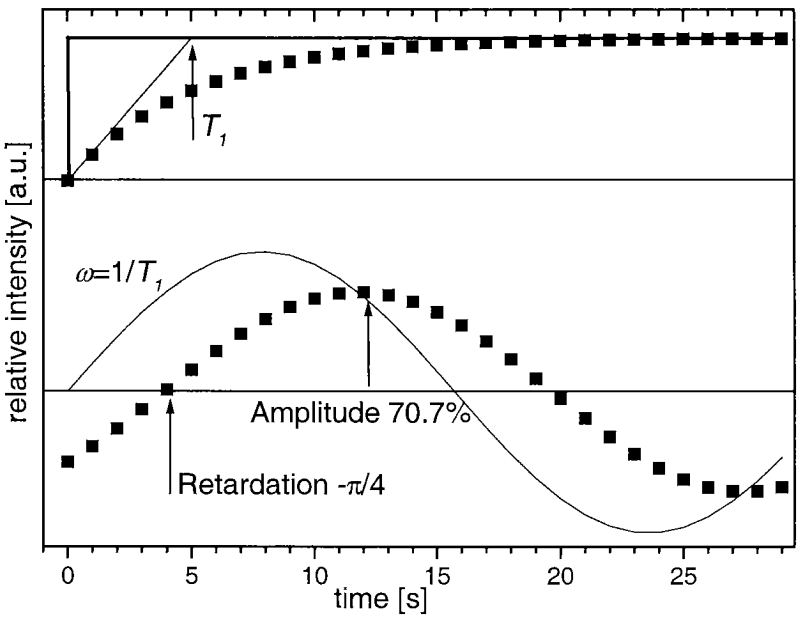

Figure 3-3: Comparison between different input signals (solid line) and the corresponding output signals (dotted line). **Top:** step up/step down experiment with the determination of the value of T_1. **Bottom:** shift and amplitude of the output signal using $\omega_e = T_1^{-1}$ as modulation frequency.

The characteristic parameter of the considered delay element is obtained as follows. From the plot of a step up/step down experiment, T_1 is estimated (see Figure 3-3, top). Using the same amplitude K of the step up/step down experiment and the *Edge Frequency* $\omega_e = T_1^{-1}$ as modulation frequency, the intensity of the obtained signal should be equal to $2^{-0.5}$ ($\approx 71\%$) of the step up/step down experiment, and a retardation of $-\pi/4$ should be observed (see Figure 3-3, bottom). Note that the PT_1 acts as a low pass filter, and that the chosen frequencyω_e is equivalent to the bandwidth frequency ω_b (see paragraph 3.3.1).

For the determination of the interesting frequency region some considerations are necessary. As explained above, an increase in the frequency reduces the general quality of the signal, and, at the edge frequency ω_e, the amplitude of the output signal is reduced by $\approx 30\%$. A retardation of $-\pi/4$ should already be achieved. To avoid the collection of data having a large uncertainty the analysed region should be between the edge frequency and $\omega = 0$.

3.3.4.3 Delay element of 2nd Order (PT_2)

The differential equations of 2nd order are described in the control system theory using a delay element of 2nd order with proportional behaviour (PT_2).

$$T_2^2 \cdot \ddot{x}_{out}(t) + T_1 \cdot \dot{x}_{out}(t) + x_{out}(t) = K \cdot x_{in}(t) \tag{3.16}$$

Equation 3.16 is solved using the Fourier transformation. The frequency response function $G(i\omega)$ is:

$$G(i\omega) = \frac{K}{1 + i\omega T_1 - \omega^2 T_2^2} \tag{3.17}$$

From Equation 3.17 amplitude and phase response are quickly derived.

$$A(\omega) = \frac{K}{\sqrt{(1-\omega^2 T_2^2)^2 + \omega^2 T_1^2}} \tag{3.18}$$

$$\varphi(\omega) = -\arctan\left(\frac{\omega T_1}{1-\omega^2 T_2^2}\right) \tag{3.19}$$

As for the PT_1, the phase response $\varphi(\omega)$ is independent from the intensity K of the input signal, but reveals an interesting evolution. At $\omega = 0$ the retardation is 0 and at $\omega \approx \infty$ $\varphi(\omega)$ approaches 0, too. A similar behaviour of the retardation can be explained by considering the PT_2 element as two separate, consecutive PT_1 elements. Using high frequencies both retardations approach the maximum value of $-\pi/2$. Hence, at $\omega \approx \infty$ the total retardation is closer to $-\pi$. At $\omega = T_2^{-1}$ the total retardation approaches $-\pi/2$, and a discontinuity is created. This last frequency is called *Eigen Frequency* ω_0 of the undamped oscillation.

$A(\omega)$ presents a more complicated evolution than for the delay element of 1st order. At $\omega \approx \infty$ the amplitude ratio approaches zero. The maximum value of $A(\omega)$ depends on the ratio T_1/T_2. If this ratio is greater or equal to $2^{0.5}$ then the amplitude has its maximum at $\omega = 0$. In the other case $A(\omega)$ reaches its maximum at the resonance frequency ω_r:

$$\omega_r = T_2^{-1}\sqrt{1-\frac{T_1^2}{2T_2^2}} \tag{3.20}$$

and the corresponding amplitude ratio $A(\omega_r)$ in given in Equation 3.21.

$$A(\omega_r) = \frac{K}{\frac{T_1}{T_2}\sqrt{1-\frac{T_1^2}{4T_2^2}}} \tag{3.21}$$

In general, an increase of the used frequencies corresponds to a decrease of the intensity of the propagated signals. Therefore, it is difficult to detect these signals and to discriminate their retardation.

Characteristic parameters of the PT_2 delay elements can be approximated using the *Inflection Tangent Approximation* [108]. This method is valid only if the ratio T_A/T_U is greater than 9.64, and if $T_1 \neq T_2$. From the plot of the output signal of a step up/step down experiment T_A and T_U are estimated (see Figure 3-4).

With the alignment chart in Figure 3-5 T_1 and T_2 are obtained. In Figure 3-6 two modulation patterns with the same amplitude but different frequencies are shown. In the first case (Figure 3-6, top) the resonance frequency ω_r is used. This has the advantage of a higher intensity of the output signals, but with a reduced retardation.

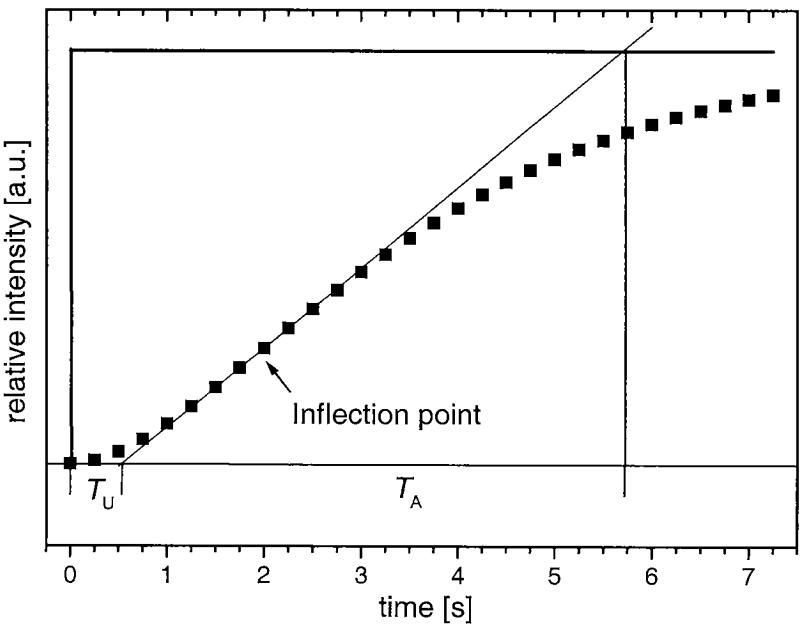

Figure 3-4: The input signal (solid line) is changed stepwise. From the inflection tangent of the output signal (dotted line) the two values T_A and T_U are calculated.

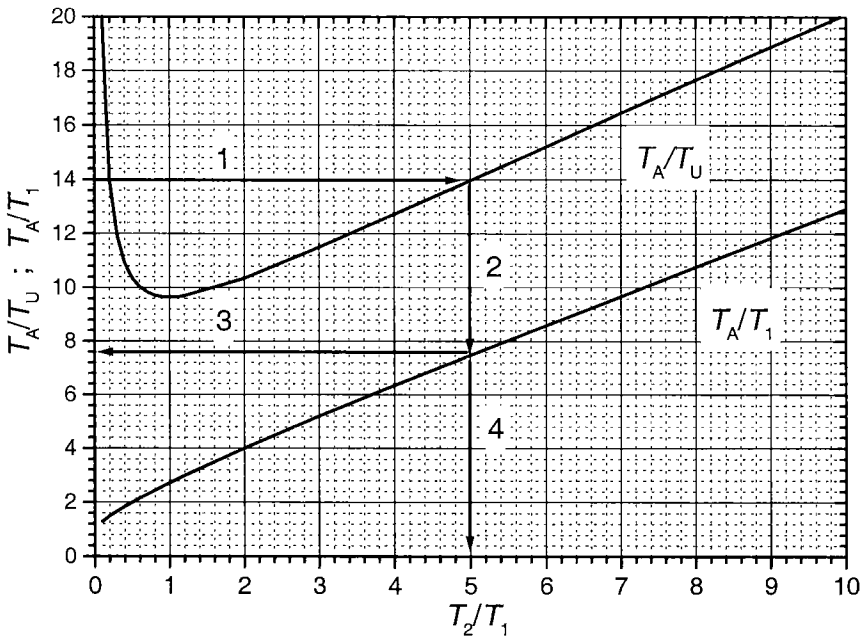

Figure 3-5: Alignment chart for the *Inflection Tangent Approximation*. From the ratio T_A/T_U (1) the ratio T_A/T_1 (2 and 3) is obtained and T_1 approximated. From the ratio T_2/T_1 (2 and 4) T_2 can be calculated [108].

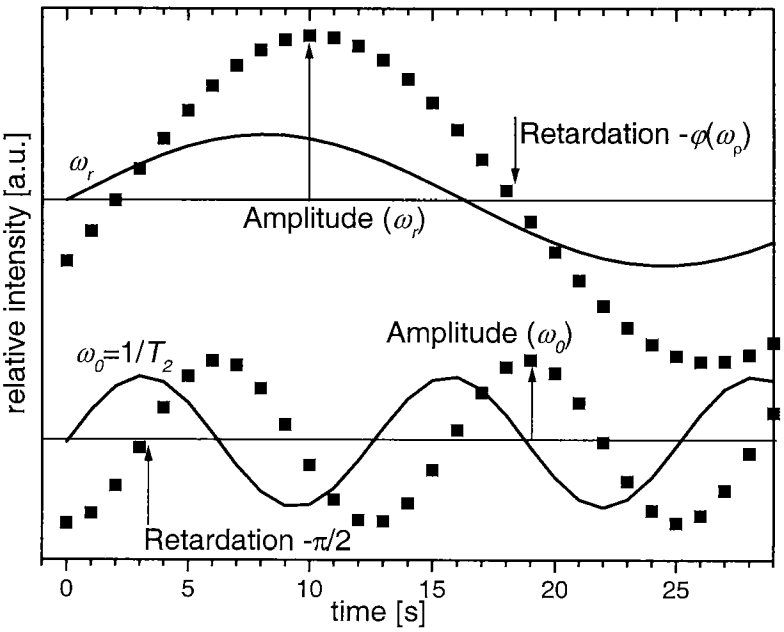

Figure 3-6: Two different input signals (solid lines) using the same amplitude but different frequencies: ω_r (top) and $\omega_0 = T_2^{-1}$ (bottom) are shown. The corresponding output signals are represented by dotted lines.

In the second case (Figure 3-6, bottom) the *Eigen Frequency* ω_0 is used, and the expected retardation approaches $-\pi/2$.

The determination of the interesting frequency region is not quite simple. As explained above, an increase of the frequency lowers the general quality of the signal, but is necessary to induce the oscillation of the PT_1 delay term elements included in the investigated PT_2. Therefore, analysis of the characteristic values: ω_0, ω_r and ω_b of the system is necessary.

As rule of thumb, a region around the *Eigen Frequency* ω_0 down to $\omega = 0$ is used as starting point. This has the advantage that a retardation ($-\pi/2$), covering one half of the maximum, has already been achieved.

3.3.5 Recording techniques

Experimental data are recorded using *time resolved FTIR spectroscopy* [109,110,111,112,113]. Essentially, there are two time resolved FTIR techniques, depending on the method used for moving the interferometer mirror: continuous moving (slow-scan [110,114] respectively rapid-scan [115,116]) or step-by-step moving (step-scan [117,118]).

In the slow-scan mode complete interferograms are recorded and immediately Fourier transformed before starting the collection of a new spectrum. In the rapid-scan mode sets of complete interferograms are collected before executing the Fourier transformation. In both cases the co-addition of complete interferograms allows an achievement of the desired Signal-to-Noise Ratio (SNR).

The slow-scan and rapid-scan technique are suitable to investigate reactions that occur in the second to milliseconds range.

In the step-scan mode the interferograms are created point by point. At each mirror position, data are collected for as long as it is necessary to achieve the desired SNR. Then the mirror is moved to the next position, the experiment is repeated and new data are collected. Using the accumulated data interferograms the Fourier transformation is performed.

Step-scan is useful for reactions in the microseconds to nanoseconds range. Due to the necessity of repeating each single experiment at each mirror position the investigated processes should be easily repeated to avoid long measurement times, examples are: photoacustic spectroscopy [119,120], liquid crystal reorientation [121] and photo-excited states investigation [122].

3.3.6 Recording parameters

Independently from the applied recording technique it is not easy to achieve a high enough SNR for plausible spectra. The SNR value can be controlled by the aperture, filters, resolution, scan velocity and number of collected spectra.

Modification of the aperture and used filters is a simple way to improve the SNR. The used parameters should allow the highest energy throughput, but any limitation of the collected frequency windows should be avoided. Scan velocity, resolution and number of averaged scans have a strong influence on the SNR. The number of photons reaching the detector should be as high as possible. The scale of the spectra and the time resolution should allow the evaluation of the observed retardation. To find the best condition test experiments are necessary.

3.4 Useful simple models

3.4.1 A few definitions in heterogeneous catalysis

A reaction is heterogeneous if it requires the presence of at least two phases to proceed at the given rate. Since more than one phase is present, the movement of material from phase to phase must be considered.

A central problem is the reaction pathway. In systems, such as solid catalysed reactions, where several series-parallel reactions are usually present, the concentration of the different intermediates is usually difficult to determine. To overcome this problem, rates are expressed in terms of overall reaction rates ($r_{overall}$). These are absolute rate expressions of the whole reaction, or of a single reaction step. Additionally to the usual chemical kinetics terms, mass transfer terms are also incorporated.

If the changes take place by parallel paths, under steady state conditions the overall rate is simply the sum of all individual rates (r_i).

$$r_{overall} = \sum_{i=1}^{n} r_i \tag{3.22}$$

On the other hand, if the overall change requires that a number of steps take place in succession, at steady state, all these steps will proceed at the same rate.

$$r_{overall} = r_i\big|_{i=1}^{n} \tag{3.23}$$

In this case the step providing the major resistance is called rate-limiting step, and can be considered alone. In Equation 3.24 the n^{th} order reaction of compound A is shown.

$$r_{overall} = k_{rate-limiting} \cdot A^n \tag{3.24}$$

This procedure leads to a very simple expression and is used whenever possible. More details about the modelling and the design of chemical reactions can be found in the literature [123,124].

3.4.2 Heterogeneous reactions in the used setup

As explained above, both used setup can be modelled as a continuous stirred tank reactor with residence time τ. The difference between the two setup can be summarised in the following way. The DRIFT cell permits the observation of gas phase and surface composition, but has a lower sensitivity towards the gas phase. The μ-reactor/gas cell system has a high sensitivity for gases, but no surface species can be detected. Therefore, a reduced amount of information can be collected and only suggestions about the reaction pathways can be obtained.

The gas cell acts as a continuous stirred tank that induces a supplementary retardation of each monitored compound. The retardation of a compound A can be represented using the following differential equation:

$$\frac{dA}{dt} = -\tau_{IR-cell}^{-1} A + \tau_{IR-cell}^{-1} A_0 \tag{3.25}$$

where A_0 is the concentration of A in the entering the gas cell from the reactor side, and $\tau_{IR\text{-}cell}$ is the residence time in the cell. The equation is resolved using the Fourier transformation (see Equation 3.3), and the retardation as a function of ω is obtained.

$$\tan\left(\varphi_A - \varphi_{A_0}\right) = \omega\tau_{IR-cell} \tag{3.26}$$

As expected the cell causes a retardation of the signals, which is only function of the residence time. The use of faster gas flows allows to reduce this value.

In the following paragraphs several simple models are presented and discussed. The reactions start always with compound A, with a concentration of A_0 in the feed gas. All the reaction rate constants k_i are considered as overall first order rate constants.

3.4.2.1 Adsorption/desorption equilibrium

The adsorption of a component is the first step in each catalysed reaction, while the desorption always follows. Knowledge about these equilibria is of great interest for an understanding of observed reaction behaviour, as well as in the formulation of plausible reaction schemes.

In this paragraph the equilibrium between an adsorbate B^* and a gas phase component A is considered. If a low partial pressure is applied, the surface concentration of vacant adsorption sites can be assumed as constant, and the following simple model can be used:

$$A \xrightarrow{k_1} B^*$$
$$A \xleftarrow{k_2} B^*$$

The system is described using the following set of differential equations.

$$\begin{cases} \dfrac{dA}{dt} = -(k_1 + \tau^{-1})A + \tau^{-1}A_0 + k_2 B^* \\ \dfrac{dB^*}{dt} = -k_2 B^* + k_1 A \end{cases} \tag{3.27}$$

This set of differential equations is solved using the Fourier transformation. The retardation as function of ω is obtained.

$$\tan\left(\varphi_A - \varphi_{A_0}\right) = \frac{\omega\left(\omega^2 + k_1 k_2 + k_2^2\right)}{\omega^2\left(k_1 + \tau^{-1}\right) + k_2^2 \tau^{-1}} \tag{3.28}$$

$$\tan\left(\varphi_{B^*} - \varphi_A\right) = \omega k_2^{-1} \tag{3.29}$$

For ***B****, the retardation is only dependent on the desorption reaction. For ***A***, a superposition is present. Considering that ω^2 is only important when high frequencies are applied, a low frequency approximation can be used.

$$\tan\left(\varphi_A - \varphi_{A_0}\right) = \omega \tau \left(k_1 k_2^{-1} + 1\right) \tag{3.30}$$

In this approximation the reaction rates are substituted by an overall equilibrium constant (k_1/k_2). The single values can be obtained using the value for k_2 estimated in Equation 3.29. If the residence time approaches zero, the retardation of ***A*** approaches zero too, and only the retardation of ***B**** can be monitored. A minor desorption or adsorption indicates a surface saturated with stable species. Therefore, the system acts as simple continuous stirred tank.

3.4.2.2 Series reactions

Series reactions consist of a sequence of two or more reaction steps. These represent the simplest form of catalytic reactions, where only one end product is formed.

In the considered system a compound ***A*** adsorbs on the surface to form ***B****, which reacts to the end product ***C***. If a low partial pressure of ***A*** is used, the surface concentration of vacant adsorption sites can be considered as constant. The use of an excess of other involved components allows the assumption of constant surface concentration. The following simplified model is used:

$$A \xrightarrow{k_1} B^* \xrightarrow{k_2} C$$

which is described by the following set of differential equations:

$$\begin{cases} \dfrac{dA}{dt} = -(k_1 + \tau^{-1})A + \tau^{-1}A_0 \\ \dfrac{dB*}{dt} = -k_2 B* + k_1 A \\ \dfrac{dC}{dt} = -\tau^{-1}C + k_2 B* \end{cases} \tag{3.31}$$

The system is resolved using the Fourier transformation and the retardation is expressed as function of ω.

$$\tan\left(\varphi_A - \varphi_{A_0}\right) = \omega\left(k_1 + \tau^{-1}\right)^{-1} \tag{3.32}$$

$$\tan\left(\varphi_{B*} - \varphi_A\right) = \omega k_2^{-1} \tag{3.33}$$

$$\tan\left(\varphi_C - \varphi_{B*}\right) = \omega\,\tau \tag{3.34}$$

For ***A*** and ***B**** the retardation is influenced by the adsorption and the reaction. For ***C*** only the residence time is important. The use of small residence times induces the retardation of ***A*** and ***C*** to approach zero. The only remaining retardation is given by Equation 3.33.

3.4.2.3 Parallel reactions

For parallel reactions, two or more reaction steps originate from the same intermediate, but different end products are obtained. Similar models are used for the case that expected as well as undesired products are generated from the same intermediate.

In the chosen example the compound ***A*** adsorbs on the surface, and the adsorbate ***B**** is created. This reacts to the end products ***C*** and ***D***. As discussed in the previous paragraph, the use of an excess of other involved components and a low partial pressure of ***A*** lead to the following simple model.

$$A \xrightarrow{k_1} B* \xrightarrow{k_2} C$$
$$B* \xrightarrow{k_3} D$$

This model is described by the following set of differential equations:

$$\begin{cases} \dfrac{dA}{dt} = -(k_1 + \tau^{-1})A + \tau^{-1}A_0 \\ \dfrac{dB*}{dt} = -(k_2 + k_3)B* + k_1 A \\ \dfrac{dC}{dt} = -\tau^{-1}C + k_2 B* \\ \dfrac{dD}{dt} = -\tau^{-1}D + k_3 B* \end{cases} \tag{3.35}$$

The set is solved and the solution is given as function of the modulation frequency.

$$\tan\left(\varphi_A - \varphi_{A_0}\right) = \omega\left(\tau^{-1} + k_1\right)^{-1} \tag{3.36}$$

$$\tan\left(\varphi_{B*} - \varphi_A\right) = \omega\left(k_2 + k_3\right)^{-1} \tag{3.37}$$

$$\tan\left(\varphi_C - \varphi_{B*}\right) = \omega\,\tau \tag{3.38}$$

$$\tan\left(\varphi_D - \varphi_{B*}\right) = \omega\,\tau \tag{3.39}$$

As expected, the retardations of compounds ***A*** and ***B**** depend on the rates of the different reaction steps. End products ***C*** and ***D*** present the same retardation, which is only dependent on the residence time. If τ approaches zero, all gas phase species show no retardation any longer, and only Equation 3.37 remains valid.

3.4.2.4 Series-parallel reactions

In series-parallel reactions different reaction steps, both in series and in parallel, are present. These represent the classical situation in heterogeneous catalysis. A reactant can

generate different products and intermediates, which can lead to various other end products.

In the considered example the compound ***A*** adsorbs on the surface to form ***B****, which can either react to the end product ***C*** or to the intermediate ***D***. The last component reacts to a separate intermediate ***E**** that further leads to the end product ***F***. If all the previously discussed simplifications about surface concentration of vacant adsorption sites and co-reactants are valid, the following simplified model can be used.

$$\begin{aligned} A &\xrightarrow{k_1} B^* \xrightarrow{k_2} C \\ B^* &\xrightarrow{k_3} D \xrightarrow{k_4} E^* \xrightarrow{k_5} F \end{aligned}$$

The system is described using the following set of differential equations:

$$\begin{cases} \dfrac{dA}{dt} = -(k_1 + \tau^{-1})A + \tau^{-1}A_0 \\ \dfrac{dB^*}{dt} = -(k_2 + k_3)B^* + k_1 A \\ \dfrac{dC}{dt} = -\tau^{-1}C + k_2 B^* \\ \dfrac{dD}{dt} = -(k_4 + \tau^{-1})D + k_3 B^* \\ \dfrac{dE^*}{dt} = -k_5 E^* + k_4 D \\ \dfrac{dF}{dt} = -\tau^{-1}F + k_5 E^* \end{cases} \tag{3.40}$$

The solutions as function of ω are the following:

$$\tan\left(\varphi_A - \varphi_{A_0}\right) = \omega\left(\tau^{-1} + k_1\right)^{-1} \tag{3.41}$$

$$\tan\left(\varphi_{B^*} - \varphi_A\right) = \omega\left(k_2 + k_3\right)^{-1} \tag{3.42}$$

$$\tan\left(\varphi_C - \varphi_{B^*}\right) = \omega\,\tau \tag{3.43}$$

$$\tan(\varphi_D - \varphi_{B^*}) = \omega\left(\tau^{-1} + k_4\right)^{-1} \tag{3.44}$$

$$\tan(\varphi_{E^*} - \varphi_D) = \omega k_5^{-1} \tag{3.45}$$

$$\tan(\varphi_F - \varphi_{E^*}) = \omega\,\tau \tag{3.46}$$

As expected, the retardations of the compounds ***A*** and ***D*** depend on both, reaction and residence time. The retardation of the intermediates (***B**** and ***E******) and of the end products (***C*** and ***F***) depends only on the reaction rates and only on the residence time, respectively. Due to the consecutive reaction, ***D*** precedes ***C*** in phase. If k_4 approaches zero the two compounds, ***C*** and ***D***, would present the same retardation. If τ approaches zero only Equations 3.42 and 3.45 remain valid, because all other retardations approach zero.

An amazing situation is possible if ***C*** and ***F*** represent the same end product. In this case, in Equations set 3.40 ***F*** disappears and the differential equation for ***C*** is:

$$\frac{dC}{dt} = -\tau^{-1}C + k_2 B^* + k_5 E^* \tag{3.47}$$

that yields the following solution:

$$\tan(\varphi_C - \varphi_{B^*}) = \frac{\omega\,\tau\left(k_2\left(\omega^2 + k_5^2\right)\left(\omega^2\tau^2 + \left(k_4\tau + 1\right)^2\right) + k_3k_4k_5\left(k_4\tau + 2k_5\tau + 1 + k_4k_5\tau^2 - \omega^2\tau^2\right)\right)}{k_2\left(\omega^2 + k_5^2\right)\left(\omega^2\tau^2 + \left(k_4\tau + 1\right)^2\right) + k_3k_4k_5\tau\left(k_5\left(1 + k_4\tau\right) - \omega^2\tau\left(2 + k_4\tau - k_5\tau\right)\right)} \tag{3.48}$$

The signal of ***C*** is obtained from a superposition of two signals, the first is generated from ***B**** and the second from ***D****. The retardation is placed between the two limits. The lower limit is given by $k_3 \approx 0$, where the solution corresponds to Equation 3.43. The upper limit is given by $k_2 \approx 0$, where the solution is obtained from Equation 3.49. This corresponds to the retardation between ***B**** and ***F*** as given in the Equations set 3.40.

$$\tan(\varphi_F - \varphi_{B^*}) = \frac{\omega\left(k_4\tau + 2k_5\tau + 1 + k_4k_5\tau^2 - \omega^2\tau^2\right)}{k_5\left(1 + k_4\tau\right) - \omega^2\tau\left(2 + k_4\tau - k_5\tau\right)} \tag{3.49}$$

In the case of a residence time approaching to zero, Equation 3.48 is mainly dependent on the value of k_2. To show this relationship better, Equation 3.48 is rewritten with new variables (X, Y and Z) and isolating τ.

$$\tan(\varphi_C - \varphi_{B^*}) = \frac{\omega\left(k_2X + Y\right)}{Z}\left(1 - \frac{\frac{X}{Z}}{\frac{X}{Z} + \frac{\tau}{k_2}}\right) \tag{3.50}$$

The new variables X, Y and Z are defined in the Equations set 3.51. The ratio τ/k_2 is very important, because from the residence time indications about k_2 can be drawn directly. If τ approaches zero, the expected retardation approaches zero too. An observed large value of the retardation indicates that k_2 approaches zero, too.

$$\begin{cases} X = \left(\omega^2 + k_5^2\right)\left(\omega^2\tau^2 + \left(k_4\tau + 1\right)^2\right) \\ Y = k_3k_4k_5\left(k_4\tau + 2k_5\tau + 1 + k_4k_5\tau^2 - \omega^2\tau^2\right) \\ Z = k_3k_4k_5\left(k_5\left(1 + k_4\tau\right) - \omega^2\tau\left(2 + k_4\tau - k_5\tau\right)\right) \end{cases} \tag{3.51}$$

3.5 Conclusions

The information potential of the *reactants modulation* technique in FTIR/DRIFT spectroscopy studies of heterogeneous catalysis has been described. The experimental procedure and the selection of the experimental conditions were discussed.

Some simple situations have been worked out to exemplify how this technique can be used to yield kinetic information and hints on reaction pathways. Equations were

derived to show the relationship between the retardation of the concentration waves and the system parameters, such as reaction rate constants and residence time. All these parameters can be calculated from the experiments without the necessity of previously established calibration curves.

This is page 84 !

This page was left intentionally blank !

4. Reaction pathway investigation

4.1 Introduction

In this chapter the modulation concept for the investigation of the reaction pathways is presented. The induced dynamic changes in the concentrations of products, intermediates and reactants were monitored by FTIR spectroscopy in the gas cell. The observed phase retardation $\Delta\varphi$ between the external perturbation of the feed gas and the signals of products, intermediates and reactants was studied depending on the modulation frequency ω.

The methanol synthesis from $CO/CO_2/H_2$ over a commercial $Cu/ZnO/Al_2O_3$ catalyst was selected. Further details on the application of the modulation concept on this system can be found elsewhere [125,126]

Methanol is a key compound in the chemical industry and a suitable energy carrier. It is the precursor of several other widely used chemicals, such as formaldehyde, acetic acid, MMA (methyl-methacrylate), DMT (dimethyl-terephthalate), MTBE (methyl-tertiary-butylether) and chloromethanes.

The application of methanol as fuel is very important. It can either be used in combustion engines, or partially oxidised to yield CO_2 and hydrogen, which is used in fuel cells. Methanol has twice the energy density of liquid hydrogen, but without the storage and transport problems. In the Rio de Janeiro agreements (1992) and Kyoto protocols (1997) the attendees agreed to notably reduce the emission of greenhouse

gases to the atmosphere in the next decade. The methanol synthesis starting from CO_2 appears to be a valid approach to lower the release of this gas to the environment.

Since the introduction of highly selective Cu/ZnO catalysts by ICI in 1960s, the industrial production of methanol is exclusively based on this technology. All currently used catalysts contain copper oxide and zinc oxide with one or more stabilising additives, mainly Al_2O_3 and graphite. In the past years numerous investigations were carried out to clarify the various aspects of the reactions involved in the methanol synthesis, and different views of the mechanism have been proposed [127,128,129,130].

For the investigated system Ovesen *et al.* [131,132,133] and Askgaard *et al.* [134] have demonstrated that the water-gas shift/reverse water-gas shift reactions are taking place via adsorbed CO and CO_2 respectively. The hydrogenation reaction starts from adsorbed CO_2 and leads, via formates and methoxy, to the methanol product.

4.2 Experimental

The used setup consists of the gas dosing system *Modulation Unit*, described in section 2.3.2, which is attached to the μ-reactor/gas cell system (see section 2.5). All spectra were recorded in the rapid scan mode with a resolution of 4 cm^{-1} and an accumulation of 8 to 64 interferograms for the time dependent spectra, and 1024 scans for background spectra. The used FTIR spectrometer is presented in section 2.6.

A commercial CO/CO_2 hydrogenation $Cu/ZnO/Al_2O_3$ catalyst, kindly provided by Haldor Topsøe A/S, was ground, sieved, and placed into the micro reactor. The reactor length was adjusted to minimise the dead volume. The catalyst was activated by reduction in 10%-H_2/N_2 with an overall flow of 2 l_N min^{-1} at 5 bar using the following temperature program: 3 K min^{-1} up to 453 K, and 1 K min^{-1} up to 523 K.

Modulation experiments were performed as follows [106]. The catalyst was activated and held under reaction conditions for approximately 30 minutes, i. e. a continuous flow of N_2 (carrier gas) and reaction gases was passed through the catalyst bed. After recording the background spectrum a modulation experiment was started by varying the inlet mass flow of the reaction gas sinusoidally using the desired modulation frequency and amplitude. Each change in the mass flow was compensated by an inverse change in the carrier gas mass flow to ensure constant pressure and overall mass flow during the experiment. After waiting at least 3 modulation periods to allow for an adjustment of the system to the external perturbation, the recording of the spectra was started.

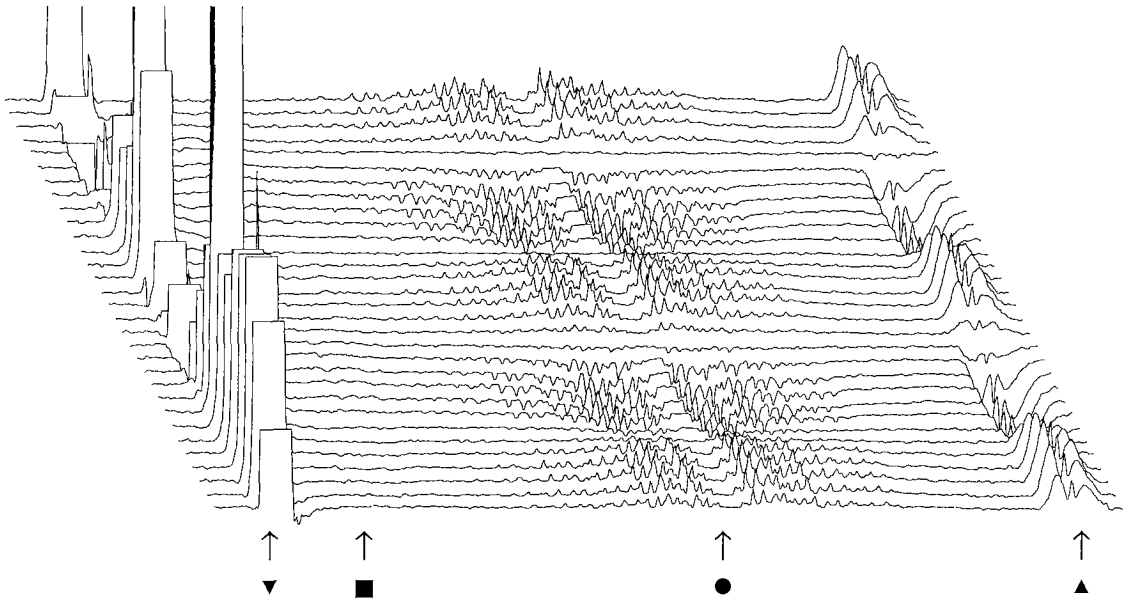

Figure 4-1: CO2 hydrogenation over $Cu/ZnO/Al_2O_3$; stack plot for the H_2 modulation frequency of 1/60 Hz with a time resolution of 4.45 s spectrum^{-1}. The assigned bands are all gas phase signal of: CO_2 (▼) at 2350 cm^{-1}, CO (■) at 2145 cm^{-1}, H_2O (●) at 1597 cm^{-1} and CH_3OH (▲) at 1032 cm^{-1}. In the displayed representation the maximum value of CO_2 was arbitrary set, because the detector is in overflow. Experiment performed at 5 bar and 473 K. Feed composition: CO_2, 0.05 l_N min^{-1}; H_2, 0.39 ± 0.1 l_N min^{-1} and N_2 up to 2 l_N min^{-1}.

In Figure 4-1 a stack plot is shown as example for the obtained spectra (first recorded trace at the top), each trace is recorded within 4.45 seconds. The assigned bands are all gas phase signals of: CO_2 (▼) at 2350 cm^{-1}, CO (■) at 2145 cm^{-1}, H_2O (●) at 1597 cm^{-1} and CH_3OH (▲) at 1032 cm^{-1}. A contour plot of Figure 4-1 is shown in Figure 4-2. The phase shift $\Delta\varphi$ is deduced by plotting the peak area as function of time.

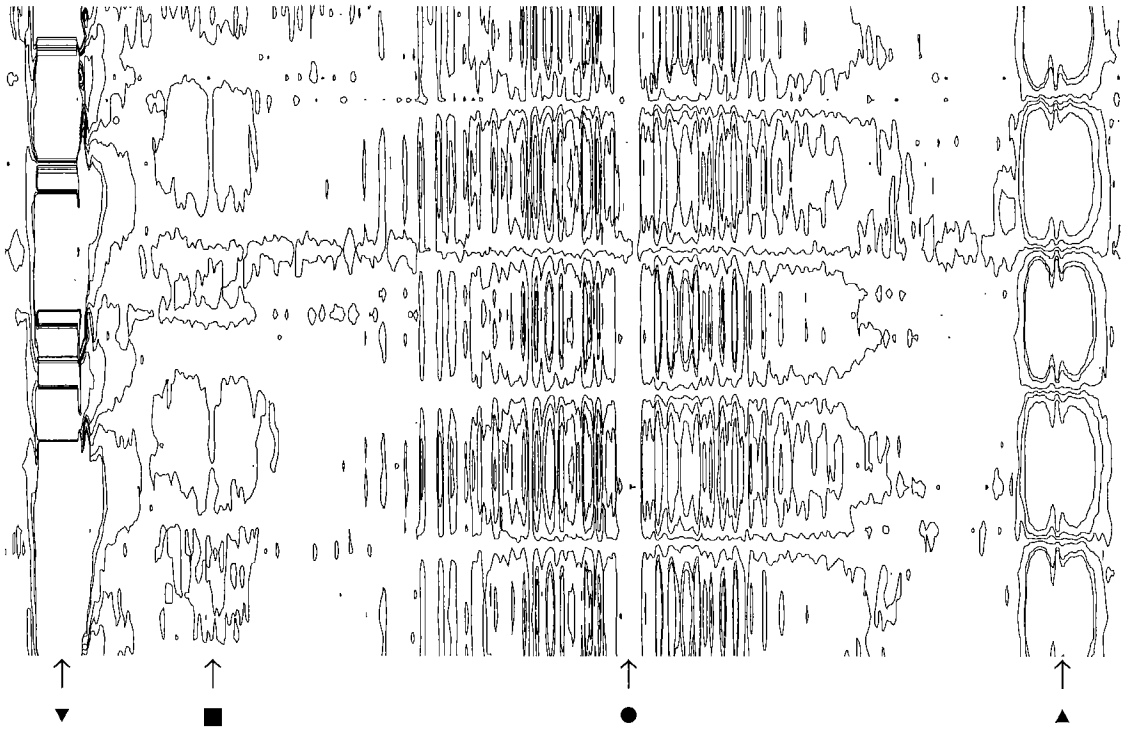

Figure 4-2: Contour plot for the H_2 modulation frequency of 1/60 Hz with a time resolution of 4.45 s $spectra^{-1}$. The assigned bands are all gas phase signal of CO_2 (▼) at 2350 cm^{-1}, CO (■) at 2145 cm^{-1}, H_2O (●) at 1597 cm^{-1} and CH_3OH (▲) at 1032 cm^{-1}. Experiment performed using the same conditions as in Figure 4-1.

A first set of measurements was performed at 5 bar and 473 K with the following feed composition: CO_2, 0.05 ± 0.025 $l_N\ min^{-1}$; H_2, 0.58 $l_N\ min^{-1}$; and N_2, up to 2 $l_N\ min^{-1}$. The second set of measurements was performed at the same pressure and temperature, with a feed composition of H_2, 0.39 ± 0.1 $l_N\ min^{-1}$; CO_2, 0.05 $l_N\ min^{-1}$; and N_2, up to 2 $l_N\ min^{-1}$.

Both, the first and the second set, were performed using different modulation frequencies.

A detailed description of the used compounds can be found in section 2.8.

4.3 Results

The procedure explained in section 3.1 is used for this experiment. In the first step possible models are developed, while in a second step the postulated models are compared to the experimental results. A discussion about the relationship between phase shift and modulation frequency can be found in section 3.4.

4.3.1 Models

In this study only the gas phase species can be detected. In view of this limitation, only one rate limiting step was postulated for the reaction [123]. Three different simplified reaction models with only one derived surface species (#, derived from adsorbed CO_2 respectively CO) are presented. These represent the surface compounds of the rate limiting step of the considered reactions. At this point the chemical nature of the different surface species is no of interest. A detailed microkinetic model for the investigated system can be found elsewhere [133].

4.3.1.1 Model 1: Parallel reactions

In this case all reactions (*R1* and *R2*) are proceeding from the same intermediate. The formation of this surface species is the rate limiting step of the whole reaction. In the case of CO_2 modulation the phase shift has to be equal for all products ($\Delta\varphi(CO) = \Delta\varphi(H_2O) = \Delta\varphi(CH_3OH)$). In the case of H_2 all compounds have the same retardation. The phase retardation of CO_2 presents a supplementary shift of π.

$$CO_2 \rightarrow [\#] \xrightarrow{H_2} CO + H_2O \qquad (R1)$$

$$CO_2 \rightarrow [\#] \xrightarrow{3\,H_2} CH_3OH + H_2O \qquad (R2)$$

4.3.1.2 Model 2: Series reactions

In this model methanol is produced in a second step from adsorbed CO (*R3*).

$$CO_2 \rightarrow [\#] \xrightarrow{H_2} CO + H_2O \qquad (R1)$$

$$CO \rightarrow [\#] \xrightarrow{2\,H_2} CH_3OH \qquad (R3)$$

During CO_2 modulation the phase shift H_2O/CO_2 and CO/CO_2 from the reverse water gas shift reaction should be the same.

However, if CO has to be consumed to obtain methanol, its absolute phase shift must be smaller than the one of H_2O. Methanol is at the end of the reaction sequence; however, if its formation from CO is sufficiently rapid, its phase shift may lie between those of CO and H_2O ($\Delta\varphi(CO) < [\,\Delta\varphi(H_2O)$ or $\Delta\varphi(CH_3OH)\,]$).

During H_2 modulation the phase shifts of CO/H_2, H_2O/H_2 and CH_3OH/H_2 should be monitored together. If CO was consumed to produce methanol, the phase shift CO/H_2 would be smaller and the phase shift CH_3OH/H_2 would be larger than the relative phase shift of H_2O/H_2 ($\Delta\varphi(CO) < \Delta\varphi(H_2O) < \Delta\varphi(CH_3OH)$). The phase shift of CO_2 would present a shift of π with respect to the water signal.

4.3.1.3 Model 3: Series-parallel reactions

Here all three reactions presented so far are assumed to proceed simultaneously.

$$CO_2 \rightarrow [\#] \xrightarrow{H_2} CO + H_2O \qquad (R1)$$

$$CO_2 \rightarrow [\#] \xrightarrow{3\,H_2} CH_3OH + H_2O \qquad (R2)$$

$$CO \rightarrow [\#] \xrightarrow{2\,H_2} CH_3OH \qquad (R3)$$

The case for CO_2 modulation is similar to those of series reactions. The sequence of absolute phase shifts will not be changed: $\Delta\varphi(CO) < [\,\Delta\varphi(H_2O)$ or $\Delta\varphi(CH_3OH)\,]$.

In case of H_2 modulation, one might expect from visual inspection that all products have the same phase shift. However, CO is used to produce methanol, and hence the phase shift CO/H_2 will be smaller and the phase shift CH_3OH/H_2 will be larger. The sequence is again: $\Delta\varphi\,(CO) < \Delta\varphi\,(H_2O) < \Delta\varphi\,(CH_3OH)$, even though at the same time CO_2 is directly reduced to CH_3OH and water. This fact is not influencing the discussed result. The phase shift CH_3OH/H_2 will be similar to the phase shift of H_2O/H_2.

4.3.2 Experimental results

In this section the above presented models are discussed in relation to the observed phase shifts to check the proposed pathways.

4.3.2.1 Modulation of CO_2

In the present system CO_2 modulation induces a modulation of all following reaction steps. As shown in Figure 4-3, the phase shifts H_2O/CO_2 and CH_3OH/CO_2 are not the same. The corresponding curves could be fitted with the phase function of a third order delay term (PT_3), suggesting more than one relevant surface species and/or several reaction pathways leading to the same products [131,132,133,134].

CO is produced first (smallest phase shift) and the curve can be fitted with the phase function of a second order delay term (PT_2), suggesting that only one relevant surface species was involved and that CO is reacting. In any case, even assuming that more surface species are involved in model 1, water should exhibit a phase shift between those of methanol and CO, because it can be produced from both reactions. This could

not be confirmed experimentally. Therefore, model 1 can be rejected; discriminating between model 2 and 3 is not yet possible.

CO is produced first (smallest phase shift) and the curve can be fitted with the phase function of a second order delay term (PT_2), suggesting that only one relevant surface species was involved and that CO is reacting. In any case, even assuming that more surface species are involved in model 1, water should exhibit a phase shift between those of methanol and CO, because it can be produced from both reactions. This could not be confirmed experimentally. Therefore, model 1 can be rejected; discriminating between model 2 and 3 is not yet possible.

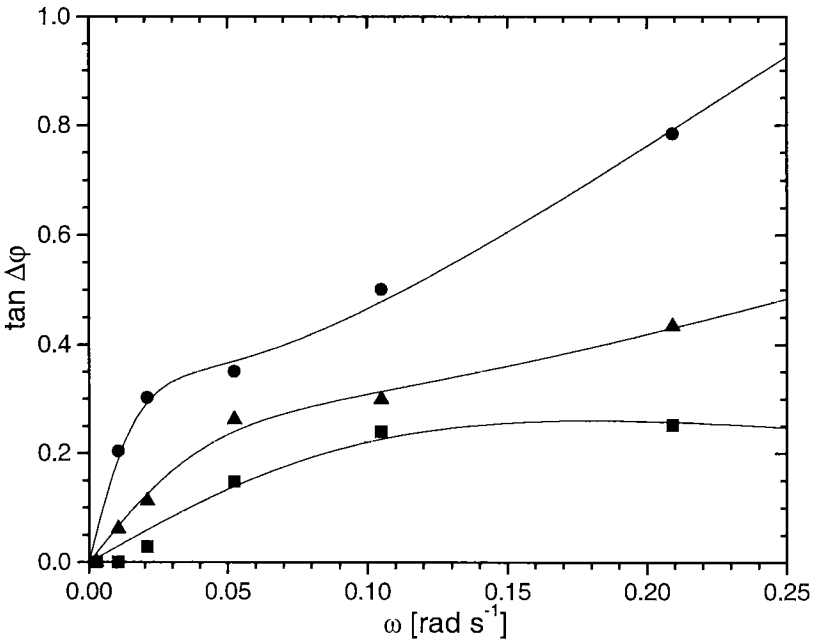

Figure 4-3: Figure 4: Phase shift between CO_2 and H_2O (●), CH_3OH (▲) and CO (■) for CO_2 modulation experiments performed at 5 bar and 473 K. Feed composition: CO_2 0.05 ± 0.025 l_N min^{-1}; H_2 0.58 l_N min^{-1} and N_2 up to 2 l_N min^{-1}.

4.3.2.2 Modulation of H_2

H_2 modulation induces a modulation of several reaction steps simultaneously. In Figure 4-4 the phase shift sequence for the different compounds is shown.

The phase shift between CO and H_2 can be fitted by a straight line (phase function of a first order delay term) indicating that only one relevant surface species is directly reduced to yield CO. This was already suggested by the first experiment. The phase shift of water could be fitted with a phase function of a second order delay term suggesting that more reactions are yielding the same product.

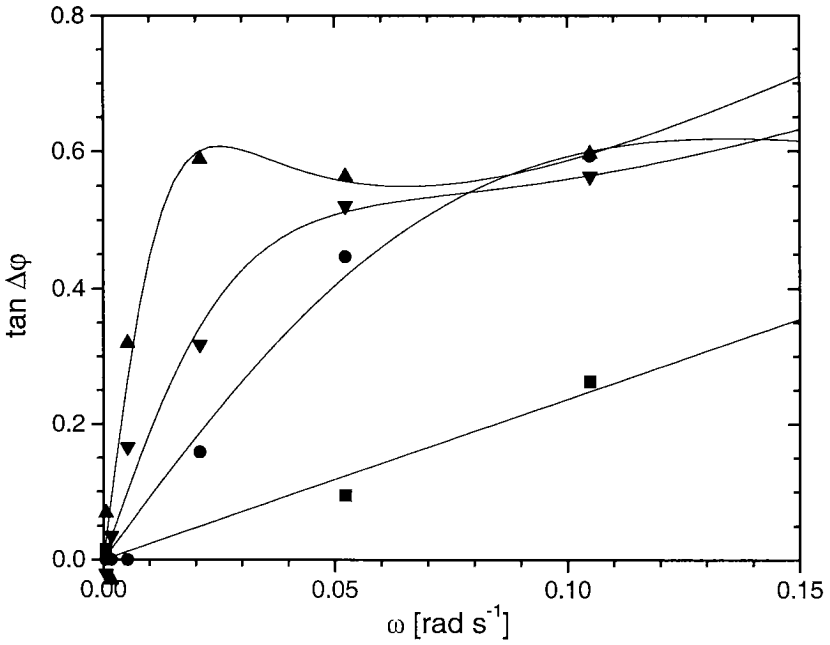

Figure 4-4: Phase shift between H_2 and CH_3OH (▲), CO_2 (▼), H_2O (●) and CO (■) and for H_2 modulation experiments performed at 5 bar and 473 K. Feed composition: CO_2, 0.05 l_N min^{-1}; H_2, 0.39 ± 0.1 l_N min^{-1} and N_2 up to 2 l_N min^{-1}.

The phase shift of methanol corresponds approximately to a phase function of a third order delay term indicating that it can be produced by more than one reaction with

several intermediates. From this information it is already possible to reject model 2 and to select model 3 as the most reasonable among the choices considered.

4.4 Discussion

In the chosen model (3), CO_2 reacts to yield CO via a derived surface species #, and CO can react to yield CH_3OH via the same derived surface species #. This is an alternate way to consider the equilibrium between CO_2 and CO established via the water-gas shift / reverse water-gas shift reactions. The formation of derived surface species # represents the rate limiting step intermediate in the hydrogenation of CO to methanol. If CO was directly converted to CH_3OH the retardation of CO_2 in Figure 4-4 would be smaller than the relative phase shift of CO. Hence, it is possible to conclude that CO and CO_2 are in equilibrium and that the reaction of CO to methanol occurs via CO_2.

This is in agreement with the microkinetic model that has been proposed for $Cu/ZnO/Al_2O_3$ catalysts [131,132,133,134], in which CO and CO_2 are in equilibrium via the water-gas shift reaction. The oxidation of adsorbed CO to adsorbed CO_2 is the rate limiting step of this latter equilibrium.

The considered model (3) assumes that carbon dioxide reacts to methanol via a surface species ($\#_{CO_2}$) derived from CO_2, where the rate limiting step is the reduction of this species.

This is also in agreement with the previously mentioned microkinetic model in which adsorbed CO_2 is hydrogenated to methanol via formates, and methoxy species [131,132,133,134]. The formation of methoxy is the rate limiting step.

The experimental results are sufficient to create a simplified model for this system. An extended version of model 3, including more surface species, has to be developed to understand the reaction pathway in more detail.

4.5 Conclusions

The periodic modulations of reactant concentrations were used to induce time dependent changes in the FTIR signals of reactant, intermediate, and products. These were monitored to obtain information on the reaction pathway of methanol synthesis over $Cu/ZnO/Al_2O_3$, where a series-parallel model was found to be most appropriate. This proofs the validity of the modulation concept in heterogeneous catalysis as monitored by FTIR.

This is page 96 !

This page was left intentionally blank !

5. Reaction rate constants investigation

5.1 Introduction

In this chapter the application of the modulation concept for studies of the reaction rate constant of solid-state catalysed reactions is presented. The dynamic variations in the concentrations of products, intermediates and reactants are monitored *in situ* in a DRIFT cell. The observed phase shift ($\Delta\varphi$) is examined depending on the modulation frequency ω. This is used to derive the rate constants, characterising the single reaction steps, and reaction orders. The repetition of experiments at different temperatures makes it possible to calculate the temperature dependent constants.

The CO oxidation over a $Pd_{25}Zr_{75}$ based catalyst is studied in detail. Further details on the application of the modulation concept on this system can be found elsewhere [106,135].

Generally, the oxidation of carbon monoxide to CO_2 by oxygen is an efficient method to remove highly diluted CO from gases. This is of practical importance for the treatment of exhaust gases of internal combustion engines. The current state of technology of fuel cells operating with the reformate gas of liquid fuel, e. g. gasoline and methanol, demands high purity CO-free feed gases, because carbon monoxide acts as poison for the electrocatalyst of the polymer electrolytes. The selective oxidation of CO in the H_2 containing reformate is a suitable procedure.

The kinetics of the CO oxidation over Pd (or Pt) based catalysts exhibits a multifaceted behaviour. Three characteristic regimes of the reaction rate can be distinguished. With

increasing CO partial pressure the reaction rate increases first linearly with CO partial pressure, then an oscillating behaviour follows, and finally a quenched reaction state is reached [136], in which the apparent order with respect to CO is negative.

A corresponding behaviour is reported for the reaction rate as a function of temperature. While at low temperatures the reaction rate is of negative order for CO, it passes through a range of oscillations with increasing temperature, and finally exhibits a linear increase with CO partial pressure at high temperatures [137]. Evidence for a Langmuir-Hinshelwood mechanism for the reaction on metal surface was reported by different authors [106,138,139,140,141]. The oscillating behaviour of the reaction rate onto Pd and Pt was intensively investigated [136,137,142,143,144,145,146].

The properties of the used PdZr catalyst have been investigated and discussed in detail by Baiker *et al.* [147,148,149,150], Ladas *et al.* [142], and Barnickel *et al.* [151]. It was found that oxygen atoms adsorb on the substochiometric zirconia (ZrO_{2-x}), whereas CO molecules adsorb and are consecutively oxidised on the surface of the palladium component. In a previous work on the same catalyst [125], the band at 2056 cm^{-1} was assigned to CO linearly bound to Pd [151,152].

5.2 Experimental

The used setup consists of the gas dosing system *Modulation Unit* (see section 2.3.2) attached to the DRIFT cell presented in section 2.4.2. The whole setup is controlled using the program presented in section 2.2. The FTIR spectrometer is described in section 2.6. All spectra were recorded in the rapid scan mode with a resolution of 4 cm^{-1}. For transient measurements 8 to 32 interferograms per spectra and 1024 scans for the background spectra were accumulated.

The amorphous $Pd_{25}Zr_{75}$ alloy catalyst for CO oxidation was prepared by the melt spinning technique [153]. A given amount (0.306 g) of catalyst was placed in the DRIFT sample cup and packed with a stamp using a pressure of 1 MPa to ensure reproducibility [31].

The experiments were performed as follows. In a first step the dead time between the gas dosing system (the mixing of the feed gas) and the cell was estimated with step up/step down experiments (see paragraph 3.3.4.1). In a second step the modulation experiments were started. To monitor the influence of the temperature on the reaction, the experiment was repeated applying different temperatures. The changes of concentrations in step up/step down and modulation experiments have the same order of magnitude.

Step up/step down and modulation experiments were performed as follows. Once the catalyst was activated [147-151], it was held under constant reaction conditions for at least 30 minutes, i. e. a continuous flow of N_2 (carrier gas) and reactants passed through the catalyst bed. After recording the background spectrum, the experiment was started. For this purpose, the inlet mass flow of the reactants was altered in one step by the desired amplitude. Simultaneously to each change in the reactant gas mass flow, the carrier gas mass flow was compensated by the inverse amount to ensure constant pressure and overall mass flow. Simultaneously, the recording of the spectra was started.

For each size of change two to four sets of spectra, containing up to 40 spectra each, were collected. The dead time between the gas dosing system and the cell was determined by plotting the peak area of the modulation gas (CO or CO_2) as function of time. The mean value of several measurements was used to reduce the error.

Before starting a modulation experiment, as previously described [106,125,135], the system was held under the same constant initial conditions for at least 30 minutes. A new background spectrum was collected, and the modulation experiment was started.

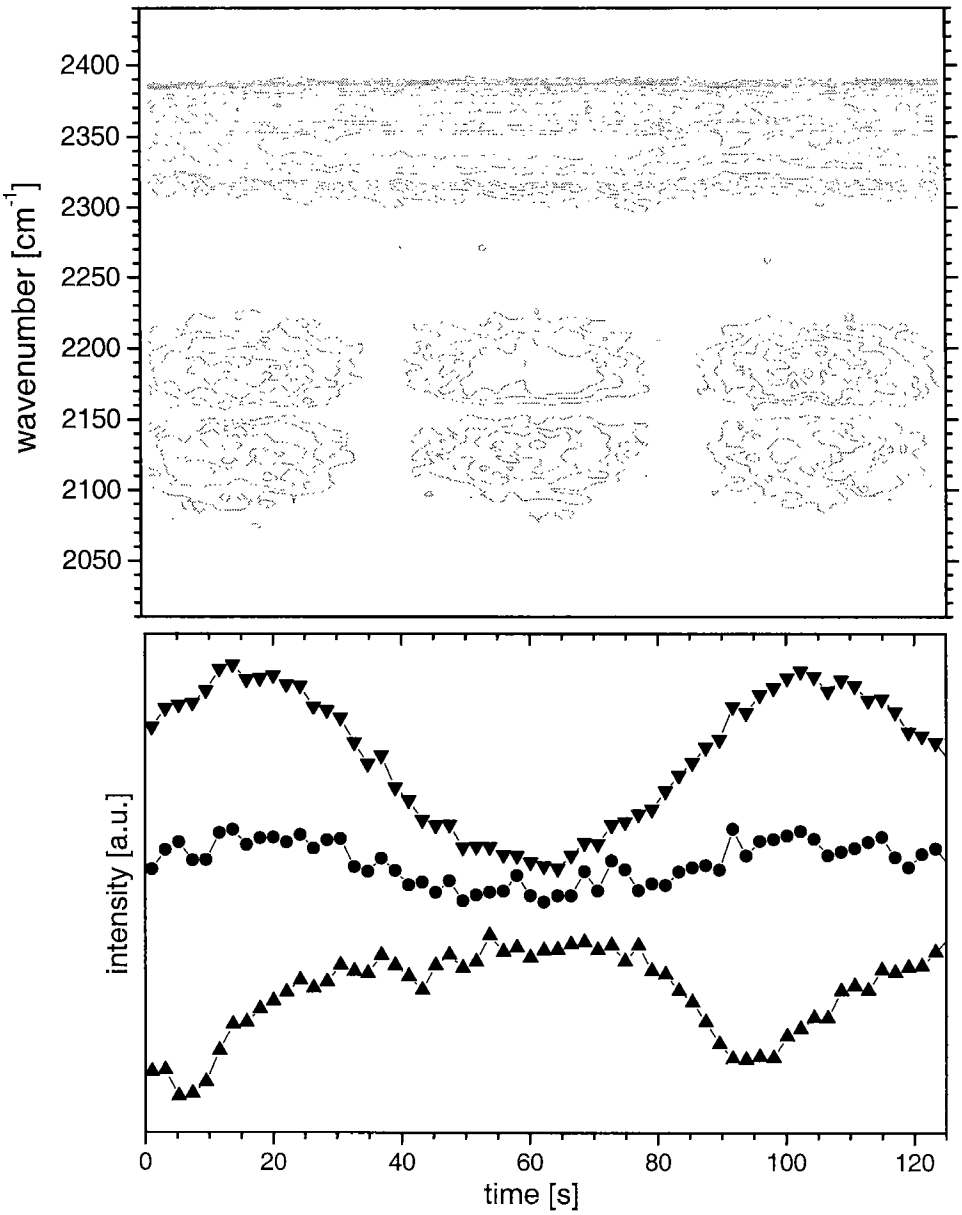

Figure 5-1: CO oxidation experiment with modulated reactant concentration. **Top:** contour plot of CO modulation experiment performed at a frequency of 1/90 Hz, with a time resolution of 4.45 s per spectrum. The assigned bands are the signals of CO_2 at 2350 cm^{-1}, CO at 2145 cm^{-1}, and CO_{ad} at 2056 cm^{-1}. **Bottom:** time dependence of peak areas of CO (▼), CO_{ad} (●) (magnified by factor 5) and CO_2 (▲) for the same modulation frequency of 1/90 Hz. The experiment was performed at 4 bar and 353 K. Feed composition: O_2, 0.01 l_N min^{-1}; 10%-CO/N_2, 0.02 ± 0.01 l_N min^{-1} and N_2 up to 0.08 l_N min^{-1}.

The concentration of the feed gas was sinusoidally varied by the desired modulation frequency and amplitude, ensuring again constant pressure and overall mass flow conditions. The recording of the spectra was started at the beginning of the modulation period. Four to five sets of spectra with the same frequency and amplitude were subsequently collected. Of these sets the first two were always rejected, because they contained the initial adjustment of the system to the external perturbation.

In Figure 5-1 (top) a contour plot is shown as example for the obtained sets of spectra (first recorded trace at the left), each trace being recorded within 4.45 seconds. The phase shift $\Delta\varphi$ is deduced by plotting the peak area as function of time, the latter corrected for the measured dead time.

To reduce the error, a mean value was calculated from each measured set of data. In Figure 5-1 (bottom) an example for the peak area evolution for the CO oxidation is shown. In the lowest trace (▲), the curve does not exhibit the expected sinusoidal behaviour. In such a case, the phase shift was instead obtained from the maxima and minima of the time-dependent intensities.

The assigned bands in Figure 5-1 (top) are the signals of: CO_2 (▲) at 2350 cm^{-1}, CO (▼) at 2145 cm^{-1}, and CO_{ad} (●) at 2056 cm^{-1}. The used integration limits are follow: CO_2: 2400-2280 cm^{-1} and 3800-3550 cm^{-1} for the first overtone; CO: 2270-2075 cm^{-1}; and CO_{ad}: 2075-1950 cm^{-1}.

All experiments were performed at a total pressure of 4 bar and at temperatures of 298 K, 326 K, 353 K, 381 K, 408 K, and 436 K. The following feed gas composition were used to investigate the questions listed below.

1. Interaction of CO with the catalyst: 10%-CO/N_2, 0.02 ± 0.01 l_N min^{-1}.

2. Interaction of CO_2 with the catalyst: CO_2, 0.05 ± 0.02 l_N min^{-1}.

3. Effect of CO in the CO oxidation reaction: 10%-CO/N_2, 0.02 $\pm$ 0.01 $l_N\,min^{-1}$; O_2, 0.01 $l_N\,min^{-1}$.

4. Effect of O_2 in the CO oxidation reaction: O_2, 0.02 $\pm$ 0.01 $l_N\,min^{-1}$; 10%-CO/N_2, 0.04 $l_N\,min^{-1}$.

Nitrogen was used as carrier and compensation gas. The overall flow was always set to 0.08 $l_N\,min^{-1}$.

Catalytic reference runs under steady state condition were performed using: 10%-CO/N_2, 0.02 $l_N\,min^{-1}$; O_2, 0.01 $l_N\,min^{-1}$. After dilution in N_2 the gases were analysed by means of a Siemens IR CO/CO_2 analyser (see section 2.7).

5.3 Results and discussion

As explained in chapter 3, the interpretation of the experimental results (phase shifts $\Delta\varphi$ or $\tan[\Delta\varphi]$) of an unknown system as a function of a perturbation (modulation frequency ω) to obtain information about its characteristics is an established method in many engineering disciplines. A set of differential equation describing the investigated system is used to obtain the relationships between observed retardation ($\tan[\Delta\varphi]$) and the data characterising the considered reaction steps (see section 3.4). From the temperature dependence, additional thermodynamic parameters of the reactions are determined.

The oxidation of CO can be described by the following microkinetic model: adsorption of CO, adsorption and dissociation of oxygen, reaction between the two surface species to form adsorbed CO_2, and finally, desorption of CO_2. For each of these steps the reverse reaction must be considered. The single steps are separately analysed, so that kinetical data of each step can be estimated. By doing so, it is possible to assess the validity of the entire microkinetic model.

5.3.1 Interaction of CO with the catalyst

5.3.1.1 Model

A modulation experiment was carried out to estimate the interaction of CO with the catalyst surface. Assuming that, for low partial pressures, the surface concentration of vacant CO adsorption sites is constant, the following simple model can be derived (see paragraph 3.4.2.1):

$$CO \underset{k_{-1}}{\overset{k_1}{\rightleftharpoons}} CO_{ad}$$

Here, k_1 and k_{-1} are effective first order rate constants. As explained in section 3.3.2 the DRIFT cell can be represented by a continuous stirred tank reactor with residence time τ. With these assumptions the system can be described with the following set of differential equations:

$$\frac{dCO}{dt} = \frac{CO_0}{\tau} - (k_1 + \frac{1}{\tau})\, CO + k_{-1} CO_{ad} \qquad (5.1)$$

$$\frac{dCO_{ad}}{dt} = k_1 CO - k_{-1} CO_{ad} \qquad (5.2)$$

where CO_0 represents the CO concentration in the feed gas, CO the concentration of carbon monoxide in the DRIFT cell, and CO_{ad} the concentration of the adsorbed species. Solving the system of differential equations for CO and CO_{ad} one obtains equations that are function of ω and ω^2 (see Equation 3.28). As explained in paragraph 3.4.2.1, ω^2 terms play a role only when high frequencies are applied, it was hence decided to employ the low frequency approximation. In this way a linearity between $\tan[\Delta\varphi]$ and the perturbation frequency is obtained:

$$\tan\ [\varphi(CO_0) - \varphi(CO)] = \omega\,\tau\,(1 + \frac{k_1}{k_{-1}}) \tag{5.3}$$

$$\tan\ [\varphi(CO) - \varphi(CO_{ad})] = \frac{\omega}{k_{-1}} \tag{5.4}$$

Note that in Equation 5.3 an equilibrium constant k_1/k_{-1} appears, rather than an individual rate constant. The temperature dependence of the residence time and of the rate constants was estimated as explained in section 3.3.2. The temperature dependence of the residence time (τ) was modelled using the ideal gas law (see Equation 3.8), and the obtained approximation is presented in Equation 3.9. For the rate constants k_1 and k_{-1}, the Arrhenius Equation was used. The pre-exponential factor k_0 was assumed to be temperature independent.

$$\tau(T) = \frac{k_\tau}{T} \tag{3.9}$$

$$k(T) = k_0 e^{-\frac{E_A}{RT}} \tag{3.10}$$

The equilibrium constant $K(T)$ of the reaction can be easily derived from Equation 3.10:

$$K(T) = \frac{k_1}{k_{-1}} = K_0 e^{-\frac{\Delta E_A}{RT}} \tag{5.5}$$

Here ΔE_A is the difference of the Arrhenius activation energies between the adsorption and desorption process. The sign of ΔE_A indicates which side of the equilibrium the process prefers.

5.3.1.2 Experimental results

An example for the evolution of the phase shifts as a function of the modulation frequency is illustrated in Figure 5-2. The lower curve (▽) displays tan[$\Delta\varphi$(CO_0-CO)]

for the lowest temperature (298 K) used and the upper curve (▲) shows tan[$\Delta\varphi(CO_0\text{-}CO)$] for the highest temperature (436 K).

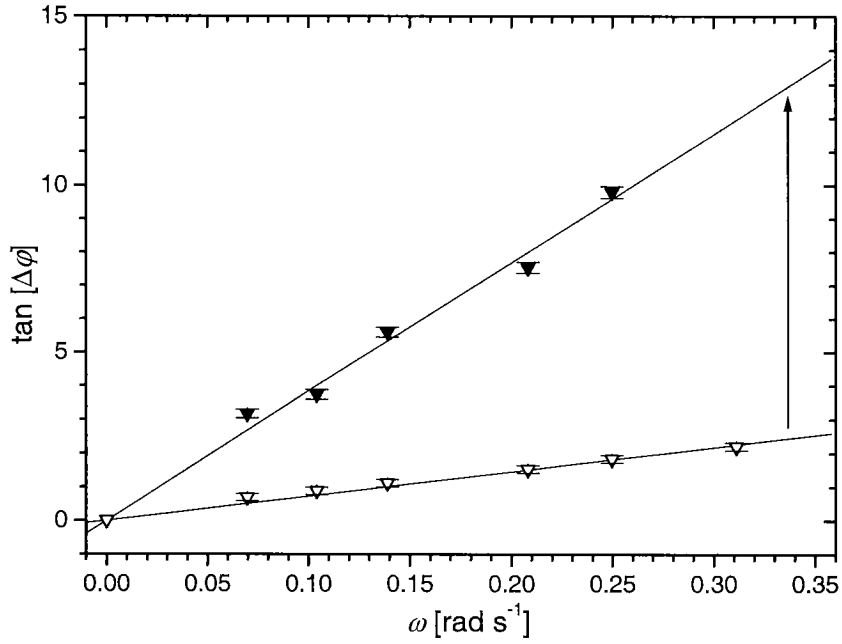

Figure 5-2: Phase shifts from CO adsorption experiment. Top: variation of tan[$\Delta\varphi(CO_0\text{-}CO)$] as function of ω for the lowest (298 K: ▽) and for the highest (436 K: ▼) temperature. The measurements were performed at 4 bar with a feed composition of 10%-CO/N_2, 0.02 ± 0.01 l_N min^{-1} and N_2 up to 0.08 l_N min^{-1}.

The arrow indicates the direction of change of the slope caused by increasing the temperature. As expected, the phase shifts can be approximated by straight lines with zero crossing. Information about the equilibrium and the residence time can be obtained from the slopes. The evolution of this value as function of the temperature is shown in Figure 5-3 (axis on the left side).

Interestingly we observe that the slope increases with rising temperature, indicating a shift of the equilibrium towards the adsorbed species. The curve can be approximated using Equation 5.3 together with Equations 3.9 and 5.5. The obtained values are:

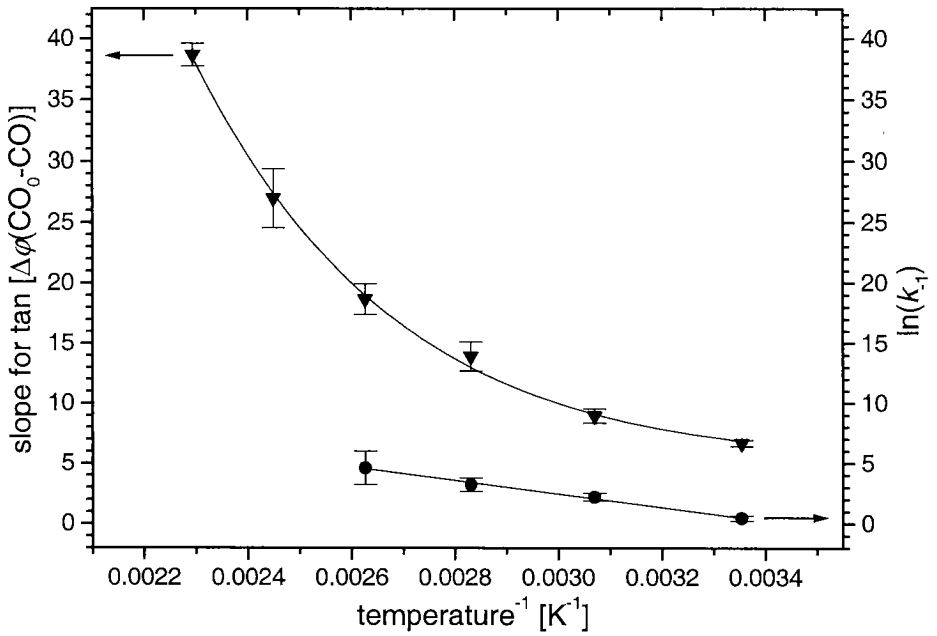

Figure 5-3: Left: Variation of the slopes for tan[$\Delta\varphi$(CO_0-CO)] (▼) as function of temperature. The curve was modelled using Equation 5.3, with Equations 3.9 and 5.5. **Right:** Arrhenius plot for the variation of the slopes of tan[$\Delta\varphi$(CO-CO_{ad})] (●) with the temperature. The curve was modelled using Equations 5.4 and 3.10. Experimental conditions as in Figure 5-2.

k_τ = 1'331 ± 267 K s $\quad$ $K_{0,1}$ = 8'841 ± 2'018 $\quad$ $\Delta E_{A,1}$ = 24.1 ± 1.4 kJ mol^{-1}

The equilibrium is characterised by $K_{0,1}$ and $\Delta E_{A,1}$, and the geometry of the reactor by k_τ. $\Delta E_{A,1}$ is positive indicating that the adsorption reaction is energy consuming. This result agrees with the observation that CO_{ad} exists spectroscopically only in the presence of gas phase CO (data not shown).

The phase shift evolution between CO and CO_{ad} provides information about the reverse reaction. The slopes obtained from the phase shifts decrease with increasing temperature. This indicates an enhanced desorption at higher temperatures. For an Arrhenius plot, Equation 3.10 was inserted into Equation 5.4 and solved for ln(k_{-1}). The experimental data for the slopes of tan[$\Delta\varphi$(CO-CO_{ad})] were analysed according to this

new equation. The temperature dependence of $\ln(k_{-1})$ is shown in Figure 5-3 (axis on the right side), from which $E_{A,-1}$ and $k_{0,-1}$ are simply estimated. The obtained values are:

$$k_{0,-1} = 1.95 \cdot 10^{8} \pm 1.81 \cdot 10^{8}\ s^{-1} \qquad E_{A,-1} = 46.1 \pm 2.6\ kJ\ mol^{-1}$$

In Figure 5-3, only the four lowest temperatures are plotted, because at high temperatures the amplitude of the variation of the concentration was not large enough to define the phase shift within an acceptable error. Even for the used values the error is already quite high for $k_{0,-1}$.

Approximated values for the Arrhenius energy and pre-exponential factor of the adsorption reaction, $E_{A,1}$ and $k_{0,1}$ respectively, can be derived from the numbers given above:

$$k_{0,1} = 1.72 \cdot 10^{12} \pm 1.64 \cdot 10^{12}\ s^{-1} \qquad E_{A,1} = 70.2 \pm 3.0\ kJ\ mol^{-1}$$

The obtained pre-exponential factor shows a relatively high error due to the uncertainty of $k_{0,-1}$. These apparent standard deviations of the pre-exponential values ($k_{0,1}$, $k_{0,-1}$) can be traced back to the assumption that k_0 is temperature independent. The obtained values should serve only as a hint for the adsorption/desorption reaction rates.

As a reference it is noteworthy that the activation energy for the desorption ($E_{A,des}$) of singly bound CO on pure Pd was estimated to be 56.4 kJ mol^{-1} [146].

5.3.2 Interaction of CO_2 with the catalyst

5.3.2.1 Model

As described above for CO, also in this experiment the interaction of a reactant gas (CO_2) with the catalyst surface was investigated (see paragraph 3.4.2.1). Under the used conditions no adsorbed CO_2 ($CO_{2,ad}$), neither reaction products like CO_{ad} nor

carbonates, were observed. However this does not exclude the existence of these species on the surface at a concentration below the detection limit of DRIFT. Therefore, it is not possible to exclude that, applying different reaction conditions, CO_2 could be adsorbed and dissociated, e. g., into CO_{ad} and adsorbed oxygen (O_{ad}). Hints about a similar reaction were already found by Nijhuis *et al.* [154] for CO_2 adsorption on Pt using a TAP reactor system.

The used model considers that a possible adsorption/desorption reaction can take place. Like in the case of CO, it was assumed that, during the experiment, the surface concentration of vacant CO_2 adsorption sites is constant. The simplified model can be written as:

$$CO_2 \underset{k_{-3}}{\overset{k_3}{\rightleftharpoons}} CO_{2,ad}$$

Like above, the same presumptions are valid in this case: a) k_3 and k_{-3} are effective first order rate constants, and b) the DRIFT cell can be represented by a continuous stirred tank reactor with residence time τ. With these assumptions, we can describe the system only by using Equation 5.1, where, however, CO should be substituted with CO_2, k_1 with k_3 and k_{-1} with k_{-3}. Equation 5.2 can not be applied, because a matching surface species was not observed. With the same considerations as in the previous section for CO, we can write:

$$\tan\,[\Delta\varphi(CO_{2,0} - CO_2)] = \omega\,\tau\,(1+\frac{k_3}{k_{-3}}) \qquad (5.6)$$

where $CO_{2,0}$ represents the gas phase concentration of carbon dioxide in the feed gas and CO_2 in the DRIFT cell. Also like in Equation 5.3, Equation 5.6 approximates an equilibrium constant. The evolution of τ is approximated with Equation 3.9 and the equilibrium constant with Equation 5.5.

5.3.2.2 Experimental results

Due to the high concentration of CO_2 in the gas phase, its concentration was derived from the peak area of the first overtone. An example for the evolution of the phase shifts as function of the modulation frequencies is illustrated in Figure 5-4.

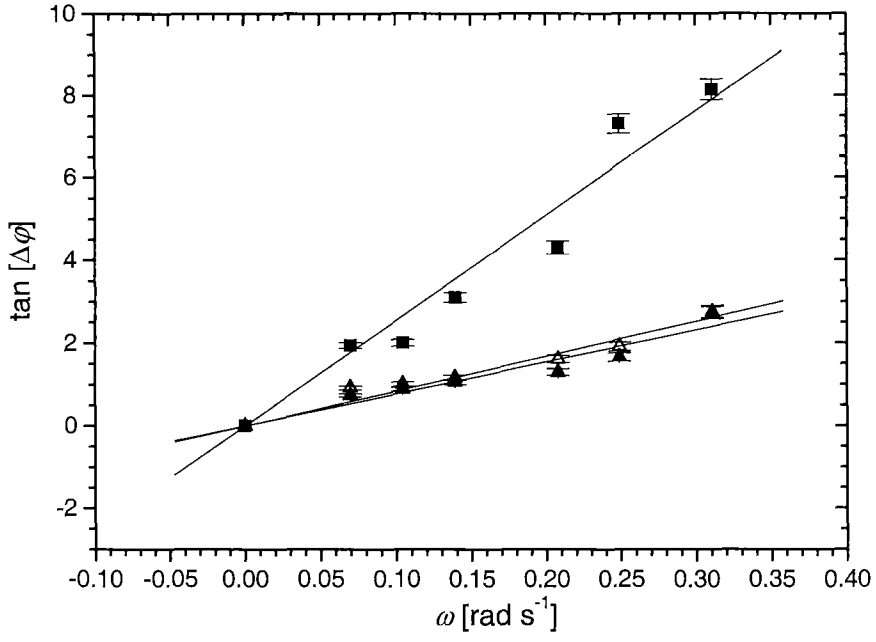

Figure 5-4: Phase shifts from CO_2 adsorption experiment: variation of $\tan[\Delta\varphi(CO_{2,0}\text{-}CO_2)]$ as function of ω for the lowest (298 K: △), for a medium (381 K: ■), and for the highest (436 K: ▲) temperature. The measurements were performed at 4 bar with a feed composition of CO_2, 0.05 ± 0.02 l_N min^{-1} and N_2 up to 0.08 l_N min^{-1}.

Open triangles (△) display the frequency dependence of $\tan[\Delta\varphi(CO_{2,0}\text{-}CO_2)]$ found for the lowest applied temperature (298 K), and filled triangles (▲) for the highest used temperature (436 K). Interestingly, the highest slope is exhibited by the curve marked with ■ (381 K). As expected, the phase shifts can be approximated by straight lines with zero crossing. The slopes thus obtained contain information about the equilibrium and the residence time. The evolution of this value as function of temperature is shown in Figure 5-5.

Interestingly, with increasing temperature, the slope increases first to a maximum and consequently decreases rapidly. This suggests that first, with increasing temperature, the equilibrium shifts towards the side of the adsorbed species.

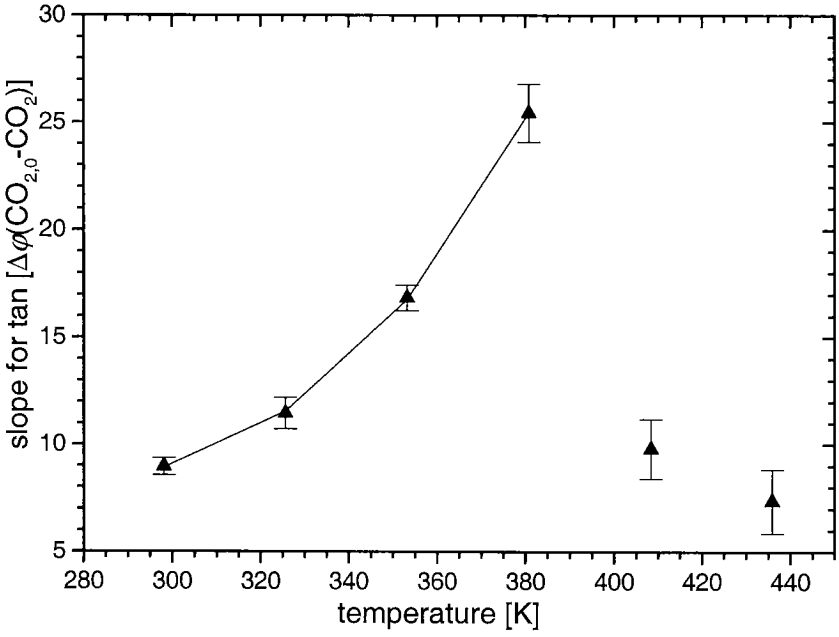

Figure 5-5: Phase shifts from CO_2 adsorption experiment: variation of the slopes for tan[$\Delta\varphi(CO_{2,0}$-$CO_2)$] (▲) as function of the temperature. The curve was modelled using Equation 5.6, with Equations 3.9 and 5.5. Experimental conditions as in the Figure 5-4.

Using temperatures above 380 K the desorption reaction is predominant. This also suggests that a change in the type of the adsorption/desorption process should be considered. In the present work spectroscopic evidence of a massive decomposition was not found. However, the evolution of the slope does suggest the existence of a decomposition reaction, because in the case of a pure adsorption/desorption process one would expect a monotone temperature dependence.

In absence of spectroscopic evidence of one or more adsorbed species and of their phase shifts evolution, the result of this experiment must be considered only as a hint for the

possible existence of a dissociative reaction. For the points at low temperature, the curve was fitted with Equation 3.9 and 5.5 inserted into Equation 5.6. The obtained values are:

$k_\tau = 1'926 \pm 90$ K s $\qquad K_{0,3} = 20'232 \pm 4'404 \qquad \Delta E_{A,3} = 27.0 \pm 0.8$ kJ mol^{-1}

Also in this case, $K_{0,3}$ and $\Delta E_{A,3}$ are the values characterising the equilibrium of the adsorption reaction and k_τ the geometry of the reactor. From the above arguments, it is clear that the equilibrium values ($K_{0,3}$ and $\Delta E_{A,3}$) are not likely to correspond to a molecular level reaction. $\Delta E_{A,3}$ is positive indicating an energy consuming adsorption reaction and consequently the equilibrium is biased towards the gas phase side.

5.3.3 Effect of CO in the CO oxidation reaction

5.3.3.1 Model

The aim of this experiment was to assess the reaction constants of the chosen kinetic model for the CO oxidation over the $Pd_{25}Zr_{75}$ catalyst. A previous modulation experiment using the same catalyst had demonstrated the validity of the Langmuir-Hinshelwood reaction mechanism [106]. Previously, other authors have demonstrated that there are different adsorption sites for CO and oxygen [151] and that a significant amount of oxygen is stored in the active catalyst [149]. With this information, and using O_2 in excess we assume that the concentration of O_{ad} is constant. As already assumed before, the concentration of the vacant CO adsorption sites is considered to be constant. Therefore, the model can be written as:

$$CO \underset{k_{-1}}{\overset{k_1}{\rightleftharpoons}} CO_{ad} \underset{k_{-2}}{\overset{k_2}{\rightleftharpoons}} CO_{2,ad} \underset{k_3}{\overset{k_{-3}}{\rightleftharpoons}} CO_2$$

To further simplify the model, the following hypotheses are made.

(1) Excess of oxygen allows to assume a saturation of O_{ad} on the surface. As a consequence the rate constant of the CO_{ad} oxidation process is faster than its back reaction ($k_2 >> k_{-2}$).

(2) As discussed in paragraph 5.3.2.2, the positive value of $\Delta E_{A,3}$ suggests that the equilibrium of the CO_2 adsorption is shifted to the side of the gas phase. Therefore, we can assume a very small CO_2 adsorption rate as compared to the desorption rate ($k_{-3} >> k_3$).

(3) As a further consequence, the desorption rate of $CO_{2,ad}$ should be much faster than the oxidation rate of CO_{ad} ($k_{-3} >> k_2$).

The two steps from CO_{ad} to gaseous CO_2 may hence be combined into one, and the four reactions (characterised by constants k_2, k_{-2}, k_{-3} and k_3) are replaced by a single one-side reaction, with rate constant k_2'. This simplification appears adequate in view of the fact that $CO_{2,ad}$ was not observed spectroscopically.

(4) Assuming that a single reaction step is rate limiting, the constants k_1 and k_{-1} of the CO adsorption/desorption process can be replaced with a net reaction constant k_1'. This constant describes the overall process as CO_{ad} production. If the CO adsorption step is rate limiting, k_1' represents a rate constant. If the CO_{ad} oxidation is rate limiting, k_1' measures the net production rate of CO_{ad} from gaseous CO.

Thus the following simple model was obtained:

$$CO \xrightarrow{k_1'} CO_{ad} \xrightarrow{k_2'} CO_2$$

Additional information about similar system can be found in paragraph 3.4.2.2. Here k_1' and k_2' are effective first order rate constants. The DRIFT cell is again represented as a continuous stirred tank reactor. Consequently, we can describe this system by the following set of differential equations:

$$\frac{dCO}{dt} = \frac{CO_0}{\tau} - (k'_1 + \frac{1}{\tau})\, CO \tag{5.7}$$

$$\frac{dCO_{ad}}{dt} = k'_1\, CO - k'_2\, CO_{ad} \tag{5.8}$$

$$\frac{dCO_2}{dt} = k'_2\, CO_{ad} - \frac{CO_2}{\tau} \tag{5.9}$$

where CO_0 represents the CO concentration in the feed gas, CO_{ad} the concentration of CO on the surface, and CO the gas concentration right above the catalytic surface. Solving this system for CO, CO_{ad} and CO_2 the phase shifts can be written as:

$$\tan\ [\Delta\varphi(CO_0 - CO)] = \omega \frac{\tau}{1 + k'_1\, \tau} \tag{5.10}$$

$$\tan\ [\Delta\varphi(CO - CO_{ad})] = \omega \frac{1}{k'_2} \tag{5.11}$$

$$\tan\ [\Delta\varphi(CO_{ad} - CO_2)] = \omega\, \tau \tag{5.12}$$

In analogy to Equation 5.4, Equations 5.10 and 5.11 contain information on the rate constants. The temperature dependence of the residence time is approximated with Equation 3.9, and those of the rate constants with Equation 3.10.

The conversion at steady state is estimated from the phase shifts. Solving Equation 5.7 for CO/CO_0 we obtain, after substitution with Equations 5.10 and 5.12:

$$\frac{CO}{CO_0} = \frac{1}{1 + k'_1\, \tau} = \omega \frac{\tau}{1 + k'_1\, \tau} \frac{1}{\omega\, \tau} \equiv \frac{\text{Slope of } \tan\ [\Delta\varphi\,(CO_0 - CO)]}{\text{Slope of } \tan\ [\Delta\varphi\,(CO_{ad} - CO_2)]} \tag{5.13}$$

5.3.3.2 Experimental results

In Figure 5-1 an example for the evolution of the different species (CO, CO_{ad} and CO_2) during a modulation experiment has been displayed. In Figure 5-6 the tangent of the phase shifts for different modulation frequencies and for temperatures of 298 K and 436 K, respectively are illustrated. All the phase shifts were approximated by straight lines with zero crossing.

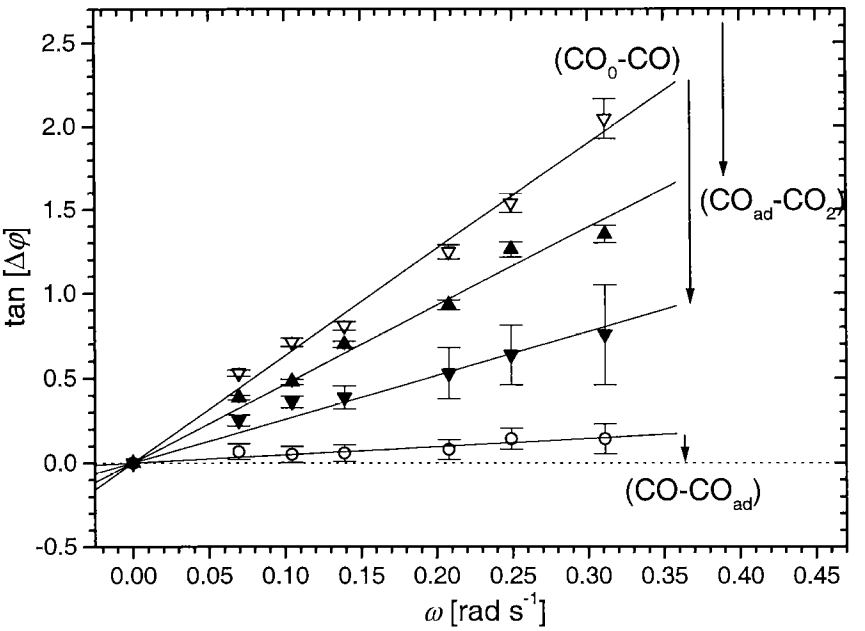

Figure 5-6: Phase shifts from CO oxidation experiment. Variation of tan[$\Delta\varphi$] for the different reaction steps as function of ω for the lowest (298 K) and for the highest (436 K) temperature. Tan[$\Delta\varphi(CO_0\text{-}CO)$] (298 K: ▽; 436 K: ▼); tan[$\Delta\varphi(CO\text{-}CO_{ad})$] (298 K: ○); tan[$\Delta\varphi(CO_{ad}\text{-}CO_2)$] (436 K: ▲). The measurements were performed at 4 bar with a feed composition of 10%-CO/N_2, 0.02 $\pm$0.01 $l_N\,min^{-1}$; O_2, 0.01 $l_N\,min^{-1}$ and N_2 up to 0.08 $l_N\,min^{-1}$.

The arrows indicate the direction of changes of the slopes caused by increasing the temperature. At low temperatures a phase shift of CO_2 was not detectable. For the highest temperature no phase shifts relative to CO_{ad} can be seen. Therefore, and only in this case, the phase shift of CO_2 was referred to CO.

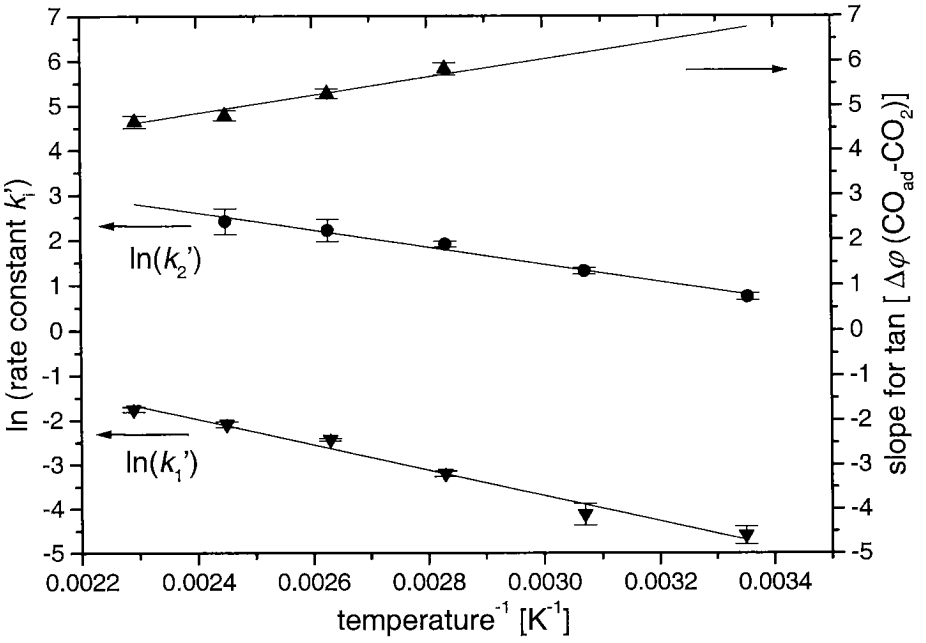

Figure 5-7: CO oxidation as function of the temperature. **Left:** Arrhenius plot obtained for the variation of the slopes of tan[$\Delta\varphi$(CO-CO_{ad})] (●) and tan[$\Delta\varphi$(CO_0-CO)] (▼) with the inverse temperature. The curve was modelled using the Equations 5.11 and 3.10, and Equations 5.10 and 3.9, respectively. In this last case for the first two temperatures, the residence time was modelled with the parameter value k_τ=2'012 ± 22 K s. **Right:** Variation of the slopes of tan[$\Delta\varphi$(CO_{ad}-CO_2)] (▲) as function of the inverse temperature. The curve was modelled with Equations 5.12 and 3.9. The measurements were performed under the same conditions as in Figure 5-6.

As described previously, the slopes of tan[$\Delta\varphi$(CO-CO_{ad})] were linearised and plotted versus the inverse of the temperature (Figure 5-7, ●). By using the Arrhenius Equation, one obtains the following Arrhenius parameters for k_2':

$$k_{0,2}' = 1'961 \pm 569\ s^{-1} \qquad E_{A,2}' = 17.0 \pm 0.7\ kJ\ mol^{-1}$$

The phase shift evolution between CO_{ad} and CO versus temperature gives information about the oxidation reaction on the surface. The ln(k_2') rises with increasing temperature, indicating an enhanced oxidation reaction. For the highest applied temperature (T^{-1} = 0.0023 K^{-1}) no point was plotted. As described before, the phase shift at this temperature was assumed to be close to zero.

As expected, the CO_{ad} oxidation process can be described with a single rate constant. The value of $E_{A,2}$' indicates a weakly activated process. The fact that $E_{A,2}$' is smaller than $\Delta E_{A,3}$ (which in turn is smaller than the activation energy $E_{A,3}$ of the CO_2 adsorption process) suggests that the oxidation of CO_{ad} followed by its desorption is favoured as compared to the adsorption of CO_2 and its subsequent decomposition. This justifies the assumptions (1), (2) and (3).

In the same Figure (Figure 5-7) the evolution of $\tan[\Delta\varphi(CO_{ad}\text{-}CO_2)]$ (▲) was plotted versus the inverse temperature. The slope of the curve yields the parameter τ. The obtained value for k_τ is:

$$k_\tau = 2012 \pm 22 \text{ K s}$$

This value depends only on the geometry of the reactor (τ). In agreement with the model, an increasing temperature corresponds to a decreasing slope. For the two lowest temperatures (298 K and 326 K) the points were omitted, because, again, it was not possible to determine the values of the phase shift evolution. This is due to the too low conversion rate of CO into CO_2.

In all cases, the phase shift $\Delta\varphi(CO\text{-}CO_2)$ was found to remain below π, indicating the reaction to be always of first order for CO. In the case of a negative reaction order, $\Delta\varphi$ has to be larger than π.

In the following section, the phase shift evolution between CO_0 and CO is discussed. Equation 3.9 for the residence time τ is inserted into Equation 5.10 and the result solved for $\ln(k_1')$. The values of τ for the first two temperatures are estimated using the above determined value for k_τ. Thus, a linear equation as function of the inverse temperature is obtained. In Figure 5-7 $\ln(k_1')$ was plotted as function of the inverse temperature. The derived values are:

$$k_{0,1}' = 132 \pm 72 \text{ s}^{-1} \qquad E_{A,1}' = 23.8 \pm 1.6 \text{ kJ mol}^{-1}$$

The CO adsorption process can be described with a single overall rate constant, as postulated in assumption (4) above. The sign of $E_{A,1}$' indicates an endothermic process. The value of $E_{A,1}$' is close to the apparent activation energies of similar catalysts (between 26.2 ± 1.0 kJ mol^{-1} and 28.1 ± 1.0 kJ mol^{-1}, [149]). A comparison between the activation energies of the two steps of the simplified model for CO oxidation (23.8 ± 1.6 kJ mol^{-1} and 17.0 ± 0.7 kJ mol^{-1}) shows that the second step is characterised by a lower energy barrier. This agrees with the observations of several authors [106,147-150].

In order to obtain more insight into the kinetics of the reaction, a comparison between the chosen and an extended version of the model is made. In this new model the CO adsorption/desorption process is included:

$$CO \underset{k_{-1}}{\overset{k_1}{\rightleftharpoons}} CO_{ad} \xrightarrow{k_2'} CO_2$$

Under quasi steady state conditions the concentration of CO_{ad} is given by the following equation:

$$\frac{CO_{ad}}{CO} = \frac{k_1}{k_2' + k_{-1}} \tag{5.14}$$

Note that, strictly speaking, the adsorption rate constant k_1 is dependent on the concentration of the free adsorption sites. A low coverage situation was assumed. This last assumption is supported by the evidence of phase shifts ($\Delta\varphi$) always less than π.

For a numerical comparison (see Figure 5-8), the values obtained in the first experiment were used for k_1 and k_{-1}. Above a temperature of 300 K, k_{-1} (●) is higher than k_2' (▲), indicating that the desorption process of CO_{ad} is faster than the oxidation. The adsorption rate, k_1 (■), is still higher than the desorption rate (k_{-1}), suggesting that CO adsorption is in quasi-equilibrium. This hypothesis is also supported by the similarity of $E_{A,1}$' (23.8 ± 1.6 kJ mol^{-1}) and $\Delta E_{A,1}$ (24.1 ± 1.4 kJ mol^{-1}). That suggests the oxidation of

CO_{ad} to be the rate limiting step. The CO_{ad} oxidation influences the CO adsorption/desorption process. Consequently, k_1' (▼) has only the meaning of an overall net production rate constant of adsorbed CO.

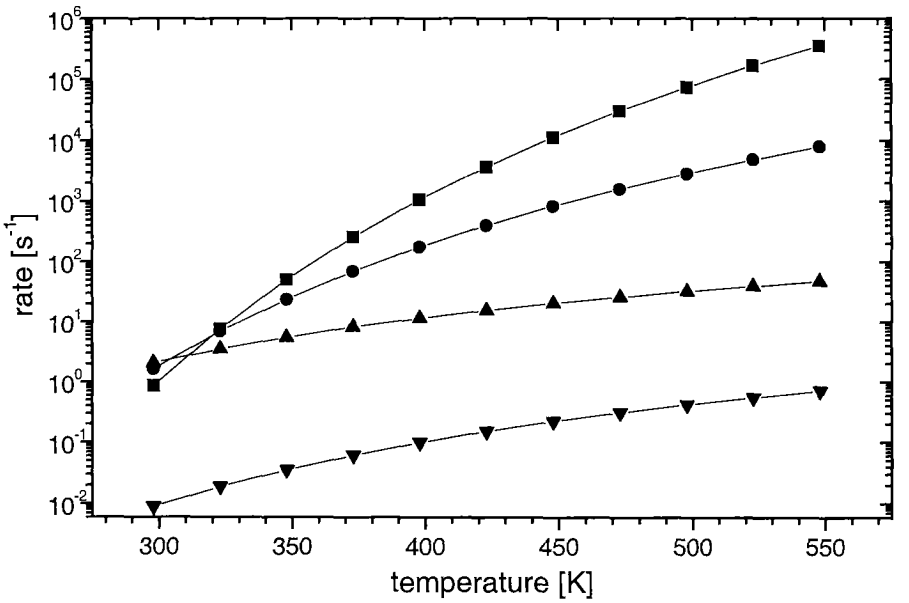

Figure 5-8: Overview of the various rate constants vs. temperature for the two models. ▼: k_1', as obtained from Figure 5-7, ●: k_{-1}, as obtained from Figure 5-3, ▲: k_2', as obtained from Figure 5-7 and ■: k_1, as determined in paragraph 5.3.1.2.

Figure 5-9 displays the CO conversion in dependence on the temperature. The curve marked with ● and a dotted line represents the obtained values from the catalytic test under steady state conditions. The CO conversion calculated from the estimated values (k_τ = 2'012 K s, $k_{0,1}$' = 132 s^{-1}, $E_{A,1}$' = 23.8 kJ mol^{-1}) is marked with ○ and a dashed line.

The determinated CO conversion, described by Equation 5.13, is marked with ▼. It is interesting to observe that the directly measured (▼) and the estimated (○) values follow quite well the obtained values for the steady state conditions (●). The error for this last curve in Figure 5-9 was estimated as ± 5% in absolute conversion. This includes

possible unstabilities (e. g. oscillations and deviations) of the steady state equilibria and instrumentation. One can easily see that the applied model agrees well with the reality.

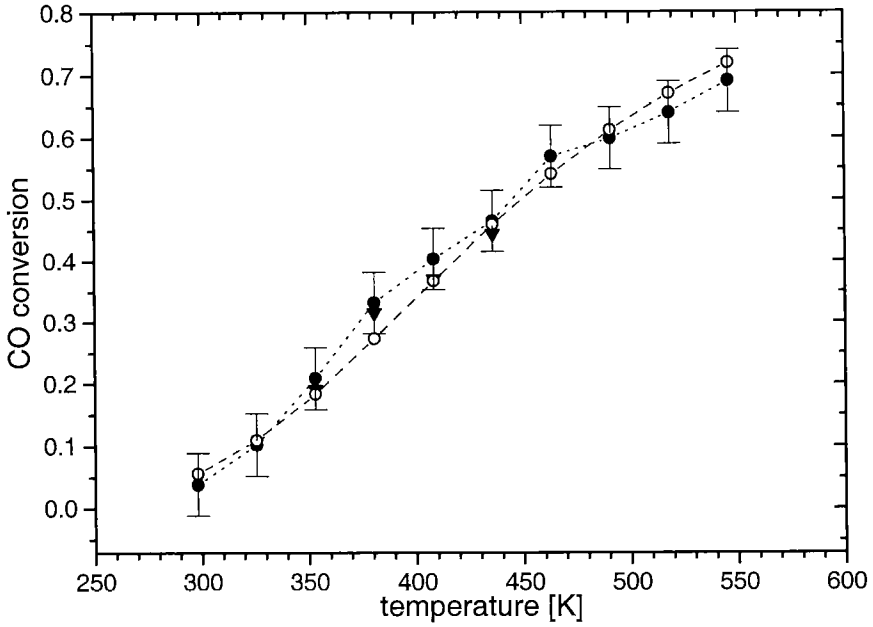

Figure 5-9: Comparison of experimental and measured CO conversions. ▼: CO conversion estimated from the slopes of the phase shifts, as given by Equation 5.13. ○ and dashed line: CO conversion calculated from the estimated values, $k_\tau = 2012$ K s, $k_0 = 132$ s^{-1}, $E_{A,1}' = 23.8$ kJ mol^{-1}. ● and dotted line: CO conversion measured under steady state conditions, no modulation, experimental error ± 0.05. The measurements under steady state conditions were performed at 4 bar with a feed composition of 10%-CO/N_2, 0.02 l_N min^{-1}; O_2, 0.01 l_N min^{-1} and N_2 up to 0.08 l_N min^{-1}.

5.3.4 Effect of O_2 in the CO oxidation reaction

5.3.4.1 Model

Finally, the influence of O_2 onto the oxidation reaction should be estimated. In analogy to the previous experiments (see section 5.3.3), CO was used in excess, and therefore the concentration of adsorbed carbon monoxide (CO_{ad}) was assumed to be constant.

Due to the impossibility to observe O_2 and O_{ad} spectroscopically with the present setup, it was necessary to use an extremely simplified model consisting of just a single reaction step:

$$O_2 \xrightarrow{k_4} CO_2$$

Also here, k_4 has to be considered as an overall first order rate constant. The model is again completed by representing the DRIFT cell as a continuous stirred tank reactor with a residence time τ. With these assumptions the system can be described with the following set of differential equations:

$$\frac{dO_2}{dt} = \frac{O_{2,0}}{\tau} - (k_4 + \frac{1}{\tau})O_2 \tag{5.15}$$

$$\frac{dCO_2}{dt} = k_4 O_2 - \frac{CO_2}{\tau} \tag{5.16}$$

$O_{2,0}$ represents the O_2 concentration in the feed gas. In the present case the overall phase shift results from several reaction steps. Solving the formulas for CO_2 and considering the observations mentioned before, it is possible to write:

$$\tan\ [\Delta\varphi(O_{2,0} - CO_2)] = \omega\tau(1 + \frac{1}{1 + k_4\tau}) \tag{5.17}$$

The temperature dependence evolution of the residence time is approximated with Equation 3.9, and those of k_4 with Equation 3.10.

5.3.4.2 Experimental results

In Figure 5-10 the frequency dependence of the CO_2 phase shift for different temperatures is shown.

With the applied conditions it was not possible to observe a change in the CO or CO_{ad} concentration. Also, no changes in the CO_2 concentration were detected for the lower tested temperature (298 K). Remarkable is the evolution as function of the temperature: the second curve (353 K: ○) comprises lower phase shifts than the first one (326 K: ■), indicating that the reaction became more rapid. The other curves (381 K: ▲; 408 K: ▽; 436 K: ♦) appear with higher phase shifts. The data for 408 K and 436 K (▽ and ♦) exibit a lower phase shift than these taken at 381 K (▲).

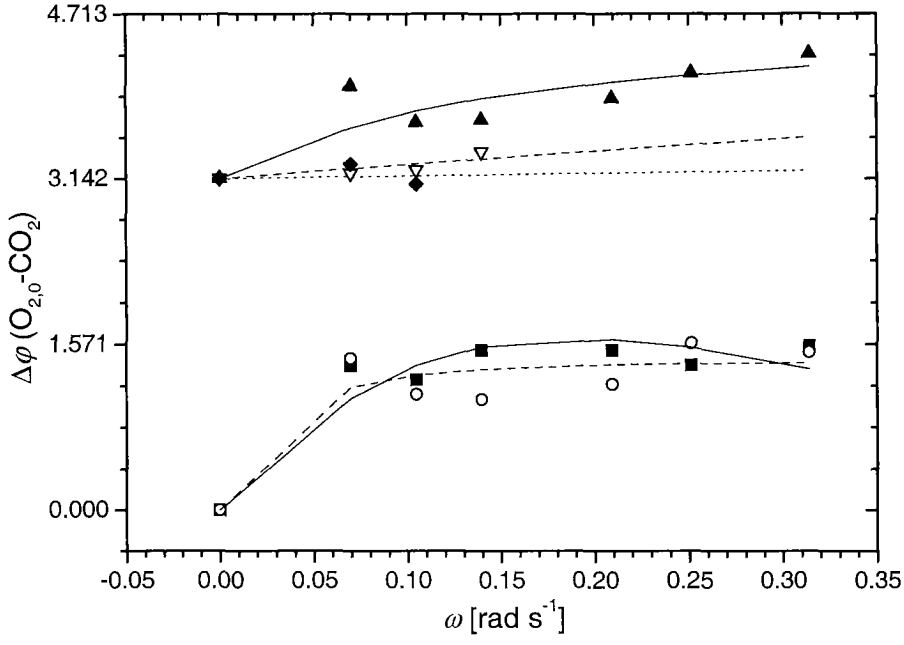

Figure 5-10: Oxygen modulation experiment. Overview on the variation of $\Delta\varphi(O_{2,0}\text{-}CO_2)$ for different temperatures (326 K: ■ and solid line; 353 K: ○ and dashed line; 381 K: ▲ and solid line; 408 K: ▽ and dashed line; 436 K: ♦ and dotted line). The measurements were performed at 4 bar with a feed composition of O_2, 0.02 ± 0.01 l_N min^{-1}; 10%-CO, 0.04 l_N min^{-1} and N_2 up to 0.08 l_N min^{-1}.

This behaviour indicates that the reaction order has changed. At low temperatures the CO_2 production is of first order with respect to oxygen, and at high temperatures it becomes of negative order. This is in agreement with the observations of Böcker *et al.* [136]. At low temperatures the CO consumption is of negative reaction order with

respect to oxygen and positive at high temperatures. The evolution of the slopes for different temperatures is given in Figure 5-11.

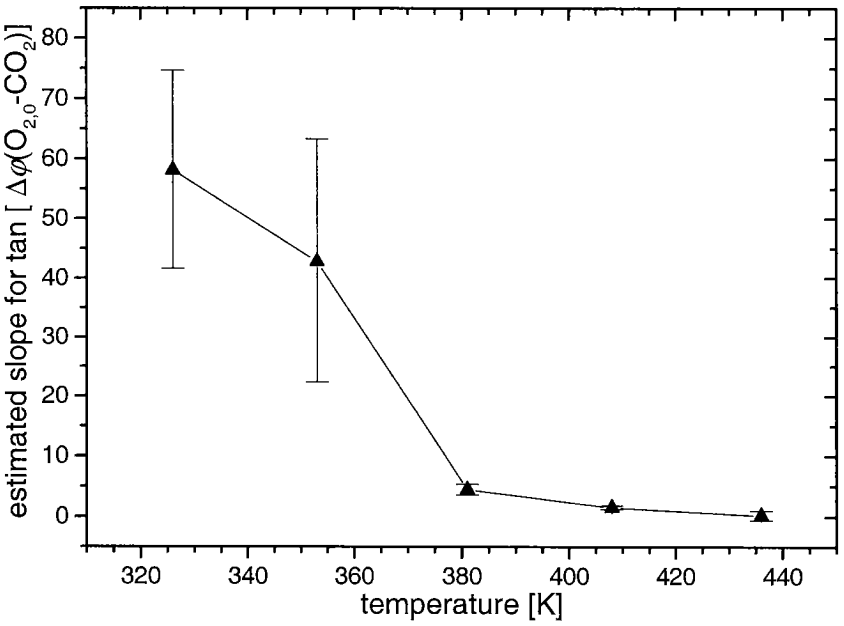

Figure 5-11: Variation of the slopes for $\Delta\varphi(O_{2,0}\text{-}CO_2)$ (▲) as function of the temperature. The curve can not be modelled with an Arrhenius temperature dependence (Equation 5.17). Experimental conditions as in Figure 5-10.

As a maximum of O_{ad} corresponds to a minimum of CO_{ad} in the regime where the rate is linear in CO, an intercept of π rather than 0 was assumed for the three highest temperatures. With increasing temperature the slope decreases, indicating an enhanced reaction velocity. As expected, a fit of the obtained curve using Equation 5.17 does not give a satisfactory result, because the first two values at low temperatures are dependent on the O_2 concentration in the gas phase, whereas the values taken at higher temperatures depend on the CO_{ad} concentration. This clearly indicates that a more complex model would have to be used for quantitative modelling.

5.4 Error sources

In this paragraph possible sources of errors and their influence on the results are discussed.

5.4.1 Signal-to-Noise Ratio (SNR)

An important error source is certainly the low Signal-to-Noise Ratio (SNR). As explained in section 3.3.4, if the SNR is not good enough, the measured signal can contain artefacts. After defining the measurement conditions (aperture, scan velocity, filter, etc.), the SNR is dependent on the number of collected scans per spectrum, the concentration of the different species, and the IR emissivity of the sample.

In our case, the number of photons is low (ca. 250 photons per second). This effect is due to the greyish-black colour of the catalyst, exhibiting a strong absorption in the mid-IR region. For each spectrum several interferograms were accumulated, but the collection time is limited by the time resolution required to resolve the phase during a modulation cycle.

5.4.2 Phase resolution

Six points per period were collected for several modulation periods, at any given modulation frequency, to reduce the error caused by the approximation of the sinusoidal curve. With this data set, it was possible to approximate the obtained points with a sinusoidal function over several periods.

5.4.3 Optical path of the DRIFT cell

As explained in section 1.3.5 the optical path within the DRIFT cell is very important. It determines the relative size of the gas phase signal. In our setup, we have a total optical path length of about 10 mm (5 mm before and 5 mm after the catalyst) in the DRIFT cell.

5.4.4 Reflectivity of the sample

The change of the reflectivity on the surface of the catalyst can strongly affect the SNR. The reflectivity also depends on the concentrations of the surface species on the catalyst surface. As a consequence, a small change of the concentrations in the feed gas is preferred, because it will induce only a small change in the reflectivity. More details about the reflectivity can be found in section 1.3.4.

5.4.5 Changes in the concentration

Another error source is based on the concentration changes of the different species. The amplitudes have to be chosen far away from the detection limits. The change in the concentration should be big enough to be detected but not so strong to saturate the detector (see section 3.3.4). A saturation of the surface of the catalysts should also be avoided, because modulation experiments are not possible under these conditions (see section 3.3.4).

Other unwanted effects, which can affect the result of the measurements, should also be avoided. As an example, a result obtained within the parameter regime of oscillating CO oxidation is shown in Figure 5-12.

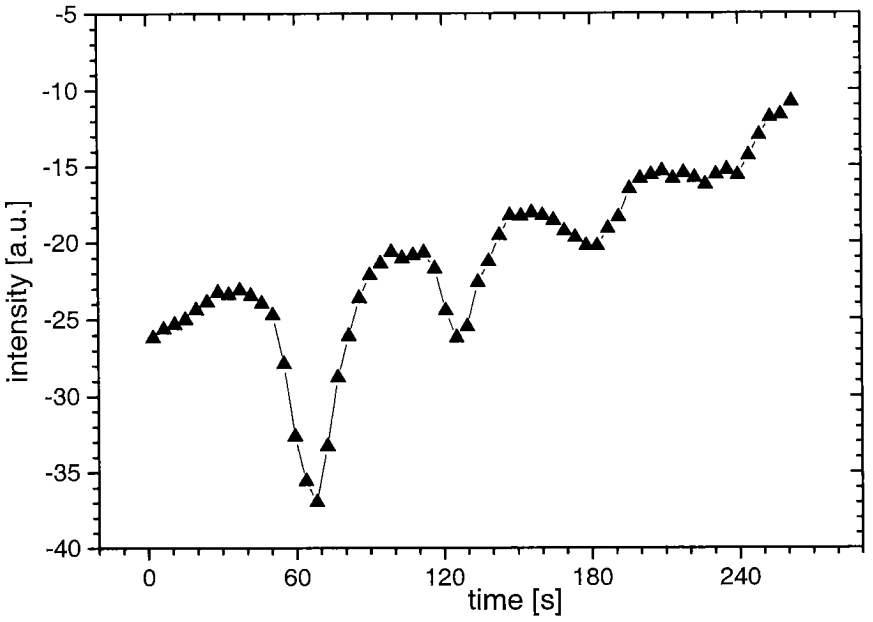

Figure 5-12: Oscillatory evolution of CO_2 concentration in the gas phase (▲) during a step down test experiment. The conditions used are: 4 bar, 353 K, 10%-CO, 0.04 - 0.01 $l_N\,min^{-1}$; O_2, 0.05 $l_N\,min^{-1}$ and N_2 up to 0.24 $l_N\,min^{-1}$.

It is easy to recognise a damped oscillation of the CO_2 concentration during a CO step down test experiment. The applied conditions were: 4 bar total pressure, 353 K, 10%-CO/N_2, 0.04 - 0.01 $l_N\,min^{-1}$; O_2 0.05 $l_N\,min^{-1}$ and N_2 up to 0.16 $l_N\,min^{-1}$.

5.4.6 Experimental errors

To minimise the experimental error *ad hoc* solutions were used. Temperature controllers and mass flow controllers have an error of ± 1 K and ± 0.002 $l_N\,min^{-1}$ respectively. The estimated trigger dead time is below 20 ms. More information about the used setup and its limits can be found in sections 2.2.2 and 2.3.2.

5.4.7 Dead time

The dead time estimation is important to define the start of a modulation period and consequently the phase shift $\Delta\varphi$ between the species (see paragraph 3.3.4.1). The dead time monitored during the different experiments at different temperatures is shown in Figure 5-13.

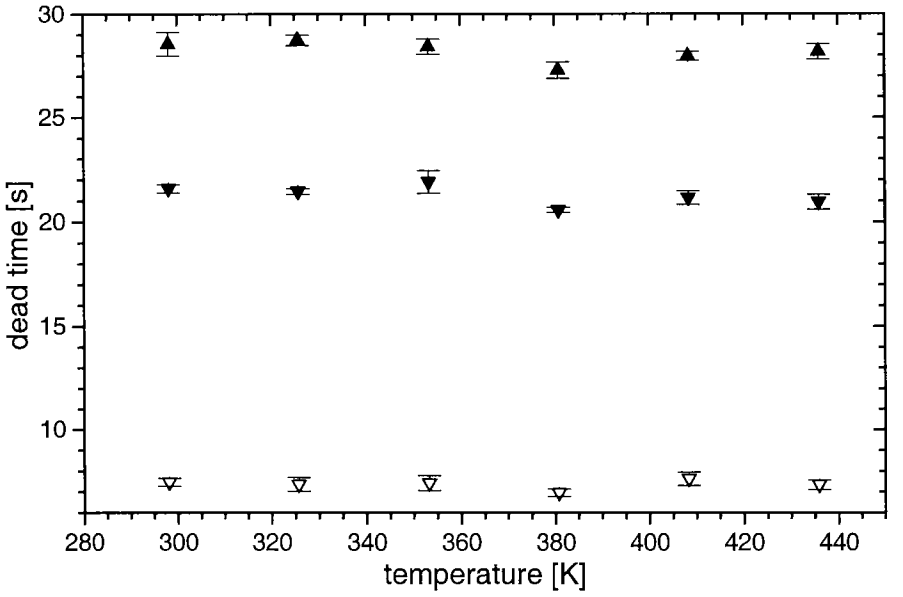

Figure 5-13: Dead time monitored during the different experiments at different temperatures. ▼: CO adsorption (section 5.3.1) ▲: CO_2 adsorption (section 5.3.2); ▽: CO oxidation (section 5.3.3).

Note the changes of the dead time for the different temperatures. These variations are due to the different conditions (temperature and pressure) present in the laboratory during the experiments. To reduce the error, the used dead time is obtained by averaging several measurements performed under identical conditions. The estimated error is around 0.2 s.

5.4.8 Selection of the model

Selecting the appropriate model is important to avoid artefacts and unrealistic results. The existence of reverse reactions together with surface effects should be carefully considered (for a complex example, see Figure 5-12). The model chosen for the temperature dependence of parameters, such as k_τ and k_1, should also be considered. As know from all fitting problems, the model should not be too complicated to induce too many degrees of freedom. A large number of variables results normally in estimated parameter values with large errors.

Using different models, it is possible that the same constant exhibits a large deviation in the estimated values. An example are the differences between the values of k_τ, approximated in the CO adsorption, in the CO oxidation, and in the CO_2 adsorption experiments. Other constants display a smaller deviation, even when several other parameters are varied. An example is E_A in Equations 5.3, 5.6 and 5.10. Even a large change of k_τ induces only a limited deviation. This is a consequence of a model describing events with defined assumptions.

More information about possible and useful models, that can be used in the heterogeneous catalysis, can be found in section 3.4.

5.4.9 Error propagation

The propagation of errors along the data reduction chain has to be considered. (1) A sinusoidal feed modulation induces a cascade of sinusoidal concentration dependencies. (2) A phase shift is derived from each sinusoidal curve. (3) From all phase shifts obtained under identical reaction conditions but with different modulation frequencies, the model parameters (e. g. a slope) are obtained. (4) From the parameters calculated at different temperatures an Arrhenius activation energy characterising the reaction is derived.

To reduce errors and to ensure the reproducibility, the experiments were performed several times under identical conditions, and averaged values were used.

5.5 Conclusions

Periodic modulations of reactant concentrations have been used to induce time dependent variations in the FTIR signals of reactant, intermediate, and product concentrations for the CO oxidation over a $Pd_{25}Zr_{75}$ catalyst. These were monitored and consecutively analysed with a micro kinetical model to obtain information on the reaction pathway and rate constants, characterising the kinetics of the reaction. Repetition of experiments at different temperatures allows to estimate the Arrhenius energy associated with each rate or equilibrium constant. The conclusions drawn from the obtained results are presented in the following sections.

5.5.1 Reaction order of CO

At low temperatures (up to 380 K) the apparent reaction order of CO in the oxidation is influenced by concentrations of O_2 and CO in the gas phase. In the CO oxidation experiments, the rate was always of apparent first order for CO. In the experiment at high CO concentration, where the effect of O_2 on the CO oxidation was investigated, the order for CO is negative.

5.5.2 Influence of the CO_2 adsorption on the oxidation reaction

The obtained ΔE_A for the CO_2 adsorption/desorption process (27.0 ± 0.8 kJ mol^{-1}), is slightly higher than for the CO adsorption. As discussed previously this value does not represent a reaction on a molecular level. CO_2 in the gas phase has probably no influence on the CO oxidation reaction. If CO_2 adsorption has an influence, the CO_{ad}

oxidation would be partly followed by $CO_{2\,ad}$ dissociation. The desorption of $CO_{2\,ad}$ would become the rate limiting step, and a phase shift between CO_{ad} and CO_2 greater than $\pi/2$ would be expected. Nothing supporting this scenario is found.

5.5.3 Energy scheme of the reaction

As previously discussed, the rate limiting step is the CO_{ad} oxidation, with an Arrhenius activation energy of 17.0 $\pm$ 0.7 kJ mol^{-1}. The CO adsorption occurs under *quasi* equilibrium condition. The associated activation energy $E_{A,1}$' (23.8 $\pm$ 1.6 kJ mol^{-1}) corresponds to an effective rate constant for net production of adsorbed CO. This assumption is supported by the similarity of the $E_{A,1}$' with the $\Delta E_{A,1}$ value (24.1 $\pm$ 1.4 kJ mol^{-1}) for the CO adsorption/ desorption process derived in the first experiment.

In Figure 5-14, a tentative energy reaction scheme for the CO oxidation reaction is shown. The total reaction energy is obtained from the known combustion enthalpy ($\Delta H°$) of CO. It was also assumed that $\Delta E_{A,3}$ characterises only the CO_2 adsorption/ desorption equilibrium. From the scheme an Arrhenius activation energy of $\approx$ 300 kJ mol^{-1} for the $CO_{2,ad}$ dissociation process can be estimated.

For CO_{ad}, the scheme would indicate a *thermodynamic* preference for oxidation over desorption. In contrast, the CO_{ad} oxidation was experimentally found to be the rate limiting step. The reason of this apparent discrepancy can be traced to the pre-exponential values of the rate constants. These values represent the influence of the standard activation entropy, $\Delta S^{\ddagger}$. Therefore, the less positive activation entropy value of the CO_{ad} oxidation is responsible for the rate limitation of the entire CO oxidation reaction sequence.

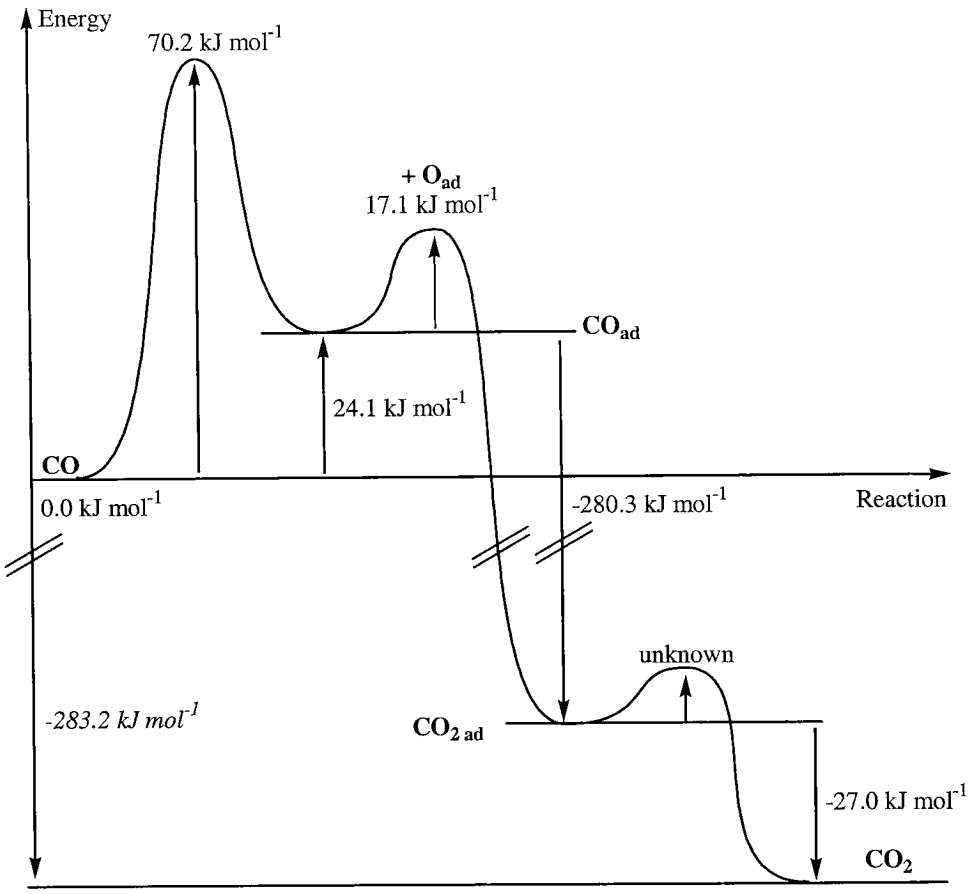

Figure 5-14: Energy reaction scheme for the CO oxidation (italic). The used total reaction energy was approximated from the combustion enthalpy ($\Delta H°$) of CO. It was assumed that $\Delta E_{A,3}$ characterises only the CO_2 adsorption/desorption equilibrium.

5.5.4 CO-CO_2 equilibrium

In case of high CO_2 concentration an equilibrium on the catalyst surface between CO_{ad}, O_{ad} and adsorbed CO_2 should be considered in the model. In the CO_2 adsorption experiment, the evolution of the slope, with increasing temperature, suggests the possibility of a reaction following the adsorption.

5.5.5 Modulation technique

The modulation concept in heterogeneous catalysis, as monitored by DRIFT, has been demonstrated. All parameters can be derived from the experiments without the need of a previously established calibration curve. Possible error sources were presented and discussed in detail.

This is page 132 !

This page was left intentionally blank !

6. Methanol synthesis pathway over Cu/ZrO_2 catalysts

6.1 Introduction

In this chapter an experiment to provide additional evidence on the pathway of methanol synthesis over Cu/ZrO_2 catalyst is proposed. A three-step *in situ* experiment was performed in a DRIFT cell. ^{13}C-labelled as well as common ^{12}C paraformaldehyde and formic acid were adsorbed and subsequently hydrogenated under reaction conditions.

More information about this experiment can be found elsewhere [155].

As already explained in chapter 4, the use of methanol in the chemical industries as reactant for other organic chemicals is increasing. Methanol plays also an important role as energy carrier. Owing to the fact that CO_2 is recognised as the major greenhouse gas, the use of this gas as an alternative feedstock replacing CO in liquid fuel production has received much attention as one of the promising emission mitigation options. Therefore, the synthesis of methanol from synthesis gas (CO, CO_2, H_2) has gained increasing importance in the last decade and is actually one of the most investigated catalytic reactions.

The formation of methanol proceeds according to the two reaction equilibria:

$$CO + 2\,H_2 \leftrightarrow CH_3OH$$
$$CO_2 + 3\,H_2 \leftrightarrow CH_3OH + H_2O$$

The use of zirconia-supported copper catalysts is of special interest due to their mechanical and thermal stability, the relatively high specific surface area, and semiconducting properties of ZrO_2. Although these catalysts have been subjected to numerous investigations, the nature of the active sites and of the intermediates continues to be discussed controversially. An issue is the question whether the route to methanol proceeds via formates or other intermediates.

For ZrO_2 supported catalysts, He *et al.* [156,157] have proposed a low temperature mechanism in which formates were hydrogenated to yield a dioxymethylene species, which could react further with hydrogen and desorb as methanol in the presence of water. Abe *et al.* [158] found for ZrO_2 experimental evidence for a mechanism proceeding via surface formates and methoxy species.

Amenomiya [159] found for Cu/ZrO_2 that CO_2 reacted directly to CH_3OH, and that the reverse water-gas shift reaction was taking place in parallel. Sun *et al.* [160] postulated for Cu/ZrO_2 a formate-to-methoxy mechanism when starting from CO as reactant.

Schild *et al.* [161, 162], Köppel *et al.* [163], Wokaun *et al.* [164], and Weigel *et al.* [165] found for Cu/ZrO_2 based catalysts that π-bonded formaldehyde, which is formed in the catalytic reaction of CO and H_2, is the key intermediate, and that subsequent reduction yields surface-bound methylate and methanol. The same authors have observed that in a first step surface formates are rapidly formed, in a second η^2-H_2CO and adsorbed H_3CO^- are produced simultaneously and in the last step gas phase H_3COH is present.

More recently, Fisher *et al.* [166, 167] found evidence of a formate $\rightarrow$ methylenebisoxy $\rightarrow$ methoxy mechanism for $Cu/ZrO_2/SiO_2$ catalysts.

6.2 Experimental and procedures

6.2.1 Catalyst

The Cu/ZrO_2 catalyst used in this study was prepared by coprecipitation of the corresponding metal nitrates at constant pH and temperature as described elsewhere [168]. It had a composition of Cu:Zr = 46:54 at.%, and a grain size of 50 - 150 μm.

6.2.2 Infrared spectroscopy

In situ experiments were performed in the DRIFT cell presented in section 2.4.1. Spectra were recorded using the Fourier transform infrared spectrometer presented in section 2.6. Spectra were recorded with a resolution of 4 cm^{-1}, with an accumulation of 128 - 512 interferograms for the time dependent spectra, and 1024 interferograms for background spectra, depending on the respective signal strengths.

The investigated catalyst has a greyish-black colour and adsorbs strongly throughout the mid IR region. Its reflectance during the reaction is higher than for the reference. This violates the basic assumptions of the Kubelka-Munk theory about a weakly absorbing substrate, as explained in section 2.4.3. Therefore reflectance units (R/R_0), rather than K-M units for the presentation of spectra are used.

Gaseous products were removed by a continuous stream of the reactant mixture passing over the sample; this resulted in a reduction of the overlap of bands between surface intermediates and gaseous species.

6.2.3 Experimental setup

The setup consists of a feed gas preparation unit connected to the DRIFT cell. Feed gases were prepared using the *Preparative Unit* and the supplementary unit presented in section 2.3.1, which was designed to introduce evaporated liquid and sublimated solid substances into the reaction chamber. The temperature in the reaction chamber was controlled by a homemade control program described in section 2.2.

The used gases and labelled compounds are described in detail in section 2.8.

6.2.4 Catalyst preparation

The catalyst was pressed for a constant time (10 seconds) in the sample holder as described in section 2.4.4.

The packed catalyst was reduced in a nitrogen/hydrogen stream (10 l h^{-1}, H_2:N_2 = 3:1) at 0.1 MPa while heating to 523 K with a rate of 10 K min^{-1}, and subsequently cooled to 423 K. Then the background spectrum was recorded.

6.2.5 Experimental procedures

6.2.5.1 ^{13}C-paraformaldehyde and ^{12}C-formic acid adsorption followed by reduction

About 0.2 g of $H_2{}^{13}CO$ (paraformaldehyde) were placed in the tube and heated to 403 K. The sublimated substance was flushed with 1 l h^{-1} N_2 at 0.5 MPa onto the catalyst, which was kept at a temperature of 423 K. After five minutes 0.1 ml of HCOOH were injected into the 1 l h^{-1} N_2 flow and flushed over the catalyst. After five additional minutes the flow was increased to 10 l h^{-1} with a gas composition of H_2:N_2 = 3:1.

6.2.5.2 ^{13}C-formic acid and ^{12}C-paraformaldehyde adsorption followed by reduction

About 0.1 ml of $H^{13}COOH$ were injected into a 1 l h^{-1} N_2 flow at 0.5 MPa and flushed over the catalyst kept at 423 K. After five minutes the N_2 flow was redirected through the heated tube (403 K) containing 0.2 g of H_2CO. Five additional minutes later the flow was raised to 10 l h^{-1} with a ratio of H_2:N_2 = 3:1 and passed over the catalyst surface.

6.3 Results and discussion

Detailed assignments of all relevant vibrational bands can be found in the pertinent literature on copper oxides and zirconia supported catalyst [72,156-162,164,165,169]. In the present chapter only few vibrational features that are important for the mechanism of methanol synthesis over the investigated catalyst are considered.

6.3.1 Frequencies of labelled substances

The peak positions of labelled substances were calculated assuming that isotopically substituted molecules just differ in the respective atomic masses, but have the same bond strengths. Consequently one can write the frequency as:

$$\tilde{\nu} = \frac{1}{2\pi c}\sqrt{\frac{k}{\mu}} \tag{6.1}$$

where k is the force constants and μ is the reduced mass:

$$\mu_{(C-Y)} = \frac{m_C\, m_Y}{m_C + m_Y} \tag{6.2}$$

Here m_C is the mass of the carbon atom and m_Y is the mass of the Y-atom bonded to the carbon. From the proportionality (Equation 6.1) one obtains:

$$\frac{\tilde{\nu}_{(^{12}C-Y)}}{\tilde{\nu}_{(^{13}C-Y)}} = \frac{\sqrt{\frac{k}{\mu_{(^{12}C-Y)}}}}{\sqrt{\frac{k}{\mu_{(^{13}C-Y)}}}} \tag{6.3}$$

Upon substitution of (6.2) into (6.3) and evaluation for the C-O and C-H bonds one finds:

$$\tilde{\nu}_{(^{13}C-O)} = 0.9778 \cdot \tilde{\nu}_{(^{12}C-O)} \tag{6.4}$$

$$\tilde{\nu}_{(^{13}C-H)} = 0.9970 \cdot \tilde{\nu}_{(^{12}C-H)} \tag{6.5}$$

The shift will be larger for C-O bonds (> 22 cm^{-1}) than for C-H bonds (< 9 cm^{-1}). In the following table some significant band frequencies are summarised [164-168].

Table 1: Summarise of the significant band frequencies observed.

Species	Vibration	Literature [cm^{-1}]	This work [cm^{-1}]	Calculated [cm^{-1}]	Figure
η^2-$H_2{}^{12}CO$	ν(C=O)	1153	1155	-	Figure 6-3
η^2-$H_2{}^{13}CO$	ν(C=O)	1127	1130	1129	Figure 6-1
$^{12}CH_3OH_{(g)}$	ν(C-O)	1034	1032	-	Figure 6-3 Figure 6-4
$^{13}CH_3OH_{(g)}$	ν(C-O)	1011	1010	1009	Figure 6-1 Figure 6-2

6.3.2 Adsorption of $H_2{}^{13}CO$ and $H^{12}COOH$

After switching on the N_2 flow containing ^{13}C-labelled formaldehyde, the spectrum (trace **a** in Figure 6-1) showed groups of peaks at 1715 cm^{-1} and around 1145 cm^{-1}. Both peaks decreased rapidly after switching to the formic acid containing N_2-flow (trace **d** in Figure 6-1).

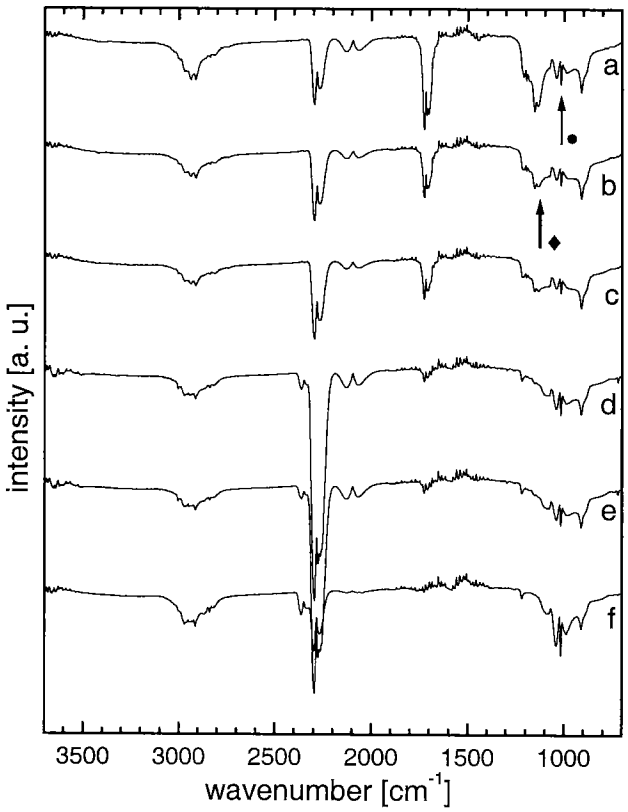

Figure 6-1: Adsorption of $H_2{}^{13}CO$ for 1, 3 and 5 minutes (**a**, **b** and **c**), followed by adsorption of $H^{12}COOH$ for 1, 3 and 5 minutes (**d**, **e** and **f**). The thin -•- and thick -♦- arrows designate marker bands of gas phase methanol and adsorbed formaldehyde, as discussed in text.

The first, above mentioned, band was assigned to $\nu(^{13}C{=}O)$ of gas phase formaldehyde, with contributions from bidentate carbonates (shoulder at 1670 cm^{-1}). The second is the result of the contributions of $\nu(^{13}C\text{-}O)$ of gas phase paraformaldehyde (1185 cm^{-1}), adsorbed paraformaldehyde (ν_{as}, 1070 cm^{-1}), η^2-$H_2{}^{13}CO$ (1130 cm^{-1}) (thick -♦- arrow in

Figure 6-1) and bidentate carbonates (ν_{as}, 1150 cm^{-1} and ν_s, 1220 cm^{-1}). ^{13}CO, from the decomposition of $H_2{}^{13}CO$, showed the corresponding doublet at 2096 cm^{-1}; on the other hand $^{13}CO_2$, due to hydrolysis/decomposition of carbonates, appeared at 2282 cm^{-1}. Labelled gas phase methanol was immediately present as evidenced by the $\nu(^{13}C\text{-}O)$ band at 1010 cm^{-1} (trace **a** in Figure 6-1; thin -•- arrow in Figure 6-1 and Figure 6-2); the R-branch contains a contribution from a methylate band ($\nu(^{13}C\text{-}O)$) at 1020 cm^{-1}.

The sharp peak at 915 cm^{-1} contains contributions from adsorbed paraformaldehyde ($\nu_s(^{13}C\text{-}O)$, 915 cm^{-1}) and bidentate carbonates ($\nu_s(^{13}C\text{-}O)$, 980 cm^{-1}). The band around 2940 cm^{-1} consists of contributions from several substances. Major peaks are the $\nu(^{13}CH_2)$ of adsorbed paraformaldehyde at 2915 cm^{-1}; the $\nu_s(^{13}C\text{-}H)$ at 2836 cm^{-1} and the shoulder of $\nu_{as}(^{13}C\text{-}H)$ at 2970 cm^{-1} of gas phase methanol. Contained within the broad peak are the $\nu(^{13}C\text{-}H)$ of methylate (ν_{as}, 2920 cm^{-1} and ν_s, 2820 cm^{-1}), of $\eta^2\text{-}H_2CO$ ($\nu_{s/as}(CH_2)$, 2810 cm^{-1}) [73,170] and of adsorbed paraformaldehyde (ν_{as}, 2910 cm^{-1}). Gas phase water, identified by the typical gas phase multiplett signal around 1620 cm^{-1}, is consumed.

Upon subsequent exposure to an N_2/HCOOH flow (traces **d**, **e** and **f** in Figure 6-1), the $^{12}CO_2$-peak (2349 cm^{-1}), resulting from the decomposition of HCOOH, is growing in intensity together with the ^{13}CO (2096 cm^{-1}), due to hydrogenation of carbonates (traces **d** and **e** in Figure 6-1). The $^{13}CO_2$-peak is also growing in intensity due to hydrolysis/decomposition of carbonates ($^*CO_3^{2-} + H_2O \leftrightarrow CO_2 + 2\ ^*OH^-$) (traces **d** and **e** in Figure 6-1).

The bands around 1700 cm^{-1} are no longer detectable. The peak around 1145 cm^{-1} is reduced in intensity, and other peaks are observable; i. e. the bidentate carbonates at 1220 cm^{-1} and peaks with contributions from $\eta^2\text{-}H_2CO$ and adsorbed paraformaldehyde. Before purging with the H_2/N_2 flow ^{13}CO and $^{13}CO_2$ are strongly decreased (trace **f** in Figure 6-1).

6.3.3 Hydrogenation of surface species

Exposing the catalyst, that has been loaded as described in the previous section, to an H_2/N_2 flow, the peaks of methanol, adsorbed paraformaldehyde and $^{13}CO_2$ (1010, 2840, 2970 cm^{-1}, 915, 1070, 2940 cm^{-1} and 2282 cm^{-1}, respectively) decrease (traces **a**, **b** and **c** Figure 6-2).

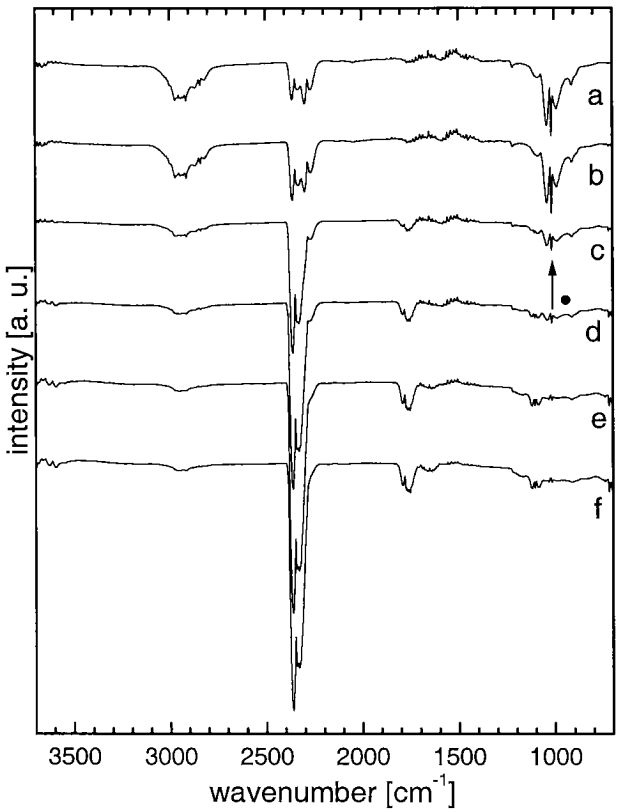

Figure 6-2: Hydrogenation of species over the catalyst surface onto which $H_2{}^{13}CO$ and $H^{12}COOH$ have been previously adsorbed. After switching to N_2/H_2, the course of hydrogenation was monitored for 1, 5, 10, 15, 25 and 45 minutes (**a**, **b**, **c**, **d**, **e** and **f**). The thin -•- arrow designates the marker band of gas phase methanol.

After some minutes the gas phase HCOOH peaks grow at 1770 cm^{-1} ($\nu(^{12}C{=}O)$) and at 1120 cm^{-1} ($\nu(^{12}C\text{-}O)$) together with the bidentate carbonate peak at 1650 cm^{-1} ($\nu(^{12}C{=}O)$). The peak at 1180 cm^{-1} has contributions from bidentate carbonates

($\nu(^{13}C\text{-}O)$ at 1220 cm^{-1} and $\nu(^{13}C\text{-}O)$ at 1070 cm^{-1}) (traces **d**, **e** and **f** Figure 6-2). Continued exposure to the H_2/N_2 flow causes a loss in intensity of the methanol bands. The CO_2 doublet becomes stronger due to increased formic acid decomposition. Gas phase water is also present, as identified from its typical multiplett of bands around 1620 cm^{-1}.

6.3.4 Adsorption of $H^{13}COOH$ and $H_2{}^{12}CO$

Spectra of a catalyst exposed to a flow of ^{13}C-labelled formic acid in N_2 (traces **a** and **b** in Figure 6-3) showed the gas phase formic acid bands at 1730 cm^{-1} ($\nu(^{13}C{=}O)$), at 1095 cm^{-1} ($\nu(^{13}C\text{-}O)$) and a less intensive band around 2920 cm^{-1} ($\nu(^{13}C\text{-}H)$).

The broad band around 1180 cm^{-1} is caused by the bidentates carbonates ($\nu(^{12}C\text{-}O)$ and $\nu(^{13}C\text{-}O)$); also the two weak peaks at 1415 cm^{-1} and at 1385 cm^{-1} can be assigned to ν_{as}(O-C-O) of ^{13}C- and ^{12}C-monodentate carbonates (traces **c** and **d** in Figure 6-3).

The shoulder at 1525 cm^{-1}, that becomes a sharp peak after several minutes (traces **b** and **c** in Figure 6-3), and the less intensive peak at 1335 cm^{-1} can be assigned to $\nu_{as}(^{13}C\text{-}O)$ and to $\nu_s(^{13}C\text{-}O)$ respectively, which, together with the $\nu(^{13}C\text{-}H)$ at 2860 cm^{-1} can be assigned to ^{13}C-formate (traces **a**, **c** and **f** in Figure 6-3). In the same way the peak at 1570 cm^{-1} (trace **a** in Figure 6-3) that becomes a shoulder in later spectra is a contribution of $\nu_{as}(^{12}C\text{-}O)$ of formates. $^{12}CO_2$ is probably due to the presence of residual air in the injection system.

After switching to the $N_2/^{12}C$-paraformaldehyde gas stream gas phase unlabelled methanol is immediately present (traces **e** and **f** in Figure 6-3) as identified by the ν(C-O) signal at 1032 cm^{-1} (thin -•- arrow in Figure 6-3 and Figure 6-4). Gas phase water is now present. Carbonate peaks at 1415 cm^{-1} and 1385 cm^{-1} are decreasing, due to hydrolysis/decomposition, and simultaneously $^{13}CO_2$ and $^{12}CO_2$ peaks are growing (traces **e** and **f** in Figure 6-3). The peak at 1735 cm^{-1} shifts to around 1750 cm^{-1} due to

contribution of gas phase formaldehyde ($\nu(^{12}C{=}O)$ at 1755 cm^{-1}). Gas phase paraformaldehyde is also present, as visible from the shoulder at 1210 cm^{-1} ($\nu(^{12}C\text{-}O)$). η^2-$H_2{}^{12}CO$ (1155 cm^{-1}) (thick -♦- arrow in Figure 6-3) is formed and finally becomes the predominant peak around 1150 cm^{-1}.

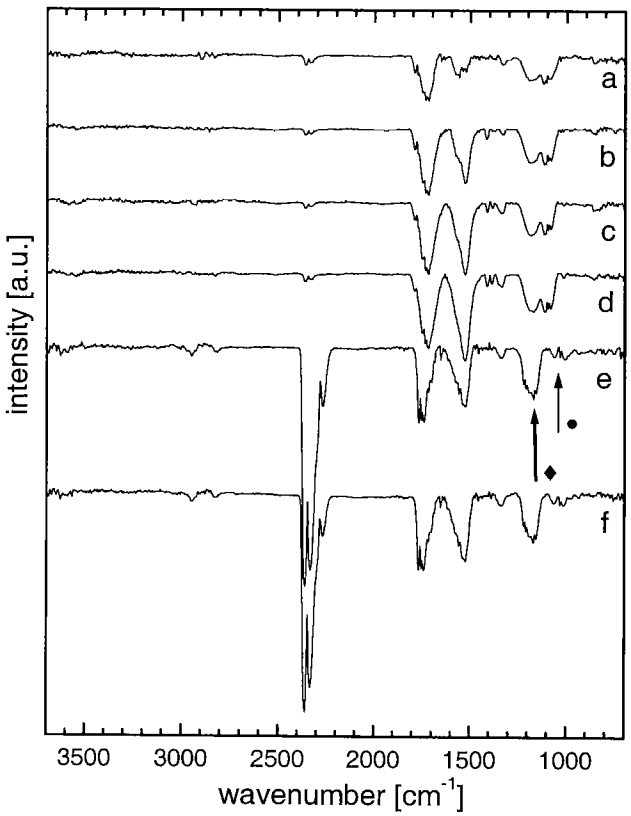

Figure 6-3. Adsorption of $H^{13}COOH$ for 1, 3 and 5 minutes (**a**, **b** and **c**), followed by adsorption of $H_2{}^{12}CO$ for 1, 3 and 5 minutes (**d**, **e** and **f**). The thin -●- and thick -♦- arrows designate marker bands of gas phase methanol and adsorbed formaldehyde, as discussed in text.

The weak peak at 1650 cm^{-1} can be assigned to the $\nu(C{=}O)$ of bidentate carbonates. The peak around 2950 cm^{-1} contains contributions from $\nu(C\text{-}H)$ of paraformaldehyde (2915 cm^{-1}) and methanol (2975 cm^{-1}), the peak at 2820 cm^{-1} is assigned to adsorbed formaldehyde.

6.3.5 Hydrogenation of surface species

Exposing the surface of the catalyst, that had been loaded as described in section 6.3.4, to an H_2/N_2 flow causes a rise of the gas phase ^{12}C-methanol peak at 1032 cm^{-1}, and a minor increase of the ^{12}CO peak at 2144 cm^{-1}, due to the hydrogenation of carbonates and H_2CO decomposition (traces **b**, **c** and **d** in Figure 6-4). After 10 minutes a small decrease of the 1525 cm^{-1} peak indicates that ^{13}C-formates are reduced (traces **a** and **d** in Figure 6-4). A small amount of monodentate carbonates (ν_{as}(O-C-O) at 1415 cm^{-1}) is formed on the surface. Gas phase water is present as always.

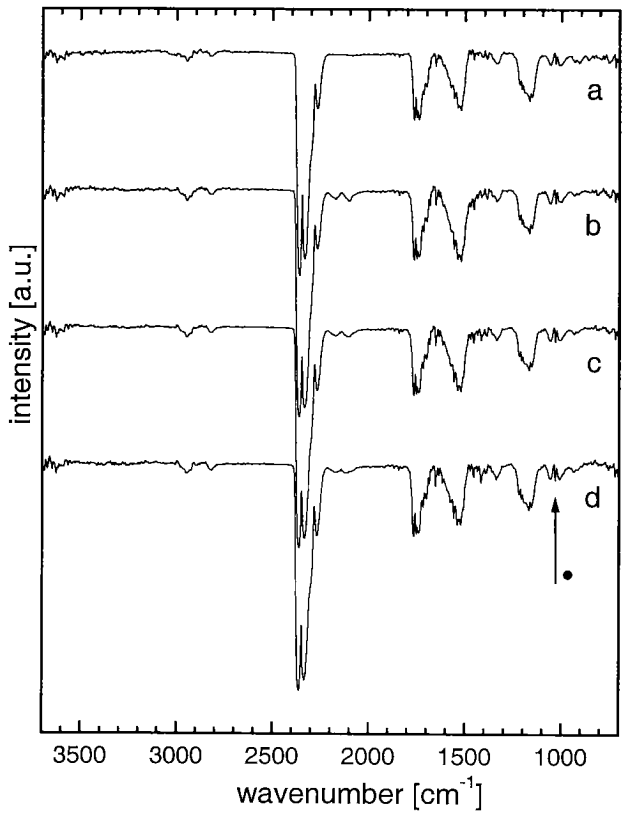

Figure 6-4: Hydrogenation of species over the catalyst surface onto which $H^{13}COOH$ and $H_2{}^{12}CO$ have been previously adsorbed. After switching to N_2/H_2, the course of hydrogenation was monitored for 1, 3, 5 and 10 minutes (**a**, **b**, **c** and **d**). The thin -•-arrow designates the marker band of gas phase methanol.

6.4 Conclusions

In the first described experiment, adsorption of ^{13}C-labelled paraformaldehyde led to the formation of adsorbed paraformaldehyde and surface-bound formaldehyde (η^2-H_2CO), which was consumed after switching to the H_2/N_2. Surface carbonates were formed from carbon monoxide (^{13}CO), which was generated by H_2CO decomposition. In the gas phase ^{13}C-labelled methanol was clearly detected with its $\nu(^{13}C\text{-}O)$ signal at 1010 cm^{-1}. Subsequent adsorption of ^{12}C-formic acid resulted in the decomposition of HCOOH into H_2 and CO_2 and consequently hydrogenation of some carbonates into ^{13}CO.

Hydrogenation of the surface led to a reduction of all present paraformaldehyde species. Part of the carbonates were hydrolysed/decomposed to release $^{13}CO_2$; besides, additional non-reactive carbonates were formed. Labelled methanol was always present. Neither surface bound ^{13}CO, nor labelled surface formates were observed, even after long exposure and hydrogenation times. No detectable change in the concentration of surface hydroxyl groups was observed.

In the second experiment, the adsorption of ^{13}C-labelled formic acid generated surface carbonates and surface formates. No methanol or methylate signals were observed. Subsequently, adsorption of $H_2{}^{12}CO$ led rapidly to a formation of gas phase unlabelled CH_3OH ($\nu(^{12}C\text{-}O)$ band at 1032 cm^{-1}), and to the hydrolysis/decomposition of carbonates (rising $^{13}CO_2$ band). No labelled adsorbed paraformaldehyde was detected.

Under reducing atmosphere, a rise of ^{12}CO due to decomposition of $H_2{}^{12}CO$ together with a small decrease of formates and formation of carbonates were observed. No adsorbed CO was detected. Neither detectable production, nor decrease of surface hydroxyl groups were observed.

6.4.1 Water gas shift reaction

The observations suggest that CO and CO_2 can be interconverted via surface carbonates, according to the equilibria:

$$CO + 2\,{*}OH^- \leftrightarrow {*}CO_3^{2-} + H_2 + *$$
$${*}CO_3^{2-} \leftrightarrow {*}O^{2-} + CO_2$$
$$* + {*}O^{2-} + H_2O \leftrightarrow 2\,{*}OH^-$$

where * designates an adsorption site. This scheme is supported by the following observations. In the first experiment (Figure 6-1) the ^{13}C source is the ^{13}CO. $^{13}CO_2$ and ^{13}C-carbonates must be generated from this source. In the presence of water (consumption of gas phase water) carbonates will be hydrolysed/decomposed and $^{13}CO_2$ will be formed.

During the hydrogenation step some $^{12}CO_2$ is present and a little gas phase water is consumed (traces **e** and **f** in Figure 6-2), as the system is close to equilibrium. In the second experiment (Figure 6-3) ^{12}C-carbonates are generated from $^{12}CO_2$. During the hydrogenation step (Figure 6-4) ^{12}C-carbonates are reduced and some ^{12}CO together with gas phase water is produced. This result is also in agreement with previous observations [164-168].

6.4.2 Methanol formation

Additional useful information is provided on the methanol synthesis route. The observations suggest that surface-bound formaldehyde is the key intermediate according to the equilibria:

$${*}\eta\text{-}H_2CO + {*}OH^- \xleftrightarrow{H_2} {*}H_3CO^- + {*}OH_2$$
$${*}H_3CO^- + {*}OH_2 \leftrightarrow * + {*}OH^- + H_3COH$$

This is supported by the fact that it was not possible to find methylate or methanol without the presence of η^2-H_2CO on the surface (Figure 6-1, Figure 6-3, Figure 6-4), and that even after long exposure to the hydrogen atmosphere no surface formates species were reduced to methanol (Figure 6-2 and Figure 6-4), i. e. no methanol was observed with the same carbon isotope as in the formates.

Most importantly, the isotope of the carbon atom of methanol and of the adsorbed formaldehyde were always of the same (Figure 6-1, Figure 6-3, Figure 6-4). It was never possible to observe CO bound to the surface.

Hence, it is possible to conclude that the C-source of the methanol carbon is always the formaldehyde carbon respectively the η^2-H_2CO carbon. This result confirms the mechanism proposed from previous observations [73,164-168].

This is page 148 !

This page was left intentionally blank !

7. Investigation of a complex system

7.1 Introduction

In this chapter the application of the modulation concept to study the reaction pathway and the reaction rate constants of a complex solid-state catalysed reactions system is described.

Kinetic data of different reaction steps can be calculated by performing modulation experiments using different gas feed composition. The dynamic variations in the concentrations of products, intermediates and reactants are monitored *in situ* in the DRIFT cell. The observed phase shift ($\Delta\varphi$) is examined depending on the modulation frequency ω. This method is used to derive equilibrium constants and overall rate constants characterising the investigated reaction steps. By repeating the experiments at different temperatures, constant such as Arrhenius activation energies can be assessed.

The methanol synthesis starting from H_2/CO and H_2/CO_2 was chosen as test reaction. As described in sections 4.1 and 6.1, methanol is an important key compound in chemical industry. Nowadays, CH_3OH is mainly produced from H_2 and CO and/or CO_2 (synthesis gas [171]). At first sight, it might be suggested from a stoichiometric point of view, that carbon monoxide is directly hydrogenated to methanol. The CO_2 hydrogenation is more complicated, because the reverse water gas shift and the hydrogenation reactions occur simultaneously (see sections 6.1 and 6.4).

The classical catalysts for the methanol synthesis are based on copper-zinc oxide-alumina systems. CH_3OH synthesis over $Cu/ZnO/Al_2O_3$-based catalysts proceeds

via adsorption of carbon dioxide and hydrogen on the surface, to form formate species, which have been suggested as an intermediate of the methanol synthesis [172,173,174,175,176] and the water-gas shift reaction [177,178].

The hydrogenation of formates to methoxy-species is considered to be the rate determining step of the synthesis reaction, which starts from carbon oxides [179,180,181]. Neophytydes *et al.* [182] observed that formate species, which are created by the hydrogenation of carbon dioxide and are adsorbed on copper, are the key intermediates in the methanol synthesis. Performing experiments with labelled $^{14}CO_2$, Chinchen *et al.* [183] confirmed that CO_2 is the precursor of methanol.

$H_2 + 2* \leftrightarrow 2*H$	01
$CO_2 + * \leftrightarrow *CO_2$	02
$*CO_2 + * \leftrightarrow *CO + *O$	03
$CO + * \leftrightarrow *CO$	04
$O_2 + 2* \leftrightarrow 2*O$	05
$*CO_2 + *H \leftrightarrow *HCOO + *$	06
$*HCOO + *H \leftrightarrow *H_2CO_2 + *$	07
$*H_2CO_2 + *H \leftrightarrow *H_3CO + *O$	08
$*H_3CO + *H \leftrightarrow *H_3COH + *$	09
$H_3COH + * \leftrightarrow *H_3COH$	10
$*H_2CO_2 + * \leftrightarrow *H_2CO + *O$	11
$H_2CO + * \leftrightarrow *H_2CO$	12
$*H_2CO + *H \leftrightarrow *H_3CO + *$	13
$H_2O + * \leftrightarrow *H_2O$	14
$*H_2O + * \leftrightarrow *OH + *H$	15
$*OH + * \leftrightarrow *O + *H$	16
$2*OH + * \leftrightarrow *H_2O + *O$	17

Figure 7-1: Microkinetic reaction model for the methanol synthesis via CO_2 hydrogenation over Cu(100) [184]. The symbol * represents an adsorption site.

The complete reaction scheme is quite complicated, because several steps, which can be equilibrium processes, are involved. In Figure 7-1 a complete microkinetic model for the methanol synthesis via hydrogenation of CO/CO_2 over Cu(100) is presented [184]. It is noteworthy that in this model carbonates are not included. Similar models for the synthesis of CH_3OH over Cu single crystal were also proposed by other authors [133,134].

Previous studies performed on Cu/ZrO_2-based catalysts by Wokaun and co-workers [73,155,161-165,185,186] had shown that carbon oxide hydrogenation over copper/zirconia to yield methanol proceeds via a complete different reaction pathway.

Starting from CO_2, carbonates and formates are formed rapidly on the reduced surface. CO_3^{2-} is hydrogenated to CO and water, whereas the surface formate concentrations remain in *quasi* steady state. This step represents the reverse water gas shift reaction.

CO is adsorbed on the surface, hydrogenated, and surface-bound formaldehyde and formates are generated. Reduction of η-H_2CO leads to the formation of the methylate and subsequently methanol, whereas surface formates do not react to further intermediates or products [155] (see also chapter 6).

The reaction pathway of the CH_3OH synthesis is divided into different reaction steps to investigate the overall reaction in more detail. By using CO_2 it is possible to study the first part of the reaction, the reverse water gas shift reaction. With CO as reactant, the second part of the methanol synthesis reaction is examined. First, the CO and CO_2 adsorption processes are investigated to obtain information about the equilibrium rate constants and surface species. Then the CO_2 and CO hydrogenation reactions are analysed.

The application of zirconia-copper catalysts is of special interest due to their physical and thermodynamic properties (see chapter 6). A complete review about Cu/ZrO_2 catalysts can be found elsewhere [187].

7.2 Experimental

The used setup is similar to those presented in chapter 5. It consists of the gas dosing system *Modulation Unit* connected to the DRIFT cell, which was placed in the FTIR spectrometer. The whole setup is controlled using the *Lab-View* based program presented in section 2.2.

All spectra were recorded in the rapid scan mode with a resolution of 4 cm^{-1}. For transient measurements, 8 to 64 interferograms per spectrum and 1024 scans for the background spectra were accumulated.

The amorphous $Cu_{46}Zr_{54}$ alloy catalyst for CO oxidation was kindly provided by Prof. Dr. A. Baiker, and had been prepared as previously described [163]. A certain amount (0.298 g) of catalyst was placed into the DRIFT sample cup and packed as described in section 2.4.4 to ensure reproducibility [29-31].

First, some step up/step down test experiments were used to estimate the dead time between the gas dosing system *Modulation Unit* and the cell (see paragraph 3.3.4.1) as well as the ability of the catalyst to propagate a perturbation. In a second step, modulation experiments were started. The experiment was repeated applying different temperatures to monitor the influence of the temperature on the reaction. The concentration changes in step up/step down and modulation experiments exhibited the same order of magnitude.

Step up/step down and modulation experiments were performed as described in section 5.2. For the same modulation frequency two to four sets of experiments, each consisting of up to 60 spectra, were collected. The system was held under the same constant initial conditions for at least 30 minutes, before starting a new modulation experiment. A new background spectrum was collected for each new experiment. The first two sets of spectra were discarded, because they contained the initial adjustments of the system to external perturbations.

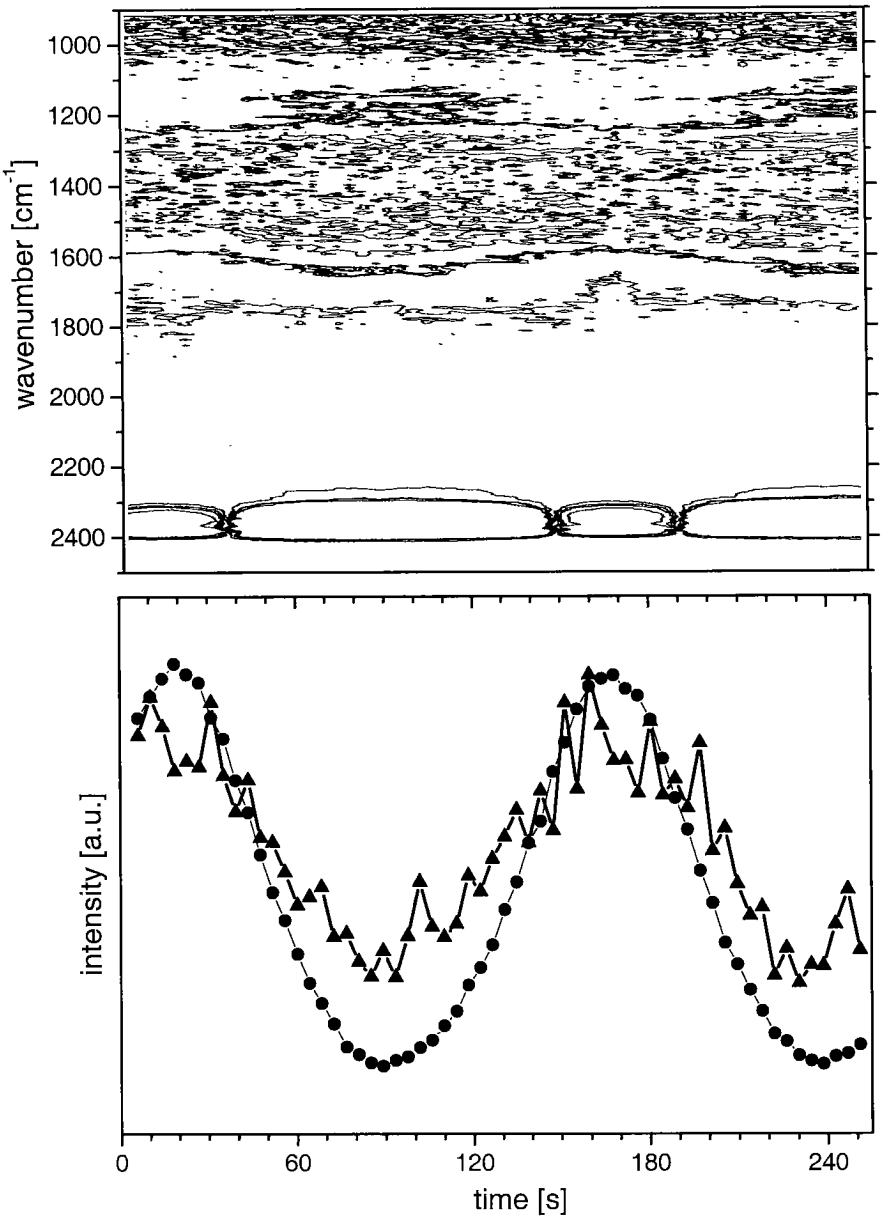

Figure 7-2: CO_2 adsorption experiment with the modulated reactant concentration. **Top**: contour plot of CO_2 modulation experiment performed at a frequency of 1/150 Hz, with a time resolution of 4.15 s per spectrum. The assigned bands are the signals of CO_2 at 2350 cm^{-1}, and of carbonate (CO_3^{2-}): broad bands located around 1600 and 1200 cm^{-1}. **Bottom**: time dependence of peak areas of CO_2 (●) and of CO_3^{2-} (▲) (magnified by a factor of 15) for the same modulation frequency of 1/150 Hz. The experiment was performed at 6 bar and 385 K. Feed composition: 10%-CO_2/N_2, 0.01 ± 0.0095 l_N min^{-1} and N_2 up to 0.09 l_N min^{-1}.

The used method to evaluate the collected spectra is described in detail in chapters 3 and 5. The dead time between the gas dosing system and the cell was determined by plotting the peak area of the modulated gas (CO or CO_2) as a function of time. The effective phase shift $\Delta\varphi$ of other components is deduced by plotting the peak area as a function of time, which was corrected for the measured dead time. In both cases, a mean value was calculated from each measured set of data to reduce the error.

In Figure 7-2 (top) a contour plot is shown as example for the obtained spectra during the CO_2 adsorption (first recorded trace at the left), where each trace is recorded within 4.15 seconds. At the bottom the corresponding peak area evolutions for the CO_2 adsorption are shown. The assigned bands are the signals of: CO_2 (●) at 2350 cm^{-1}, and the broad adsorption around 1600 cm^{-1} [169,182,188] for CO_3^{2-} (▲). The used integration limits are: CO_2: 2480-2250 cm^{-1} and CO_3^{2-}: 1800-1480 cm^{-1}.

In Figure 7-3 (top) a contour plot and (bottom) the corresponding peak area evolution, obtained during the CO adsorption experiment, are shown. Each trace is recorded within 4.16 seconds (first recorded trace at the left). The assigned bands are the signals of: CO (♦) at 2150 cm^{-1}, and adsorbed CO -CO_{ad}- (▼) at 2040 cm^{-1}. The used integration limits are: CO: 2250-2065 cm^{-1} and CO_{ad}: 2065-2015 cm^{-1}.

All experiments were performed at a total pressure of 6 bar and at the following temperatures of 328 K, 385 K, 442 K, 499 K, and 556 K. The feed gas compositions in the experiments are:

1. CO_2 adsorption: 10%-CO_2/N_2, 0.01 ± 0.0095 l_N min^{-1}.

2. CO adsorption: 10%-CO/N_2, 0.02 ± 0.0195 l_N min^{-1}.

3. CO_2 hydrogenation: 10%-CO_2/N_2, 0.01 ± 0.0095 l_N min^{-1}; H_2, 0.02 l_N min^{-1}.

4. CO hydrogenation: 10%-CO/N_2, 0.02 ± 0.0195 l_N min^{-1}; H_2, 0.02 l_N min^{-1}.

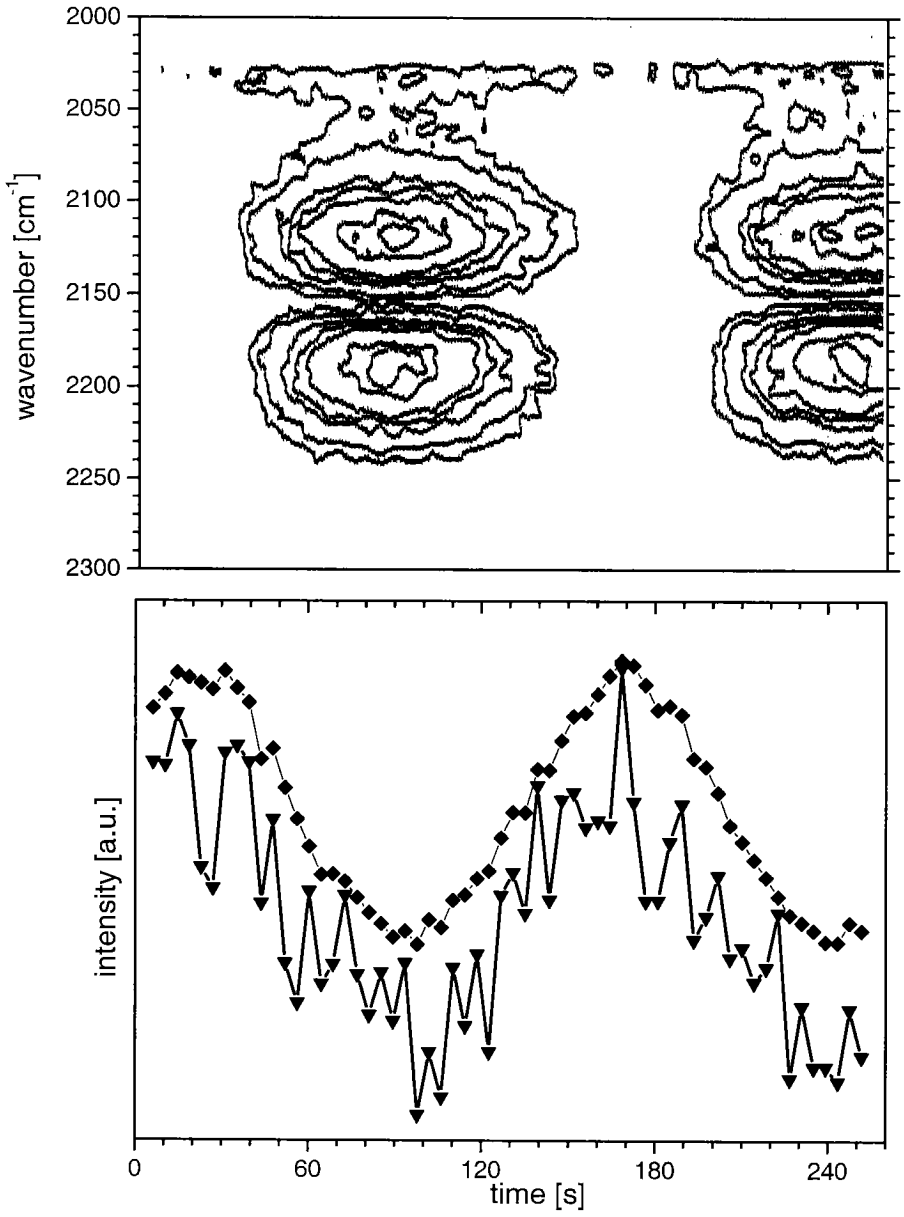

Figure 7-3: CO adsorption experiment with the modulated reactant concentration. **Top**: contour plot of the CO experiment performed at a frequency of 1/150 Hz, with a time resolution of 4.16 s per spectrum. The assigned bands are the signals of CO at 2150 cm^{-1}, and of CO adsorbed (CO_{ad}) at 2040 cm^{-1}. **Bottom**: time dependence of the peak areas of CO (♦) and of CO_{ad} (▼) (magnified by a factor 15) for the same modulation frequency of 1/150 Hz. The experiment was performed at 6 bar and 385 K. Feed composition: 10%-CO/N_2, 0.02 ± 0.0195 $l_N\ min^{-1}$ and N_2 up to 0.09 $l_N\ min^{-1}$.

Nitrogen was used as carrier and compensation gas. The overall flow was always kept constant at 0.09 l_N min^{-1}.

7.3 Results and discussion

As explained in chapter 3, the interpretation of the resulting retardations (phase shifts $\Delta\varphi$ or $\tan[\Delta\varphi]$) as function of a perturbation (modulation frequency ω) is an established method to obtain information about an unknown system.

A set of equations is used to model the investigated system (see section 3.4). From the temperature dependence, additional thermodynamic parameters of the reactions are determined.

The synthesis of methanol can be described by the following microkinetic model: adsorption of the C-supplying compound (CO or CO_2), adsorption and dissociation of hydrogen, reaction between the C-containing surface species and hydrogen to form intermediates, which react further to form new intermediates, and so on. The end products are methanol and, for CO_2, also water. The interactions of CO and CO_2 with the catalyst in an inert and hydrogen containing atmosphere are analysed separately, to estimate the kinetic data characteristic of each reaction step.

For all experiments the C-supplying reactant (CO or CO_2) was modulated. Unfortunately, only modifications in the concentration of the first surface species could be detected. It was, however, not possible to deduce any phase shift between gas phase and surface species within an acceptable error, because the signal of the adsorbed species was always in phase with the signal of the reactant in the gas phase (see also Figure 7-2 and Figure 7-3). Test experiments using higher modulation frequencies were performed to resolve the phase shifts. The resulting amplitude of the concentration variation was unfortunately not large enough to define the retardation.

Additional test experiments with higher amplitudes and longer periods were performed for the CO_2 and CO hydrogenation reactions to study the perturbation of further intermediates and products. The resulting signals were again not strong enough to identify these compounds or to define a retardation $\Delta\varphi$ within an acceptable error.

7.3.1 CO_2 adsorption on the reduced catalyst

7.3.1.1 Model

A modulation experiment was carried out to estimate the interaction of a reactant gas (CO_2) with the catalyst surface (see section 7.3.2). Under the used conditions it was not possible to distinguish between carbonite ($CO_2^{\delta-}$), which has the asymmetric stretching vibration around 1540 cm^{-1} [185,189,190] and carbonates, which have a broad absorption band around 1600 cm^{-1}. The existence of carbonates on the surface was confirmed by the presence of the bands around 1200 cm^{-1} [185]. However, this does not exclude the existence of $CO_2^{\delta-}$ species on the surface at concentrations below the detection limit of DRIFT, or as high frequency part of the carbonate bands at 1600 cm^{-1}.

The used model implies that carbon dioxide adsorbs and generates carbonates [73] immediately. To obtain a better propagation of the perturbation, the largest possible amplitude was used. The lowest possible partial pressure was applied in order to avoid unwanted effects, such as saturation of the surface as well as an influence of the concentration of vacant adsorption sites. Applying a reduced carbon dioxide partial pressure has the consequence that the changes in the gas phase concentration are limited. Therefore, it is possible to assume that the surface coverage is low and that the number of vacant CO_2 adsorption site remains *quasi* constant. The following simple model can be derived:

$$CO_2 \underset{k_{-1}}{\overset{k_1}{\rightleftharpoons}} CO_3^{2-}$$

Here, k_1 and k_{-1} are effective first order rate constants. As explained in section 3.3.2, the DRIFT cell can be represented by a continuous stirred tank reactor with a residence time τ. Therefore, the system can be described with the following set of differential equations:

$$\frac{dCO_2}{dt} = \frac{CO_{2,0}}{\tau} - (k_1 + \frac{1}{\tau})\, CO_2 + k_{-1} CO_3^{2-} \tag{7.1}$$

$$\frac{dCO_3^{2-}}{dt} = k_1 CO_2 - k_{-1} CO_3^{2-} \tag{7.2}$$

$CO_{2,0}$ represents the gas phase concentration of carbon dioxide in the feed gas and CO_2 in the DRIFT cell, CO_3^{2-} is the surface concentration of carbonates. The set of differential equations is solved for CO_2 and CO_3^{2-}. Equations as function of ω and ω^2 (see Equation 3.28) are obtained. As explained in paragraph 3.4.2.1, the ω^2 terms are only important when high frequencies are applied. Therefore, the low frequency approximation can be applied and the linearity between the tangent of the phase shift ($\tan[\Delta\varphi]$) and the perturbation frequency (ω) is obtained:

$$\tan\,[\Delta\varphi(CO_{2,0} - CO_2)] = \omega\,\tau\,(1 + \frac{k_1}{k_{-1}}) \tag{7.3}$$

$$\tan\,[\varphi(CO_2) - \varphi(CO_3^{2-})] = \frac{\omega}{k_{-1}} \tag{7.4}$$

In Equation 7.3 an equilibrium constant k_1/k_{-1} appears, rather than an individual rate constant as in Equation 7.4 (see paragraph 3.4.2.1). The temperature influence was estimated, as explained in chapter 3. The residence time (τ) is modelled using Equation 3.9, which was derived from ideal gas law (see Equation 3.8). For the rate constants k_1

and k_{-1} the Arrhenius Equation was used (see Equation 3.10). The pre-exponential factor k_0 was assumed to be temperature independent.

$$\tau(T) = \frac{k_\tau}{T} \tag{3.9}$$

$$k(T) = k_0 e^{-\frac{E_A}{RT}} \tag{3.10}$$

As explained in section 5.3.1 the equilibrium constant $K(T)$ of the reaction can be easily derived from Equation 3.10:

$$K(T) = \frac{k_1}{k_{-1}} = K_0 e^{-\frac{\Delta E_A}{RT}} \tag{5.5}$$

Here ΔE_A is the difference of the Arrhenius activation energies between the adsorption and desorption process. The sign of ΔE_A indicates whether the equilibrium process favours reactants or products.

7.3.1.2 Experimental results

In Figure 7-2 a contour plot and the peak area evolution for a CO_2 adsorption experiment are shown. An example for the evolution of the phase shifts as a function of the modulation frequencies is illustrated in Figure 7-4. Open triangles (△) display the frequency dependence of $\tan[\Delta\varphi(CO_{2,0}\text{-}CO_2)]$ found for the lowest applied temperature (328 K), and filled triangles (▲) for the highest temperature (556 K). As expected, the phase shifts can be approximated by straight lines with zero crossing. The arrow indicates the direction of the slope change caused by increasing temperatures.

The obtained slope contains information about the reaction ($K_{1,0}$ and $\Delta E_{A,1}$) as well as the residence time (k_τ). The evolution of the slope values as function of temperature is shown in Figure 7-5. A monotonous temperature dependence of the adsorption/

desorption process was found. The curve was fitted with Equation 3.9 and 5.5 inserted into Equation 7.3. The obtained values are:

$k_\tau = 9'904 \pm 1'928$ Ks $\quad K_{0,1} = 51 \pm 11$ $\quad \Delta E_{A,1} = 13.2 \pm 1.7$ kJ mol^{-1}

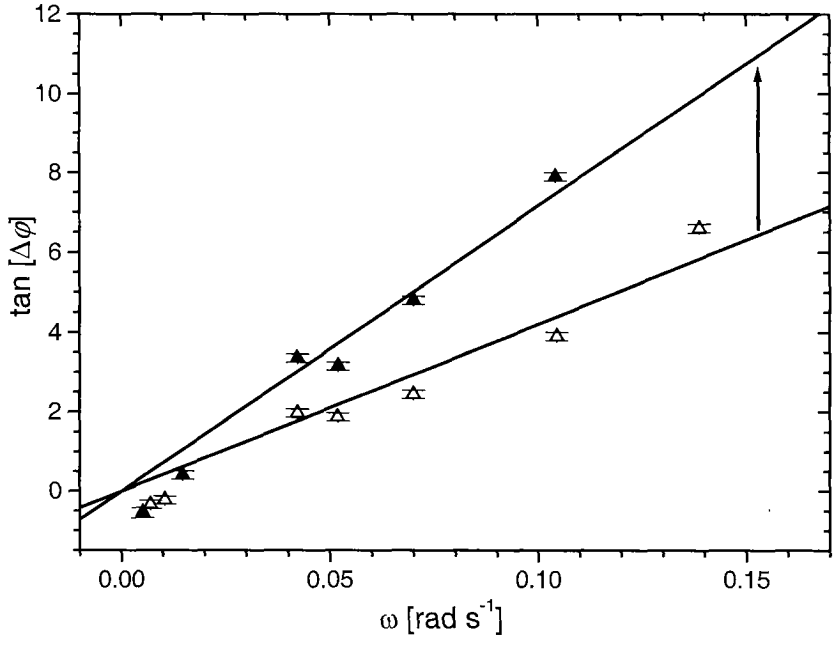

Figure 7-4: Phase shifts from CO_2 adsorption experiment: variation of $\tan[\Delta\varphi(CO_{2,0}\text{-}CO_2)]$ as function of ω for the lowest (328 K: △), and for the highest (556 K: ▲) temperature. The measurements were performed at 6 bar with a feed composition of 10%-CO_2/N_2, 0.01 ± 0.0095 l_N min^{-1} and N_2 up to 0.09 l_N min^{-1}.

The equilibrium values ($K_{0,1}$ and $\Delta E_{A,1}$) are not likely to correspond to a molecular level reaction, but describe an overall equilibrium reaction. $\Delta E_{A,1}$ is positive, indicating an energy consuming adsorption reaction and a shift of the equilibrium to the side of the gas phase. With increasing temperature the slope increases, suggesting the equilibrium shifts towards the adsorbed species.

The adsorption of CO_2 on Cu(100) single crystals has an adsorption energy of 27.3 kJ mol^{-1} [133].

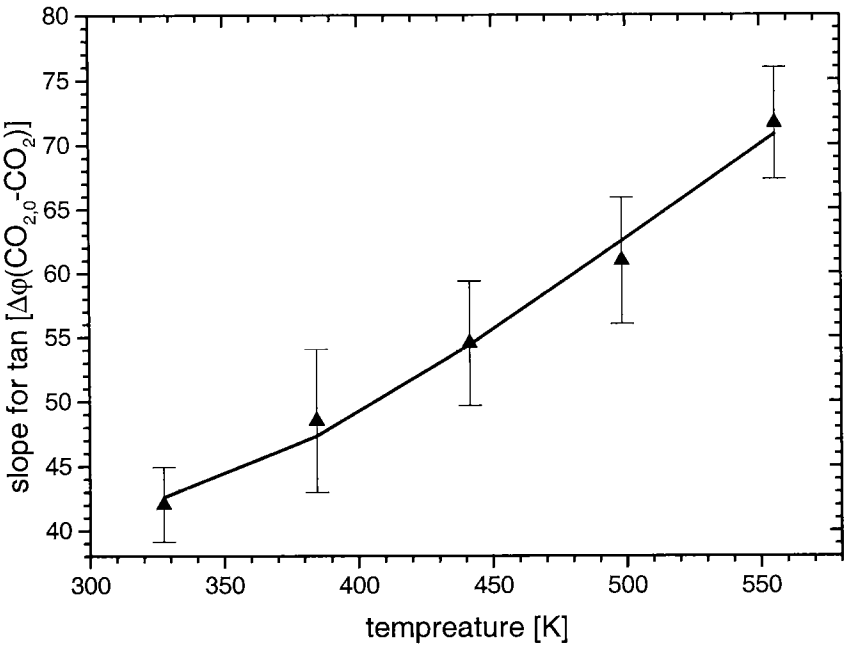

Figure 7-5: Variation of the slopes for tan[$\Delta\varphi(CO_{2\ 0}\text{-}CO_2)$] (▲) as a function of the temperature. The curve was modelled using Equation 7.3, with Equations 3.9 and 5.5. Experimental conditions are the same as in Figure 7-4.

The impossibility to resolve the phase shift between gas phase (CO_2) and surface (CO_3^{2-}) compounds indicates a rapid equilibrium adjustment, which supports the observation of a positive $\Delta E_{A,1}$ for the adsorption/desorption process, as well as the assumption that adsorbed CO_2 is immediately converted into carbonates.

7.3.2 CO adsorption on the reduced catalyst

7.3.2.1 Model

In this experiment the interaction of a reactant gas (CO) with the catalysts surface was investigated. Similar to CO_2, a large amplitude and a low partial pressure of the modulating gas were used. As in the previous section (7.3.1), it was assumed that,

during the experiment, the surface concentration of vacant CO adsorption sites was constant.

An additional advantage of a low partial pressure is the reduced influence of the carbon monoxide gas phase signal (2150 cm^{-1}) on the quality of CO surface signal (2040 cm^{-1}). For large modulation amplitudes, no strong changes in the intensity of the CO band are induced.

The simplified model can be written as:

$$CO \underset{k_{-3}}{\overset{k_3}{\rightleftharpoons}} CO_{ad}$$

The same assumptions are also valid in this case: a) k_3 and k_{-3} are effective first order rate constants, and b) the DRIFT cell can be represented by a continuous stirred tank reactor with the residence time τ. According to these assumptions, the system can be describe using Equations 7.1 and 7.2, where, CO_2 should be substituted by CO, k_1 with k_3 and k_{-1} with k_{-3}.

$$\frac{dCO}{dt} = \frac{CO_0}{\tau} - (k_3 + \frac{1}{\tau})\, CO + k_{-3} CO_{ad} \tag{7.5}$$

$$\frac{dCO_{ad}}{dt} = k_3 CO - k_{-3} CO_{ad} \tag{7.6}$$

where CO_0 represents the CO concentration in the feed gas, CO the concentration of carbon monoxide in the DRIFT cell, and CO_{ad} the concentration of the adsorbed species. Equations 7.5 and 7.6 are solved under the same assumptions as in the previous section for CO_2. Linear relations between the tangent of the phase shift and the modulation frequency are obtained:

$$\tan\ [\varphi(CO_0) - \varphi(CO)] = \omega\,\tau\,(1 + \frac{k_3}{k_{-3}}) \tag{7.7}$$

$$\tan\ [\varphi(CO) - \varphi(CO_{ad})] = \frac{\omega}{k_{-3}} \tag{7.8}$$

As in Equation 7.3, Equation 7.7 contains a rate constant describing an equilibrium (k_3/k_{-3}). The temperature dependence of τ is approximated with Equation 3.9 and the equilibrium with Equation 5.5.

7.3.2.2 Experimental results

In Figure 7-3 a contour plot and the peak area evolution for a CO adsorption experiment are presented.

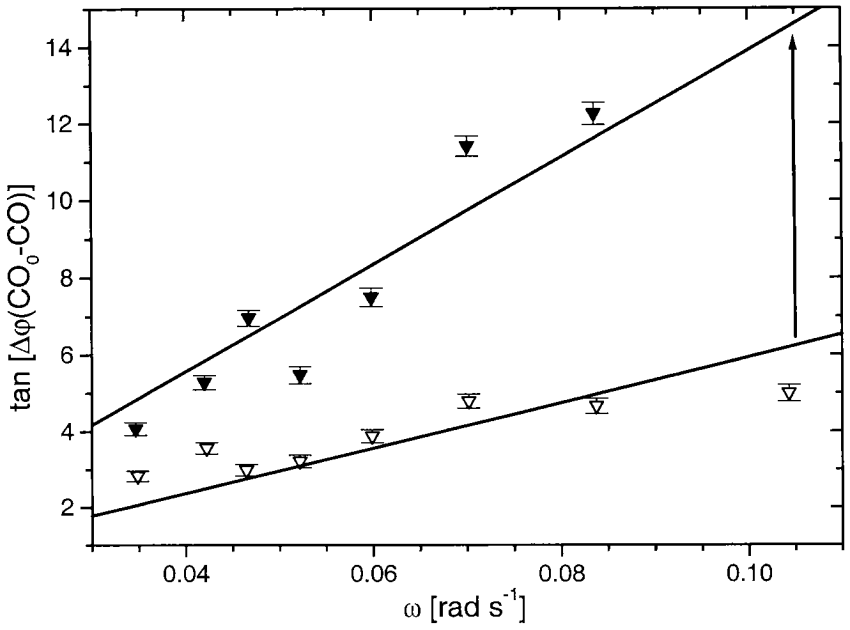

Figure 7-6: Variation of tan[$\Delta\varphi$(CO_0-CO)] as function of ω for the lowest (328 K: ▽) and for the highest (556 K: ▼) temperature during the CO adsorption experiment. The measurements were performed at 6 bar with a feed composition of 10%-CO/N_2, 0.02 ± 0.0195 $l_N\ min^{-1}$ and N_2 up to 0.09 $l_N\ min^{-1}$.

An example for the evolution of the phase shifts as function of the modulation frequency is illustrated in Figure 7-6. The lower curve (▽) displays the tan[$\Delta\varphi$(CO_0-CO)] for the lowest temperature (328 K) and the upper curve (▼) shows tan[$\Delta\varphi$(CO_0-CO)] for the highest temperature (556 K). The phase shifts can be approximated by straight lines with zero crossing. The arrow indicates the direction of the slope change caused by increasing temperatures.

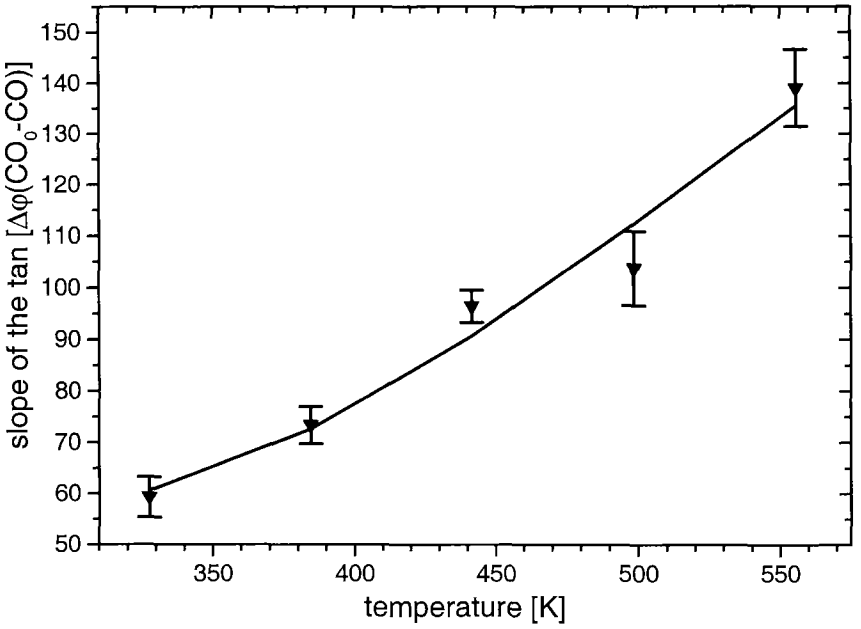

Figure 7-7: Variation of the slopes for tan[$\Delta\varphi$(CO_0-CO)] (▼) as a function of the temperature. The curve was modelled using Equation 7.7 together with Equations 3.9 and 5.5. Experimental conditions are the same as in Figure 7-6.

In Figure 7-7 the evolution of the slope as function of the temperature is shown. Information about the equilibrium ($K_{0,3}$ and $\Delta E_{A,3}$) and the geometry of the reactor (k_τ) can be obtained from the slopes. The curve is fitted using Equation 7.7 together with Equations 3.9 and 5.5. The obtained values are:

k_τ = 13'530 ± 6'078 K s $K_{0,3}$ = 121 ± 58 $\Delta E_{A,3}$ = 15.1 ± 4.1 kJ mol^{-1}

The expectancy value for k_τ differs slightly from the value obtained for the CO_2 adsorption/desorption process in the previous experiment (see section 7.3.1). The difference is probably due to the reduced quality of the data. This hypothesis is supported by the large standard deviations, making the difference between the two k_τ values insignificant.

It is noteworthy that the adsorption energy obtained in this experiment (15.1 kJ mol^{-1}) is very different from the value ($\approx$ 53.9 kJ mol^{-1}) of CO on Cu(100), Cu(110) or Cu(111) [133]. The large difference between the values indicates an important influence of the support (zirconia) on the physico-chemical characteristic of the copper catalyst.

The positive value of $\Delta E_{A,3}$ suggests that the adsorption reaction is energy consuming and that the equilibrium is on the side of the gas phase compound. The increase of the slope, with increasing temperature, indicates a shift of the equilibrium towards the adsorbed species. This result agrees with the observation that, in absence of gas phase CO, the CO_{ad} concentration decreases rapidly below the detection limit (data not shown). Chorkendorff *et al.* have demonstrated, by using temperature programmed desorption experiments in ultra high vacuum (TPD-UHV), that on a pure copper single crystal (100) no carbon monoxide can be adsorbed on the surface at temperatures above 293 K [191,192].

The evidence that the signals of CO and CO_{ad} are always in phase (see also Figure 7-3) confirms the rapid equilibrium adjustment between the two species and supports the observation of a positive $\Delta E_{A,3}$.

7.3.3 CO_2 hydrogenation reaction

7.3.3.1 Model

This modulation experiment was carried out to investigate the influence of the carbon dioxide during CO_2 hydrogenation reaction over the Cu/ZrO_2-based catalyst.

Several authors report [161-165,185,186] that the CO_2 hydrogenation over these catalysts has the following reaction pathway: CO_2 adsorbs on the reduced surface, generating formates and carbonates. Carbonates are converted to CO via the reverse water gas shift reaction. Subsequent hydrogenation of adsorbed carbon monoxide results in the formation of surface-bound formaldehyde and methylate. No reaction of formates to further intermediates or products could be detected [155] (see also chapter 6).

The following assumptions were made to assess a simplified model for CO_2-modulation.

(1) As explained in section 7.3.1, it was not possible under the used conditions to discriminate between carbonite ($CO_2^{\delta-}$) and carbonates (CO_3^{2-}). It is assumed that gas phase carbon dioxide is adsorbed and forms immediately carbonates.

(2) It is assumed that the CO_3^{2-} decomposition process to CO_2 is much faster than the carbonates hydrogenation reaction, which results in an undefined surface intermediate species [#].

The validity of these assumptions is supported by the evidence that the applied perturbations do not propagate observably further along the reaction pathway; and no changes of formates, surface-bound formaldehyde and methylate bands could be detected. Only the concentrations of carbon dioxide and carbonates are changing.

(3) H_2 is used in excess. This allows the assumption of a saturation of hydrogen on the surface. As a consequence the rate constants of the different reaction steps are not

dependent on hydrogen surface concentration. Furthermore, the equilibrium of any reversible hydrogenation reaction step would be shifted towards the product side, and any possible dehydrogenation (reverse) reactions would be inhibited. Therefore, an overall first order rate constant (k_2') describing the CO_3^{2-} hydrogenation reaction was used.

A low CO_2 partial pressure and a large amplitude are used and a *quasi* constant concentration of vacant CO_2 adsorption sites is assumed (see section 7.3.2). A simple model is chosen to describe the reaction.

$$CO_2 \underset{k_{-1}}{\overset{k_1}{\rightleftharpoons}} CO_3^{2-} \xrightarrow{k_2'} [\#]$$

k_1, k_{-1} and k_2' are effective first order rate constants. As explained in section 3.3.2 the DRIFT cell is represented by a continuous stirred tank reactor with residence time τ. With these assumptions the system can be modelled using differential equations 7.1 and 7.9.

$$\frac{dCO_2}{dt} = \frac{CO_{2,0}}{\tau} - (k_1 + \frac{1}{\tau})\, CO_2 + k_{-1} CO_3^{2-} \qquad (7.1)$$

$$\frac{dCO_3^{2-}}{dt} = k_1 CO_2 - (k_{-1} + k_2')\, CO_3^{2-} \qquad (7.9)$$

Solving this system for CO_2 and CO_3^{2-}, with the same procedure as in the previous sections and assuming $k_{-1} >> k_2$' (see assumption 2 above) the phase shifts can be written as:

$$\tan\,[\Delta\varphi(CO_{2,0} - CO_2)] = \omega \frac{(1 + \frac{k_1}{k_{-1}})}{(\tau^{-1} + \frac{k_1}{k_{-1}} k_2')} \qquad (7.10)$$

$$\tan\ [\varphi(CO_2) - \varphi(CO_3^{2-})] = \frac{\omega}{k_{-1} + k_2'} \qquad (7.11)$$

In Equation 7.10 the equilibrium constant k_1/k_{-1} appears together with the individual rate constant k_2' (see paragraph 3.4.2.1). If k_2' approaches zero, equations 7.10 and 7.11 are transformed into equations 7.3 and 7.4. As in the previous sections, the temperature dependence of the residence time and of the rate constants are estimated using equations 3.9, 3.10 and 5.5.

7.3.3.2 Experimental results

In Figure 7-8 the tangents of the phase shifts for different modulation frequencies and temperatures (328 K (▽) and 499 K (■)) are illustrated.

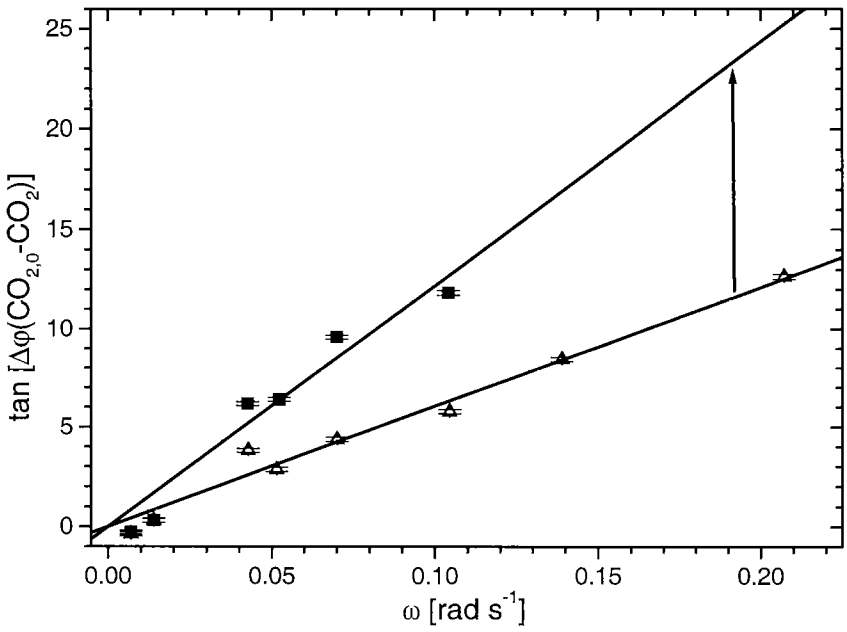

Figure 7-8: Phase shifts evolution for the CO_2 hydrogenation experiment. Variation of tan[$\Delta\varphi(CO_{2,0}$-$CO_2)$] as function of ω for the lowest (328 K: ▽) and for the temperature with the highest slope (499 K: ■). The measurements were performed at 6 bar with a feed composition of 10%-CO_2/N_2, 0.01 ± 0.0095 $l_N\ min^{-1}$; H_2, 0.02 $l_N\ min^{-1}$ and N_2 up to 0.09 $l_N\ min^{-1}$.

All phase shifts are approximated by straight lines with zero crossing. The arrow indicates the direction of the slope changes caused by increasing the temperature.

The slopes contain information about the equilibrium reaction between CO_2 and CO_3^{2-}, the hydrogenation reaction of carbonates (k_2'), and the residence time of the DRIFT cell. To assess the temperature dependence of the different parameters the slopes of $\tan[\Delta\varphi(CO_{2,0}\text{-}CO_2)]$ are plotted versus the temperature (see Figure 7-9).

With increasing temperature, the slope increases first and consequently decreases again. This suggests that, with increasing temperature, the CO_2 adsorption reaction becomes more pronounced.

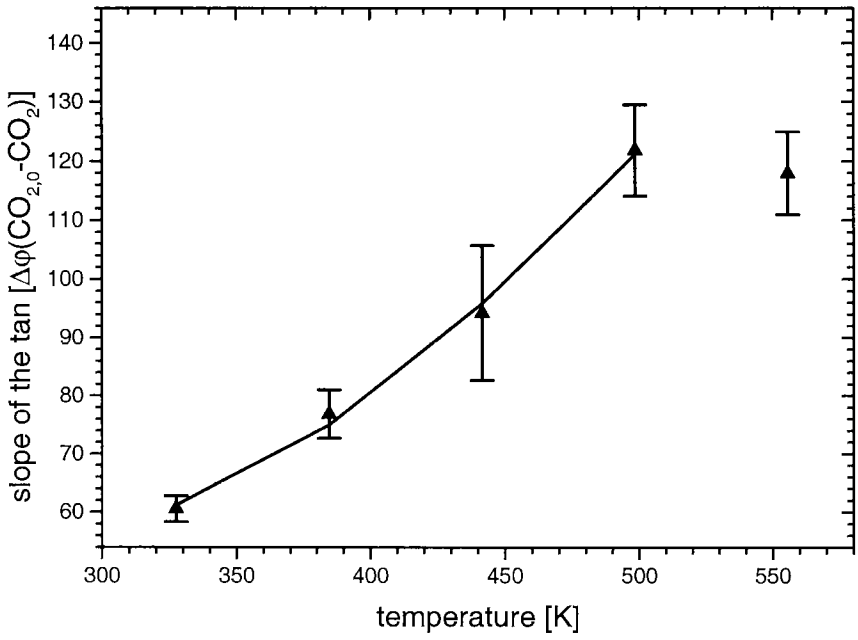

Figure 7-9: Variation of the slopes for $\tan[\Delta\varphi(CO_{2,0}\text{-}CO_2)]$ (▲) as a function of the temperature. The curve was modelled using Equation 7.10, with Equations 3.9 and 5.5. k_1/k_{-1} was approximated using the values estimated in section 7.3.2. Experimental conditions are the same as in Figure 7-8.

Using temperatures above 500 K another reaction becomes more pronounced. In section 7.3.1 the evolution of the adsorption/desorption reaction was not found to indicate an increased desorption for the higher temperatures (556 K). Therefore, an increase in the carbonate hydrogenation reaction can be deduced.

In a first step, the curve plotted in Figure 7-9 was fitted using equations 3.9, 3.10 and 5.5 substituted in equation 7.10. The values describing the equilibrium between CO_2 in the gas phase and on the surface (k_1/k_{-1}) were substituted by the parameters estimated in section 7.3.1. The parameters deduced from the fit would suggest an enhanced dehydrogenation ($k_{0,2}' < 0$) of the undefined intermediates [#], indicating that the applied model is not adequate.

Therefore, it was assumed that the carbonate hydrogenation reaction can be neglected ($k_2' \approx 0$). The curve shown in Figure 7-9 was fitted using equation 7.3. Due to this simplification assumption 3 is not any longer valid. New parameters describing the adsorption/desorption equilibrium (k_1'/k_{-1}') are estimated. The obtained values are:

$k_\tau = 13'497 \pm 2'787$ K s $\qquad K_{0,1}' = 151 \pm 50 \qquad \Delta E_{A,1}' = 15.6 \pm 2.3$ kJ mol^{-1}

The calculated activation energy ($\Delta E_{A,1}'$) is close to the value obtained in the previous section (7.3.1) for the CO_2 adsorption, suggesting that the CO_3^{2-} hydrogenation reaction is of minor importance, and that an adsorption/desorption equilibrium is the dominant process. This result confirms assumptions 1 and 2. The values of the pre-exponential factor ($K_{0,1}'$) and residence time (k_τ) have a large standard deviation. This is probably due to the presence of hydrogen, and represents an indirect evidence for a CO_3^{2-} hydrogenation reaction.

The CO_3^{2-} and CO_2 signals are always in phase, suggesting that the equilibrium between these two species is the dominant step. This observation confirms also the validity of assumptions 1 and 2.

7.3.4 CO hydrogenation reaction

7.3.4.1 Model

The modulation experiment was carried out to investigate under reaction conditions the interaction between CO and the surface of the Cu/ZrO_2 catalyst. As reported by several authors [161-165,185,186] CO is adsorbed on the surface of the catalyst, then reduced to surface-bound formaldehyde and subsequently to methoxy species. The generated formates show an improved stability even in a strong reducing atmosphere [185].

To assess a simplified model for CO-modulation experiments, the following assumptions are made.

(1) Adsorbed carbon monoxide (CO_{ad}) can desorb or react with hydrogen surface groups to form an undefined surface species [#]. The desorption process is much faster than the CO_{ad} hydrogenation reaction.

The validity of this assumption is supported by the fact that perturbations do not propagate along the reaction pathway observably. Only changes in the concentration of CO_{ad} can be clearly monitored, whereas modification of other surface species concentration can not be detected.

(2) Using an excess of H_2 allows one to assume a saturation of hydrogen on the surface. As a consequence, the rate constants of the different reaction steps are not dependent on the hydrogen surface concentration. Furthermore, each hydrogenation reaction step is shifted towards the product side, and any possible dehydrogenation (reverse) reaction is inhibited. Therefore, an overall first order rate constant (k_4') can be used to describe the CO_{ad} hydrogenation reaction.

As in the previous section a large amplitude and a low CO partial pressure are applied, and a *quasi* constant concentration of vacant CO adsorption sites is assumed. In view of these limitations a simple reduced model can be chosen.

$$CO \underset{k_{-3}}{\overset{k_3}{\rightleftharpoons}} CO_{ad} \xrightarrow{k_4'} [\#]$$

k_3, k_{-3} and k_4' are effective first order rate constants, with the same assumptions as described previously for the DRIFT cell (see section 3.3.2). The following set of differential equations is used to describe the system:

$$\frac{dCO}{dt} = \frac{CO_0}{\tau} - (k_3 + \frac{1}{\tau})\, CO + k_{-3} CO_{ad} \tag{7.5}$$

$$\frac{dCO_{ad}}{dt} = k_3 CO - (k_{-3} + k_4')\, CO_{ad} \tag{7.12}$$

The system is solved for CO and CO_{ad}, in an analogous way to the previous sections, and assuming $k_{-3} >> k_4$' (see assumption 1 above). The linear relationship between retardation (tan[$\Delta\varphi$]) and perturbation (ω) can be written as:

$$\tan\,[\Delta\varphi(CO_0 - CO)] = \omega \frac{(1 + \frac{k_3}{k_{-3}})}{(\tau^{-1} + \frac{k_3}{k_{-3}} k_4')} \tag{7.13}$$

$$\tan\,[\varphi(CO) - \varphi(CO_{ad})] = \frac{\omega}{k_{-3} + k_4'} \tag{7.14}$$

In Equation 7.13 an equilibrium constant k_3/k_{-3} appears together with an individual rate constant k_4' (see paragraph 3.4.2.1). If k_4' approaches zero, the equations 7.13 and 7.14 describe only the adsorption/desorption process (see section 7.3.2). As in previous sections, the temperature dependence of the residence time and of the rate constants are estimated using equations 3.9, 3.10 and 5.5.

7.3.4.2 Experimental results

In Figure 7-10 the tangents of the phase shifts for different modulation frequencies and for temperatures of 328 K (▽) and 556 K (▼) are illustrated. All phase shifts are approximated by straight lines with zero crossing. The arrow indicates the direction of the slope changes caused by increasing the temperature.

The slopes contain information about the adsorption/desorption equilibrium of CO, the hydrogenation reaction (k_4') of the adsorbed carbon monoxide species, as well as the residence time of the DRIFT cell. The temperature dependence of the different parameters is obtained by plotting the slopes of tan[$\Delta\varphi$(CO_0-CO)] versus the temperature (see Figure 7-11).

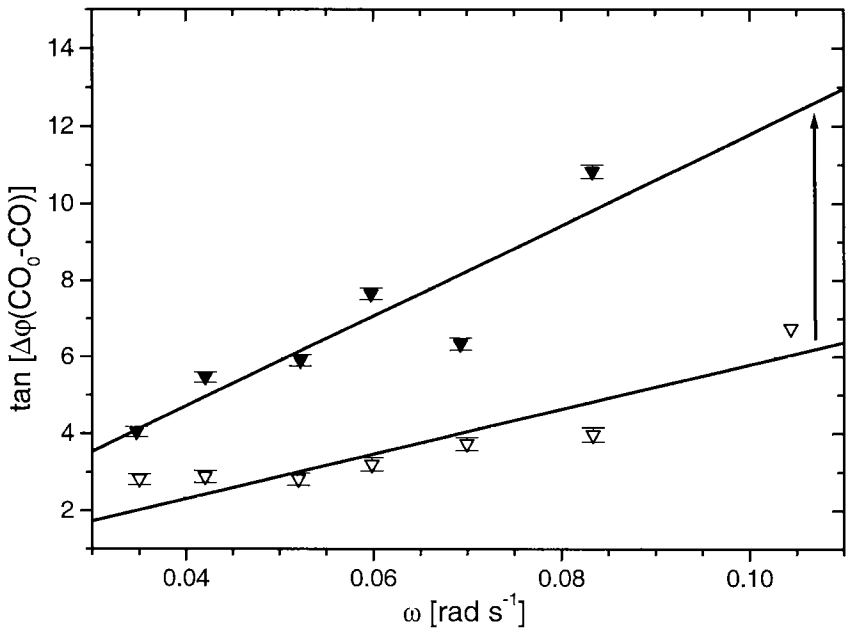

Figure 7-10: Phase shifts evolution for the CO hydrogenation experiment. Variation of tan[$\Delta\varphi$(CO_0-CO)] as function of ω for the lowest (328 K: ▽) and for the highest (556 K: ▼) temperature. The measurements were performed at 6 bar with a feed composition of 10%-CO/N_2, 0.02 ± 0.0195 l_N min^{-1}; H_2, 0.02 l_N min^{-1} and N_2 up to 0.09 l_N min^{-1}.

The increase of the slope with increasing temperature indicates that the CO adsorption/desorption process is the dominant reaction. This result confirms assumption 1 (see above). A change between increasing and decreasing behaviour, as for CO_2 hydrogenation experiments, is not observed.

The curve plotted in Figure 7-11 is fitted using equations 3.9, 3.10 and 5.5 inserted in equation 7.13. The values describing the equilibrium between CO in gas phase and on the surface (k_3/k_{-3}) are substituted with the parameters estimated in section 7.3.2. The obtained values are:

$k_\tau = 13'507 \pm 117$ K s $\qquad k_{0,4}' = 20.0 \pm 0.4 \cdot 10^{-3}$ s $\qquad E_{A,4}' = 31.3 \pm 1.2$ kJ mol^{-1}

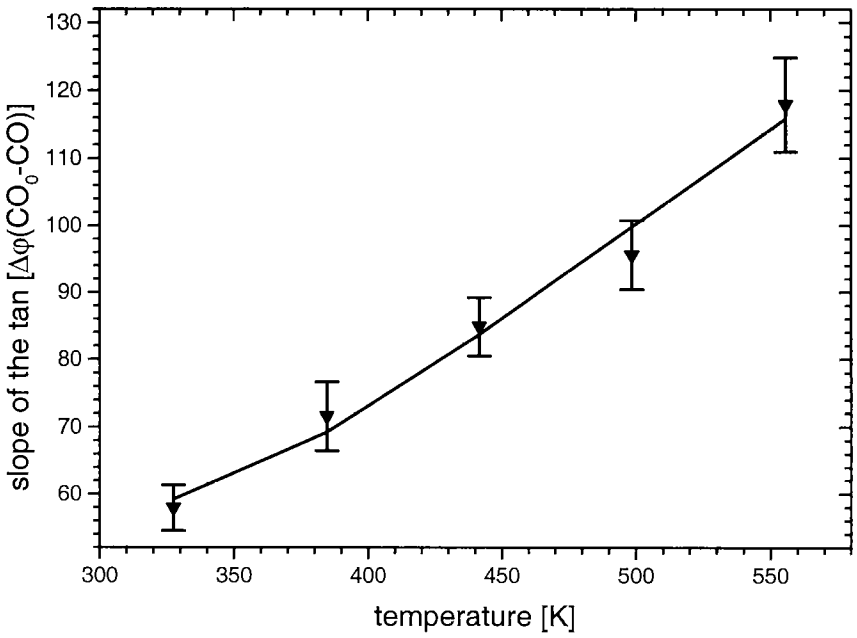

Figure 7-11: Variation of the slopes for tan[$\Delta\varphi(CO_0\text{-}CO)$] (▼) as a function of the temperature. The curve was modelled using Equation 7.13, with Equations 3.9 and 5.5. k_3/k_{-3} was approximated using the values estimated in section 7.3.2. Experimental conditions are the same as in Figure 7-10.

As expected, the CO_{ad} hydrogenation reaction can be approximated with an overall first order rate constant (k_4'). This suggests that the hydrogenation of carbon monoxide on

the surface is faster than the dehydrogenation of the intermediate [#]. This confirms assumption 2 (see above).

The signals of CO and CO_{ad} are always in phase, indicating a rapid equilibrium adjustment between the two species. This result suggests that the desorption reaction should be at least fast as the CO_{ad} hydrogenation, again confirming assumption 1 (see above). If the hydrogenation process would be faster the slopes for $\tan[\Delta\varphi(CO_0\text{-}CO)]$ would decrease with increasing temperature (see section 5.3.3).

7.4 Conclusions

7.4.1 Methanol synthesis via hydrogenation of CO

Tracing the propagation of perturbations along the reaction pathway is very difficult. For modulation of carbon monoxide in the gas phase, oscillatory components in the DRIFT signals could be detected only for adsorbed CO (CO_{ad}). Gas phase and surface CO are always in equilibrium, as demonstrated by the problems to estimate a rate constant for the desorption reaction. In the presence of hydrogen, the existence of an intermediate, which is formed by hydrogenation of CO_{ad}, is supported by the fact that it is possible to estimate the rate constant k_4'. The nature of the latter intermediate [#] could not be established from the present experiment due to a strong attenuation of the propagated modulation amplitudes.

Test experiments with modifications of hydrogen concentration were used to investigate whether the signals of the intermediates remain insensitive to perturbations. Hydrogen is active in several steps of the reaction pathway (see Figure 7-1). Therefore, changes in the H_2 concentration would be expected to induce modifications of surface concentration of various compounds (see chapter 4). As example, the peak area

evolution of the different species during a hydrogen step up/step down test experiment is shown in Figure 7-12.

The reduction of the hydrogen concentration in the gas phase induces a decrease of the consumed carbon monoxide, which corresponds to an increase of the gas phase concentration (▼ in Figure 7-12, magnified by 0.2). Carbon dioxide (▲ in Figure 7-12) is rapidly formed and after 2.5 minutes decreases in intensity. The concentration of adsorbed CO (● in Figure 7-12) increases. Carbonates and formates (data not shown) increase similarly to adsorbed CO. Meanwhile, the concentration of η-H_2CO (■ in Figure 7-12) is decreasing. No changes in the concentration of surface methylate could be detected.

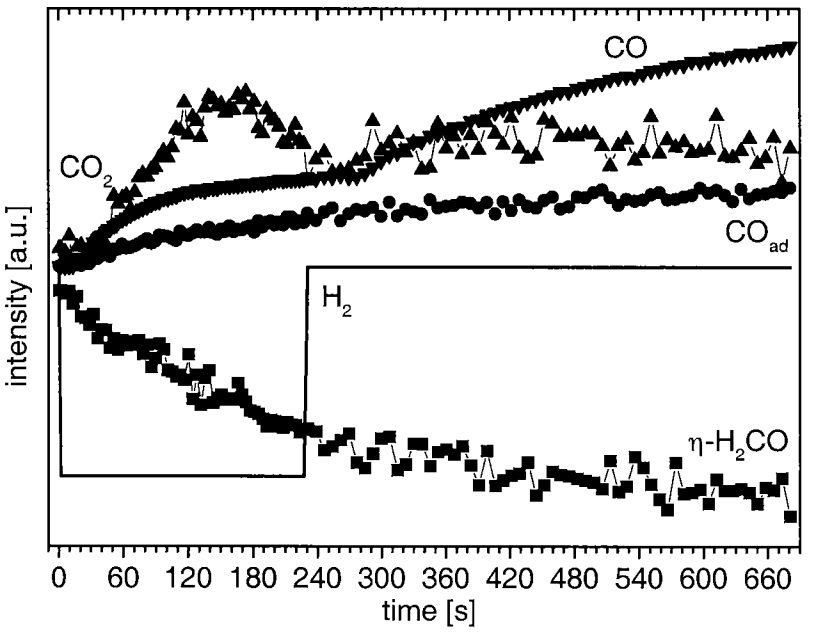

Figure 7-12: Peak area evolution of CO (▼), CO_2(▲), η-H_2CO (■), and CO_{ad}(●) during a H_2 step down/step up test experiment. The continuous line represents the changes of the hydrogen concentration in the feed gas. The experiment was performed at a total pressure of 6 bar and at a temperature of 521 K. With a feed gas composition of: CO, 0.010 l_N min^{-1}; H_2, 0.020 ± 0.0195 l_N min^{-1}; and N_2 up to 0.09 l_N min^{-1}.

After approximately 4 minutes the hydrogen concentration in the feed was restored to the initial value. This H_2 increase induces a further pronounced decrease of the consumed CO. All other compounds are not affected by this change and maintain the previously exhibited increasing/decreasing behaviour (see Figure 7-12). Here, no change in the concentration of surface methylate could be detected.

This result suggests that large changes in the reactant concentrations (CO or H_2) were not followed by the expected consequential changes in all derived surface species concentrations. An influence of feed gas composition history on the kinetics of the different reaction steps might be present. This can be due to changes of the catalyst morphology or of the physico-chemical properties of the surface layer.

Influences of feed gas composition on the structure of Cu-based catalysts were already reported by several authors [133,193,194,195]], who found modifications of the morphology of copper on the catalysts [128,129,196,197,198].

Changes of the physico-chemical properties of the surface layer were reported by several authors [191,199,200,201,202]. The influence of the surface adsorbates on the surface properties of different single crystal metals were observed. This behaviour can be explained by a change of the electronic states of the adsorbates, due to the interaction of the adsorbate bonding/anti-bonding orbitals with the sp-electrons of the metal surface. These different electronic states of the adsorbates interact then with the metal d-states [203,204,205].

7.4.2 Methanol synthesis via hydrogenation of CO_2

The propagation of perturbations along the reaction pathway is again difficult to observe. Perturbations generated by modulation of gas phase carbon dioxide induces only oscillations in carbonate (CO_3^{2-}) concentrations. The equilibrium between these two species is very rapid, as suggested by the problems to estimate a rate constant for

the desorption reaction. The rate constant describing the hydrogenation of carbonate, could not be determined. The existence of such a reaction is suggested by the pre-exponential factor ($K_{0,1}$') and residence time (k_τ) of the CO_2 hydrogenation reaction, which differ from the values obtained for the CO_2 adsorption experiments.

Test experiments, using modification of the hydrogen concentration, were also carried out for the CO_2/H_2 system. The results give information about the influence of the gas phase reactants on the different reaction steps. Only overall increasing/decreasing behaviours of the surface species concentrations could be observed. These results suggest that, also in the case of the carbon dioxide hydrogenation, the feed composition has an influence on the kinetics of the different reaction steps [133,193-195].

7.4.3 Tentative energy scheme

According to Wokaun and co-workers [73,155,161-165,185,186] carbon dioxide is converted, via the reverse water gas shift reaction, into CO, which is hydrogenated to methanol. Using these data a tentative reaction scheme can be presented (Figure 7-13).

The total reaction energies (italic) are calculated from the reaction enthalpies ($\Delta H°$) of the water gas shift reaction and from the CO hydrogenation reaction to yield methanol [206,207]. It is assumed that the obtained ΔE_A and E_A' values characterise only the reaction equilibria of the different steps.

H_{ad} represents surface hydrogen. The not determined steps and energies are identified with *unknown*. It is assumed that CO_2 adsorbs and is immediately converted to carbonates. The used equilibrium energy for CO_2 adsorption/desorption process is the calculated ΔE_A of section 7.3.1. It was not possible to identify the intermediates of the hydrogenation of CO_{ad}. Therefore, the energy reaction scheme was simplified without indicating intermediates of the hydrogenation reaction.

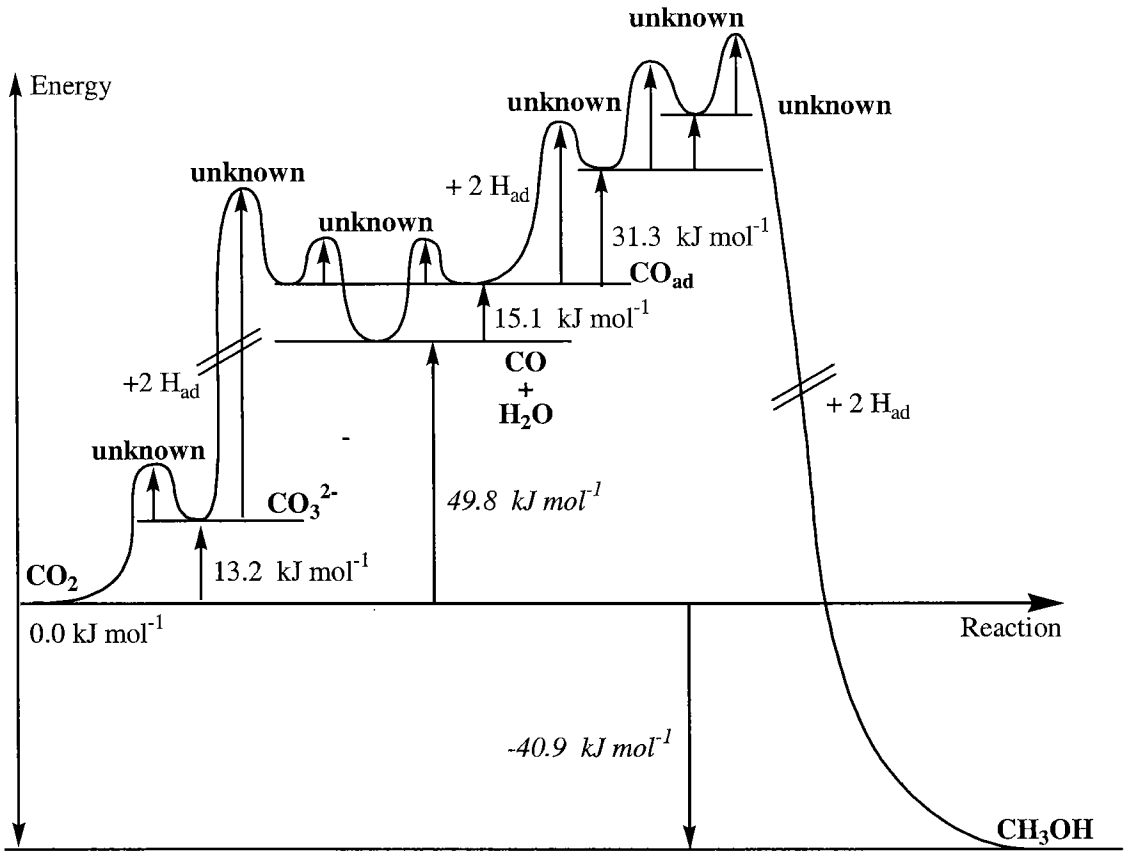

Figure 7-13: Energy reaction scheme for the CO_2/CO hydrogenation to yield methanol. The used total reaction energies (italic) are calculated from the reaction enthalpies ($\Delta H°$) of the water gas shift reaction and the CO hydrogenation to methanol [206,207]. It is assumed that the calculated ΔE_A values characterise only the reaction equilibria. H_{ad} represents surface hydrogen.

The high energy barrier between carbonates and adsorbed CO ($\Delta E_A > 50$ kJ mol^{-1}) and the following reduced reaction rate could explain the problems to monitor this step, as described in section 7.3.3. This value suggests that the reduction step is the rate limiting step in the reverse water gas shift reaction.

The problems to identify the intermediate [#] in the CO hydrogenation experiment suggest that the formation (CO_{ad} hydrogenation) of [#] is the rate limiting step. Decrease of the H_2 partial pressure in the gas phase causes a reduction of the intensity of η-H_2CO (see Figure 7-13), which supports the previous argumentation. This suggests that the

undefined intermediate [#] may be identical with surface-bounded formaldehyde [73,155,161-165,186,185].

A more detailed discussion about rate limiting steps, conversion or selectivity of the methanol synthesis is not possible, because the information about this reaction is insufficient.

The following activation energies were reported by Köppel *et al.* [208] for the CO_2 hydrogenation to yield methanol over a similar copper/zirconia catalyst: 47.9 kJ mol^{-1} for the methanol synthesis reaction and 93.2 kJ mol^{-1} for the reverse water gas shift reaction.

7.4.4 Modulation technique

The above results show that the modulation concept in heterogeneous catalysis, monitored by DRIFT, is a promising tool, where parameters can be derived from the experiments without any previously established calibration curves. Even in the case of complicated reactions, useful information can be obtained. Specific modulation experiments, e. g. using precursors of intermediates to observe specific adsorbed compounds, could be used to trace down further reaction steps and to obtain more details about the reaction.

A complete discussion of the possible error sources is compiled in section 5.4.

8. Conclusions

8.1 Introduction

In this work a new experimental FTIR and DRIFT spectroscopy based method has been presented. The method is applicable to both qualitative and quantitative measurements in heterogeneous catalysis. The basis of modulation theory, as well as several examples of applications are described.

In this chapter advantages and boundaries of this method are discussed and an outlook is presented.

8.2 Advantages of the method

8.2.1 Simplicity

The method is based on the action/reaction idea and quite simple. The transformation of a perturbation signal into response signals depends on the different characteristics of the system. The analysis of the differences between input and output signals is the key to obtain information about the investigated system.

Sinusoidal modulations of the reactant concentrations are chosen as perturbations. The advantage of this method is the possibility to follow selective modifications of different intermediates and products along the reaction pathway. Information is obtained about

the various reaction steps. Even in the case of complicated reactions information can be obtained.

8.2.2 Flexibility

The method is flexible. The modulation technique can be applied to quantitative as well as qualitative investigations of heterogeneously catalysed reactions, independently of the optical properties (reflectivity) of the used catalyst. The problem of the refractive index (see sections 1.3 and 3.2), which is the main limiting factor for qualitative measurements, is solved by using a sinusoidal pattern as perturbation function. In this case the output signal is also sinusoidal, and maxima respectively minima in the concentrations correspond to maxima and minima in the measured values.

Using the modulation technique, it is possible to perform investigations about several aspects of heterogeneous catalysis, e. g. rate limiting steps or activation energies. In chapters 4, 5 and 7 the utilisation of the method to different case studies has been presented.

8.2.3 Speed

The method is fast. As explained above, several parameters are collected at the same time during the same measurement. The accumulated data provide information about the different characteristics of the investigated system, e. g. reaction pathway and rate constants. From these data, other kinetic and thermodynamic parameters can be derived, e. g. activation energies, rate limiting steps, conversion and selectivity. In gas phase FTIR spectroscopy the use of sinusoidal functions as perturbation patterns eliminates the need for calibration curves. In DRIFT spectroscopy the use of complicated *ad hoc* developed mathematical models becomes unnecessary.

8.2.4 Economic

The method is economic. As presented in chapter 2, the setup is quite simple. It consists of the same components used in standard studies of heterogeneous catalysed reactions. The setup includes mainly commercial components. The construction of the dedicated electronic unit is not complicated, and basic commercially available electronic components are used. The required software for the control of the whole setup can be easily programmed by the user and no special know-how is necessary.

8.3 The boundaries of the method

The limiting elements can be divided into four groups, which are closely related to each other (see Figure 8-1). To achieve the best working conditions, all possible parameters have to be considered and tested. Very often trial and error processes are necessary (see chapter 3 and section 5.4).

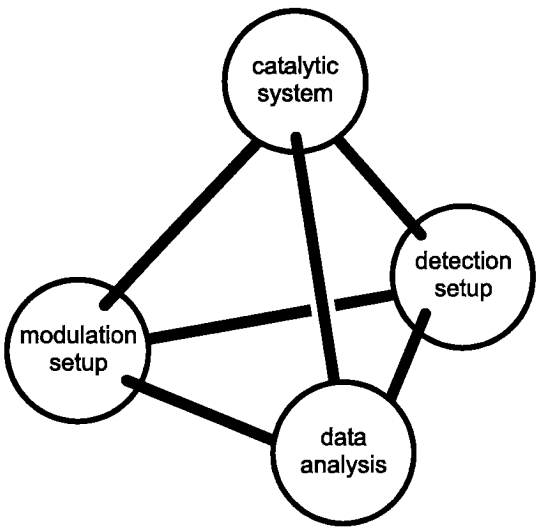

Figure 8-1: The four limiting element groups.

8.3.1 The detection setup

FTIR spectrometers are flexible and powerful instruments, but have several limitations. The Signal-to-Noise Ratio (SNR) of the obtained spectra depends on the number of photons per time reaching the detector (ADC-Counts). A large *ADC-Counts* number produces a high SNR signal and therefore spectra of high quality.

There are several ways to ensure a sufficient SNR. A high intensity IR source or a better detector can be used. A larger aperture is another possibility, but this can limit the observable range of the electromagnetic spectrum. The lowpass filtering of the collected signal can be eliminated, but the additional noise is added to the spectrum. Other solutions are an increase in the number of collected scans per spectrum or the reduction of the detector velocity. Both of these parameters are closely related to the time resolution.

8.3.2 The analysis of the data

The time resolution of the FTIR determines the shortest detectable modulation period, because a minimal number of points per period have to be measured, to fit the sinusoidal curve. By reducing the modulation frequency the resolution of the retardation is also reduced.

The collected data are analysed using an appropriate model. The choice of the model is very important. It has to be simple, because a large number of degrees of freedom gives rise to parameter values with large errors, artefacts and unrealistic results.

Additionally, the used gas flow can influence the resolution of the phase shift. The induced effects depend on the reaction step. A reaction step taking place on the surface is not influenced by the total gas flow. A reaction step involving gas phase species, e. g. an adsorption/desorption process, results in a better resolved phase shift with a smaller

gas flow, because the residence time τ is larger, and τ defines the highest possible time retardation.

To develop a good model it is necessary to monitor the largest accessible number of intermediates and products. Due to the attenuation of the intensity of the modulated signal component along the reaction pathway, the largest possible amplitude of the perturbation signal must be applied.

8.3.3 The modulation setup

The generation of the desired perturbation pattern is limited in frequency and amplitude.

The reaction and adjustment times of the used mass flow controller (MFC), together with the chosen amplitude, limit the applicable frequency. An excessively high modulation frequency, or a too large amplitude prohibits the correct implementation of the desired feed gas composition, because changes in the setpoints are faster than the adjustment of the output.

The amplitude is limited by the minimum and maximum flow of the MFC. The use of a wide range MFC can not really help, because the regulation of reduced flows or small amplitudes is very unprecise due to the sensitivity of the instrument. Preferable hence is the use of pre-mixed gases with different reactant-to-inert gases ratio.

The used concentrations should be high for detection, but below the saturation of the detector or the surface of the catalyst.

8.3.4 The catalytic system

The investigated catalytic system requires detailed consideration. Experimental conditions must be chosen away from regimes, which causes unwanted effects. The

used catalyst has to react to the induced perturbations and produce a response signal. The concentration change of the surface species on the catalyst induces a modification of the reflectivity of the sample, which can strongly affect the SNR of the spectra. From this point of view a small change of the concentrations in the feed gas is preferred, because the induced modification of the reflectivity is limited.

8.4 Outlook

The method can be improved in several ways.

8.4.1 Better detection

The experimental setup can be improved by using a synchrotron IR beam as source, which has a higher intensity within a well defined emission range compared to a common SiC globar source (with *Boltzmann distribution* of a black-body emission).

Advantages are: an expected large improvement of the SNR, resulting in an improvement of the time resolution (lower number of necessary scans); better detection limits, allowing measurements of smaller concentrations. It is also possible to perform experiments with a large IR beam without limitations in the range of the electromagnetic spectrum.

An estimation of the possible improvements, which can be achieved by a synchrotron source, is given below, using data from test measurements of KBr in the DRIFT cell. In the best case (CO oxidation) with an aperture of 3.5 mm and collecting 64 scans (4.16 s) per spectrum, a mean value for the SNR of 500 was achieved. Collecting a minimal number of 5 to 6 spectra per modulation period, gives a lower limit of 25 s per period. If a 1000 times more intense source (e. g. synchrotron) is used, the same SNR could

theoretically be achieved by collecting only one scan (0.065 s) with an aperture of 0.3 mm diameter.

8.4.2 Faster measurements

The test experiments necessary to establish the optimum experimental conditions are a time consuming process. To save time, a standard method for the test measurements must be established. Test patterns different from step up/step down can be considered.

The data resolution to obtain phase shift can be improved by collecting spectra over several modulation periods, calculating the desired integral values, combining together the obtained values, and performing a *Fast Fourier Transform* (FFT). In a single step, frequency and retardation are obtained.

Another way to reduce the measurement time is the application of perturbation patterns which are generated by the combination of sinusoidal curves of different frequencies. However, due to the non linear relation between concentration and IR intensity *ghost* frequencies can be obtained in the fitting routine. Therefore, it is important to choose an adequate fitting algorithm.

Additional errors due to changes in the optical reflectivity should be also considered.

8.4.3 Improved experiments

To elucidate complex catalytic systems, it is possible to use specific precursors to obtain adsorbed intermediate compounds, which are expected to be involved in the reaction. This would allow to bypass difficult steps and to derive more details about the investigated system. The modulation setup can be improved to allow the introduction of calibrated amounts of sublimated compounds, which would expand the above possibilities described.

The development of the necessary models is not trivial, therefore, simplest model should be chosen.

8.4.4 Additional investigations

The creation of a data base of systems in heterogeneous catalysis which have been successfully investigated by the modulation technique would be most helpful. Preliminary test experiments as well as complete studies using a variety of catalysts would be useful. At the moment there is no way to asses *a priori* which catalysts are suitable for these experiments.

The concept of modulation technique can also be applied to investigations in the homogeneous catalysis and in material exchange processes. The relationships between retardations and process parameters can be obtained analogously as explained in chapter 3.

8.5 Final remarks

The modulation technique expands the range of application of FTIR and DRIFT spectroscopy in heterogeneous catalysis. It is noteworthy that it is possible to collect data and to perform quantitative measurements without calibration curves or *ad hoc* mathematical models for calibration.

This method is a powerful tool, which can still be improved in the future. In this work, the basis of the modulation theory, as well as several examples of applications have been reported. Further implementations and investigations of other catalytic systems are necessary to fully exploit the potential of this technique.

Curriculum vitae

Personal

Enrico Eugenio Ortelli, from Meride (TI), single, born December 3, 1971 in Lugano, Switzerland.

Education

Sept.'77 - June '82 :	Primary School in Lugano
Sept.'82 - June '86 :	Secondary School in Lugano
Sept.'86 - June '91 :	Scientific College in Lugano GCE-A level: Scientific including English Major Topics: Computer science Electronics
Nov.'91 - April '96 :	Swiss Federal Institute of Technology (ETH) in Zürich, Diploma in Chemical Engineering. Advisor: Prof. Dr. A. Baiker. Major Topics: Biological Reaction Techniques Layout and Computation of Technical Equipment Analytical Methods of Technical Chemistry
June '96 - May '00 :	Ph.D. thesis at the Swiss Federal Institute of Technology (ETH) in Zürich, with experimental work carried out at the Paul Scherrer Institut in Villigen. Advisor: Prof. Dr. A. Wokaun

Referred Publications

Publications *in preparation*, and *submitted* are not listed.

D. Franzke, J. Kritzenberger, E. E. Ortelli, A. Baindl, O. Nuyken and A. Wokaun, "Photolysis and thermolysis of diaryl(pentazadiene) compounds in solid matrix investigated by infrared spectroscopy", *J. Photochem. Photobiol. A: Chem.* **112** (1998), 63-72.

E. E. Ortelli, J. M. Weigel and A. Wokaun, "Methanol synthesis pathway over Cu/ZrO_2 catalysts: a time-resolved DRIFT ^{13}C-labelling experiment", *Catal. Lett.* **54** (1998), 41-48.

E. E. Ortelli and A. Wokaun, "Use of periodic variations of reactant concentrations in time resolved FTIR studies of heterogeneously catalysed reactions", *Vib. Spectrosc.* **19** (1999), 451-459.

M. A. Reiche, E. Ortelli and A. Baiker, "Vanadia grafted on TiO_2-SiO_2, TiO_2 and SiO_2 aerogels Structural properties and catalytic behaviour in selective reduction of NO by NH_3", *Appl. Catal. B: Environmental* **23** (1999), 187-203.

E. E. Ortelli, J. Wambach, A. Wokaun, "Use of periodic variations of reactant concentrations in time resolved DRIFT studies of heterogeneously catalysed reactions", *App. Catal. A: General* **192** (2000), 137-152.

T. Lippert, E. Ortelli, J.-C. Panitz, F. Raimondi, J. Wambach, J. Wei and A. Wokaun, "Imaging-XPS/Raman Investigation on the Carbonization of Polyimide after Irradiation at 308 nm", *Appl. Phys.* **A69** (1999), 651-654.

E. E. Ortelli, F. Geiger, T: Lippert, J. Wei and A. Wokaun, "UV-Laser Induced Decomposition of Kapton Studied by Infrared Spectroscopy", *Macromolecules*, in print.

Other publications

E. E. Ortelli and A. Wokaun, "Evidence of intermediates in methanol synthesis over Cu/ZrO_2 catalysts: A time resolved, ^{13}C-labelled experiment in DRIFT", PSI Annual Report, Annex V, Villigen, 1998.

E. E. Ortelli and A. Wokaun, "Use of periodic variations of reactant concentrations in time resolved FTIR studies of CO oxidation on Pd/ZrO_2 catalysts", PSI Annual Report, Volume V, Villigen, 1999.

E. E. Ortelli, J. M. Wambach and A. Wokaun, "Determination of kinetical Data: a novel application of DRIFT Modulation spectroscopy", PSI Annual Report, Volume V, Villigen, 2000.

Posters

E. E. Ortelli and A. Wokaun, "Use of Periodic Variations of the Reactant Concentrations in Time Resolved FTIR Studies of Heterogeneous Catalyzed Reactions", AIRS III, Wien, July 5-8, 1998.

T. Lippert, E. Ortelli, J.-C. Panitz, F. Raimondi, J. Wambach, J. Wei and A. Wokaun, "Imaging-XPS/Raman Investigation on the Carbonization of Polyimide after Irradiation at 308 nm", COLA'99, Göttingen, July 19-23, 1999.

J. A. Anna Selvan, D. Grützmacher, E. Müller, E. Ortelli, A. Wokaun, H. Sigg, S. Stutz and J. Gobrecht "Building Blocks for the Development of Thin Film Si Solar Cells", National Photovoltaic Conference '99, Zürich, November 10-11, 1999.

Talks

E. E. Ortelli and A. Wokaun, "Periodic Variations of the Reactant Concentrations in Time Resolved FTIR Studies of Heterogeneously Catalysed Reactions", CERC3, Helsinki, May 20-23, 1999.

Bibliography

[1] J. Weidlein, U. Müller and K. Dehnicke, *Schwingungsspektroskopie*, G. Thieme Verlag, Stuttgart, New York, 1982.

[2] H.-H. Perkampus, *Spektroskopie*, VCH, Weinheim, New York, Basel, Cambridge, 1993.

[3] A. A. Michelson, in *Light Waves And Their Use*, Univ. of Chicago Press, 1902.

[4] R. Bracewell, *The Fourier Transform and Its Applications*, McGraw-Hill, New York, 1965.

[5] A. Papoulis, *The Fourier Integral and Its Applications*, McGraw-Hill, New York, 1962.

[6] P. B. Fellgett, *J. Phy. Radium*, **19** (1958), 237.

[7] P. Jacquinot, *Rep. Prog. Phys.* **13** (1960), 267.

[8] J. W. Cooley and J. W. Tuckey, *Math. Comput.* **19** (1965), 297.

[9] J. Connes and P. Connes, *J. Opt. Soc. Am.* **56**, (1966), 896.

[10] R. P. McDonald and P. A. Wilks, *Appl. Spectrosc.* **42** (1988), 151.

[11] P. R. Griffiths and J. A. de Haseth, *Fourier Transform Infrared Spectrometry*, vol. 83 of *Chemical Analysis: A Series of Monographs on Analtical Chemistry and Its Applications*, J. Wiley & Sons, New York, 1986.

[12] J. R. Ferraro and K. Krishnan, *Practical Fourier Transform Infrared Spectroscopy*, Academic Press, San Diego, 1990.

[13] P. Kubelka and F. Munk, *Z. Tech. Phys.* **12** (1931), 593.

[14] P. Kubelka, *J. Opt. Soc. Am.* **38(5)** (1948), 1067.

[15] P. Kubelka, *J. Opt. Soc. Am.* **44** (1954), 330.

[16] G. Kortum, *Spectrochim. Acta* **6** (1957), 534.

[17] G. Kortum, *Trans. Faraday Soc.* **58** (1962), 1624.

[18] G. Kortum, W. Braun and G. Herzog, *Angew. Chem. Intern. Ed.* **2** (1963), 333.

[19] N. T. Melamed, *J. Appl. Phys.* **34(3)** (1963), 560.

[20] P. D. Johnson, *J. Appl. Phys.* **35(2)** (1964), 334.

[21] W. W. Wendlandt and H. G. Hecht, in *Reflectance Spectroscopy*, Interscience Publishers, New York, London, 1966.

[22] W. K. Van Every and P. R. Griffiths, *Appl. Spectrosc.* **45(3)** (1991), 347.

[23] E. M. Suzuki and W. R. Gresham, *J. For. Sci.* **31** (1986), 931.

[24] M. T. McKenzie and J. L. Koenig, *Appl. Spectrosc.* **39(3)** (1985), 408.

[25] R. G. Messerschmidt, *Appl. Spectrosc.* **39(4),** (1985), 737.

[26] R. Marbach and H. M. Hesse, in 8^{th} *International Conference on Fourier Transform Spectroscopy*, 288-289, H. M. Heise, E. H. Korte and H. W. Siesler, 1575 SPIE, 1991.

[27] D. J. J. Fraser and P. R. Griffiths, *Appl. Spectrosc.* **44(2)** (1990), 193.

[28] M. Milosevic, *Mikrochim. Acta*, **II** (1988), 137.

[29] M. L. E. TeVrucht and P. R. Griffiths, *Appl. Spectrosc.* **43(8)** (1989), 1492.

[30] S. A. Yeboah, S.-H. Wang and P. R. Griffths, *Appl. Spectrosc.* **38(2)** (1984), 259.

[31] Z. Krivácsy and J. Hlavay, *J. Spec. Acta*, **50A(1)** (1994), 49.

[32] K. Moradi, C. Depecker and J. Corset, *Appl. Spectrosc.* **48(12)** (1994), 1491.

[33] A. A. Christy, Y. Liang, C. Hui, O. M. Kvalheim and R. A. Velapoldi, *Vib. Spectrosc.* **5** (1993), 233.

[34] N. E. Sharpless and D. A. Gregory, *Appl. Spectrosc.* **17** (1962), 47.

[35] R. K. Vincent and G. R. Hunt, *Appl. Opt.* **7** (1968), 7.

[36] K. Moradi, C. Depecker, J. Barbillat and J. Corset, *Spectrochimica Acta A: Mol and Biomol. Spectrosc.* **55(1)** (1999), 43.

[37] I. M. Hamadeh, S. A. Yeboah, K. A. Trumbull and P. R. Griffiths, *Appl. Spectrosc.* **38(4)** (1984), 486.

[38] F. Boroumand, J. E. Moser and H. Van den Bergh, *Appl. Spectrosc.* **46(12)** (1992), 1874.

[39] D. Reinecke, A. Jansen, F. Fister and U. Schernau, *Anal. Chem.* **60** (1988), 1221.

[40] R. S. S. Murthy and D. E. Leyden, *Anal. Chem.* **58** (1986), 1228.

[41] J. M. Chalmers and M. W. MacKenzie, in *Advances in Applied Fourier Transform Infrared Spectroscopy*, J. Wiley & Sons, Chichester, 1988.

[42] R. W. Frei, D. E. Ryan and V. T. Lieu, *Canadian J Chem.* **44** (1966), 1945.

[43] E. L. Simmons, *Appl. Opt.* **14(6)** (1975), 1380.

[44] H. G. Hecht, *Anal. Chem.* **48(12)** (1976), 1775.

[45] T. Hattori, K. Shirai, M. Niwa and Y. Murakami, *Bull. Chem. Soc. Jpn.* **54** (1981), 1964.

[46] A. A. Christy, O. M. Kvalheim and R. V. Velapoldi, *Vib. Spectrosc.* **9** (1995), 19.

[47] S. K. Loyalka and C. A. Riggs, *Appl. Spectrosc.* **49(8)** (1995), 1107.

[48] B. Azambre, O. Heintz, M. Schneider, A. Krzton and J. V. Weber, *Talanta*, **50(2)** (1999), 359.

[49] K. Tamaru, *Adv. Catal.* **15** (1964), 65.

[50] M. Kobayaski and K. Kobayaski, *Catal. Rev.-Sci. Eng.* **10** (1974), 139.

[51] C. O. Bennett, *Ibid.* **15** (976), 121.

[52] S. F. Parker, A. Amorelli, Y. D. Amos,C. Hughes, N. Porter and J. R. Walton, *J. Chem. Soc. Faraday Trans.* **43(91)** (1995), 517.

[53] W. W. Coblentz, *J. Franklin Inst.* **172** (1911), 309.

[54] M. P. Fuller and P. R. Griffiths, *Anal. Chem.* **50** (1978), 1906.

[55] M. P. Fuller and P. R. Griffiths, *Amer. Lab.* **10** (1978), 69.

[56] M. P. Fuller and P. R. Griffiths, *Appl. Spectrosc.* **34(5)** (1980), 533.

[57] LabVIEW, *Tutorial*, National Instruments.

[58] Troutmann, 5^{th} *programming postulate*, in *Murphy's Law*, A. Bloch, Methuen, London, 1985.

[59] Mass Flow Controller, *Operating Manual*, Bronkhorst.

[60] Liqui Flow, *Operating Manual*, Bronkhorst.

[61] Controlled Evaporator Mixer, *Operating Manual*, Bronkhorst.

[62] T-Control 94C, *Operating Manual*, Eurotherm.

[63] T-Control 847, *Operating Manual*, Eurotherm.

[64] T-Control 904A, *Operating Manual*, Eurotherm.

[65] Model 0030-100, *Operating Manual*, Spectra Tech.

[66] Model 0030-0XX, *Operating Manual*, Spectra Tech.

[67] Environmental Chamber 19930, *Operating Manual*, Grasby-Specac.

[68] Selector Diffuse Reflectance Accessory 19900, *Operating Manual*, Grasby-Specac.

[69] M. R. Praire, A. Renken, J. G. Highfield, K. R. Thampi and M. Grätzel, *J. Catal.* **129** (1991), 130.

[70] J. M. Olinger and P. R. Griffiths, *Anal. Chem.* **60** (1988), 2427.

[71] N. R. Smyrl, E. L. Fuller Jr. and G. L. Powell, *Appl. Spectrosc.* **37(1)** (1983), 39.

[72] C. Schild, A. Wokaun and A. Baiker, *J. Mol. Cat.* **63** (1990), 243.

[73] J. M. Weigel, Ph. D. thesis, ETH, Zürich, 1996.

[74] OPUS/IR, *Operating Manual*, Bruker GmbH.

[75] H. J. Güntherodt, in *Rapidly Quenched Metals*, vol. 2, 1591, S. Steeb & H. Warlimont, Elsevier, Amsterdam, 1985.

[76] C. Fröhlich, R. A. Köppel, A. Baiker, M. Kilo and A. Wokaun, *Appl. Cat. A: General,* **106** (1993), 275.

[77] R. A. Köppel, A. Baiker, Ch. Schild and A. Wokaun, *Stud. Surf. Sci. Catal.* **63** (1991), 59.

[78] R. B. Andersos and P. T. Dawson, *Experimental Methods in Catalytic Research*, vol. 1, Academic Press, New York, 1968.

[79] R. B. Andersos and P. T. Dawson, *Experimental Methods in Catalytic Research*, vol. 2, Academic Press, New York, 1976.

[80] R. B. Andersos and P. T. Dawson, *Experimental Methods in Catalytic Research*, vol. 3, Academic Press, New York, 1976.

[81] H. Unbehauen, *Regelungstechnik I*, Vieweg, Braunschweig/Wiesbaden, 1992.

[82] H. Unbehauen, *Regelungstechnik II*, Vieweg, Braunschweig/Wiesbaden, 1992.

[83] H. Unbehauen, *Regelungstechnik III*, Vieweg, Braunschweig/Wiesbaden, 1992.

[84] J. Baillieul and J. C. Willems, *Mathematical Control Theory*, Springer Verlag, New York, 1999.

[85] A. Cichocki and R. Unbehauen, *Neural Networks for Optimisation and Signal processing*, J. Wiley & Sons, Stuttgart, 1993.

[86] K. J. Aström and B. Wittenmark, *Adaptive Control*, Addison-Wesley, 1995.

[87] W. P. Aue, E. Bartholdi, R. R. Ernst, *J.Chem.Phys.* **64** (1976), 229.

[88] A. Bax, *Two dimensianal Nuclear Magnetic Resonance in Liquids,* Reidel, Boston, 1982

[89] D. L. Turner, *Prog. Nucl. Magn. Reson. Spectrosc.* **17** (1985), 281.

[90] R. R. Ernst, G. Bodenhausen, A. Wokaun, *Principles of nuclear magnetic resonance in one and two dimensions*, Clarendon Press, Oxford, 1987.

[91] I. Noda, *J. Am. Chem. Soc.* **111(21)** (1989), 8116.

[92] I. Noda, *Appl. Spectrosc.* **44(4)** (1990), 550.

[93] I. Noda, A. E. Dowrey and C. Marcott, *Appl. Spectrosc.* **47(9)** (1993), 1317.

[94] I. Noda, *Appl. Spectrosc.* **47(9)** (1993), 1329.

[95] I. Noda, Y. Liu, Y. Ozaki and M. Czarnecki, *J. Phys. Chem.* **99(10)** (1995), 3068.

[96] H. Kobayashi and M. Kobayashi, *Cat. Rev.-Sci. Eng.* **10(2)** (1974), 391.

[97] J. L. Falconer and J. A. Schwarz, *catal. Rev.sci.eng.* **25(2)** (1983), 141.

[98] A. Baiker, *Int. Chem. Ing.* **25(1)** (1985), 30.

[99] J. R. Schrieffer and J. H. Sinfelt, *J. Phys. Chem.* **94** (1990), 1047.

[100] H.-S. Liu, S.-C. Wu and S.-C. Lin, *Chem. Eng. Comm.* **164** (1998), 13.

[101] A. E. Rodrigues and M. M. Dias, *Chem. Eng. Process.* **37** (1998), 498.

[102] U. Fringeli, *Simultaneous Phase-Sensitive Digital Detection process For Time-Resolved Quasi Simultaneously Captured Data Arrays Of A Periodically Stimulated System*, PCT/CH96/00293, WO 97/08598.

[103] I. S. Park, M. Petkovska and D. D. Do, Chem. Eng. Sci. **53(4)** (1998), 819.

[104] I. S. Park, M. Petkovska and D. D. Do, Chem. Eng. Sci. **53(4)** (1998), 833.

[105] G. Marcelin, J. E. Lester and S. Mitchell, *J. Catal.* **102** (1986), 240.

[106] J. Kritzenberger and A. Wokaun, *J. Mol Catal. A: Chem.* **118** (1997). 235.

[107] M. Cavers, J. M. Davidson, I. R. Harkness, G. S. McDougall and L. V. C. Rees, *Stud. Surf. Sci. Catal.* **122** (1999), 65.

[108] J. G. Ziegler and N. B. Nichols, *Trans. ASME*, **64** (1942), 759.

[109] R. E. Murphy and H. Sakai, in *Aspen International Conference on Fourier Spectroscopy*, G. A. Vanasse, A. T. Stair and D. Baker, Air Force Geophysics Laboratory, Cambridge, 1971, 301.

[110] R. E. Murphy, F. Cook and H. Sakai, *J. Opt. Soc. Am.* **65** (1975), 600.

[111] R. A. Cracombes, A. A. Garrison and G. Mamantov, *9th International Conference on Fourier Transform Infrared Spectroscopy*, H. Sakai, *Proc. Soc. Photo-Opt. Instrum. Eng.* **289** (1981), 36.

[112] G. Durry, G. Guelachvili, D. Mathieu and A. Ubelmann, *9th International Conference on Fourier Transform Infrared Spectroscopy*, J. H. Bertie and H. Weiser, *Proc. Soc. Photo-Opt. Instrum. Eng.* **289** (1993), 110.

[113] G. Durry and G. Guelachvili, *Appl. Opt.* **34(12)** (1995), 1971.

[114] J. M. Presses, G. E. Hall, J. T. Muckermann, T. J. Sears, E. Weston, G. Guyot, J. C. Hanson, G. W. Flynn and H. Bernstein, *Rev. Sci. Instrum.* **64** (1993), 95.

[115] J. F. Durana and A. W. Mantz, *Fourier Transform Spectroscopy*, vol. 2, J. Ferraro and L. Basile, Academic, San Diego, 1979.

[116] J. J. Sloan, *7th International Conference on Fourier Transform Spectroscopy*, D. G. Cameron, *Proc. Soc. Photo-Opt. Instrum. Eng.* **145** (1989), 10.

[117] H. Sakai and R. E. Murphy, *Appl. Opt.* **17** (1978), 1343.

[118] R. A. Palmer, J. L. Chao, R. M. Dittmar, V. G. Gregoriou and S. E. Plunkett, *Appl. Spectrosc.* **47** (1993), 1297.

[119] B. O. Budevska and C. J. Manning, *Appl. Spectrosc.* **50(7)** (1996), 939.

[120] R. A. Palmer, E. Y. Jiang and J. L. Chao, *Mikrochim. Acta, Suppl.* **14** (1997), 591.

[121] S. V. Shilov, H. Skupin, F. Kremer, E. Gebhard and R. Zentel, *Liq. Cryst.* **22(2)** (1997), 203.

[122] R. A. Palmer, G. D. Smith and P. Y. Chen, *Vib. Spectrosc.* **19(1)** (1999), 131.

[123] O. Levenspiel, *Chemical Reaction Engineering*, J. Wiley & Sons, international edition, 1972.

[124] M. Baerns, H. Hoffmann and A. Renken, *Chemische Reaktionstechnik*, G. Thieme Verlag, Stuttgart, New York, 1987.

[125] E. E. Ortelli and A. Wokaun, *Vib. Spectrosc.* 19 (1999), 451.

[126] A. Bill, Ph. D. thesis, EPF, Lausanne, 1998.

[127] M. Bowker, H. Houghton and K. Waugh, *J. Chem. Soc. Faraday Trans.* **77** (1981), 3023.

[128] G. Chinchen, P. Denny, J. Jennings, M. Spencer and K. Waugh, *Appl. Catal.* **36** (1988), 1.

[129] M. Muhler, L. P. Nielsen, E. Törnqvist, B. S. Clausen and H. Topsøe, *Catal. Lett.* **14** (1992), 241.

[130] B. Denise and R. Sneeden, *Appl. Catal.* **28** (1986), 235-239.

[131] C. V. Ovesen, P. Stoltze, J. K. Nørskov and C. T. Campbell, *J. Catal.* **134** (1992), 445

[132] C. V. Ovesen, B. S. Clausen, B. S. Hammershøi, G. Steffensen, T. Askgaard, I. Chorkendorff, J. K. Nørskov, P. B. Rasmussen, P. Stoltze and P. Taylor, *J. Catal.* **158** (1996), 170.

[133] C. V. Ovesen, B. S. Clausen, J. Schiøtz, P. Stoltze, H. Topsøe and J. K. Nørskov, *J. Catal.* **168(2)** (1997), 133.

[134] T. S. Askgaard, J. K. Nørskov, C. V. Ovesen and P. Stoltze, *J. Catal.* **156** (1995), 229.

[135] E. E. Ortelli, J. Wambach and A. Wokaun, *Appl. Catal.* **192**(1) (2000), 137.

[136] D. Böcker and E. Wicke, *Ber. Bunsenges. Phys. Chem.* **89** (1985), 629.

[137] B. C. Sales, J. E. Turner and M. B. Maple, *Surf. Sci.* **114** (1982), 381.

[138] T. Engel and G. Ertl, *Advan. Catal.* **28** (1979), 1.

[139] H. Conrad, G. Ertl, and J. Küppers, *Surf. Sci.* **76** (1978), 33.

[140] T. Engel and G. Ertl, *J. Chem. Phys.* **69** (1978), 1267.

[141] T. Engel, *J. Chem. Phys.* **69** (1978), 373.

[142] S. Ladas, R. Imbihl and G. Ertl, *Surf. Sci.* **219** (1989), 88.

[143] Y. Q. Deng, T. G. Nevell and M. G. Jones, *Catal. Lett.* **34** (1995), 313.

[144] T. Ioannides, A. M. Efstathiou, Z. L. Zhang and X. E. Verykios, *J. Catal.* **156** (1995), 265.

[145] Yu. Suchorski, J. Beben and R. Imbihl, *Surf. Sci.* **405** (1998), L477.

[146] R. L. Keiski, M. Härkönen, A. Lathi, T. Maunula, A. Savimäki and T. Slotte, in *Proceedings CAPoC3 Conference*, Brussels, 1994, 53.

[147] A. Baiker, D. Gasser, J. Lenzner, *J. Chem. Soc. Chem. Commun.* (1987), 1750.

[148] A. Baiker, *Faraday Discuss. Chem. Soc.* **87** (1987), 239.

[149] A. Baiker, D. Gasser, J. Lenzner, A. Reller and S. Schlögl, *J. Catal.* **126** (1990), 555.

[150] A. Baiker, M. Maciejewski and S. Tagliaferri, *Ber. Bunenges. Phys. Chem.* **97** (1993), 3.

[151] P. Barnickel, A. Wokaun and A. Baiker, *J. Chem. Soc. Faraday Trans.* **87(2)** (1991), 333.

[152] L. M. Sander and S. V. Ghaisas, *Surf. Sci.* **391** (1997), 125.

[153] H. J. Güntherodt, *Rapidly Quenched Metals*, vol. 2, S. Steeb & H. Warlimont, Elsevier, Amsterdam, 1985, 1591.

[154] T. Nijhuis, M. Makkee, A. Van Langeveld and J. Moulijn, *Appl. Catal. A: General* **164** (1997), 237.

[155] E. E. Ortelli, J. M. Weigel and A. Wokaun, *Catal. Lett.* **54** (1998), 41.

[156] M.-Y. He and J. G. Ekerdt, *J. Catal.* **87** (1984), 238.

[157] M.-Y. He, J. M. White and J. G. Ekerdt, *J. Mol. Catal.* **30** (1985), 415.

[158] H. Abe, K. Maruya, K. Domen and T. Onishi, *Chem. Lett.* (1984), 1875.

[159] Y. Amenomiya, *Appl. Catal.* **30** (1987), 57.

[160] Y. Sun and P. A. Sermon, *J. Chem. Soc., Chem. Commun.* (1993), 1242.

[161] C. Schild, A. Wokaun and A. Baiker, *J. Mol. Cat.* **63** (1990), 223.

[162] C. Schild, A. Wokaun and A. Baiker, *Fres. J. Anal. Chem.* **341** (1991), 395.

[163] R. A. Köppel, A. Baiker, C. Schild and A. Wokaun, *J. Chem. Soc., Faraday Trans.* **87(17)** (1991), 2821.

[164] A. Wokaun, J. M. Weigel, M. Kilo and A. Baiker, *Fres. J. Anal. Chem.* **349** (1994), 71.

[165] J. M. Weigel, C. Fröhlich, A. Baiker and A. Wokaun, *Appl. Catal.* **140** (1996), 29.

[166] I. Fisher, H.-C. Woo and A. Bell, *Catal. Lett.* **44** (1997), 11.

[167] I. Fisher and A. Bell, *J. Catal.* **172** (1997), 222.

[168] C. Fröhlich, R. A. Köppel, A. Baiker, M. Kilo and A. Wokaun, *Appl. Cat. A: General* **106** (1993), 275.

[169] G. J. Millar, C. H. Rochester and K. C. Waugh, *J. Chem. Soc., Faraday Trans.* **88(15)** (1992), 2257.

[170] A. B. Anton, J. E. Parmeter and W. H. Weinberg, *J. Am. Chem. Soc* **107** (1985), 5558.

[171] K. Weissermel and H.-J. Arpe, *Industrielle Organische Chemie: Bedeutende Vor- und Zwischenprodukte*, VCH, Weinheim, 1994.

[172] M. Bowker, R. A. Hadden, H. Houghton, J. N. K. Hyland and K. C. Waugh, *J. Catal.* **109** (1988), 263.

[173] E. Ramroson, R. Kieffer and A. Kiennemann, *Appl. Catal.* **4** (1982) 281.

[174] J. F. Edwards and G. L. Schrader, *J. Catal.* **94** (1985), 175.

[175] A. Kiennemann, H. Idriss, J. Hindermann, J. Lavalley, A. Vallet, P. Chaumette and P. Courty, *Appl. Catal.* **59** (1990) 165.

[176] R. J. Klinger and J. W. Rathke, *J. Am. Soc.* **106** (1984), 7650.

[177] J. F. Edwards and G. L. Schrader, *J. Phys. Chem.* **88** (1984), 5620.

[178] A. Ueno, T. Onishi and K. Tamaru, *J. Catal.* **66** (1970), 756.

[179] M. Bowker, H. Hougton and K. C. Waugh, *J. Chem. Soc., Faraday Trans.* **77** (1981) 3023.

[180] M. Bowker, H. Hougton, K. C. Waugh, T. Giddings and M. Green, *J. Catal.* **84** (1983) 252.

[181] M. Bowker, *Vacuum* **33** (1983), 669.

[182] S. G. Neophytides, A. J. Marchi and G. F. Froment, *Appl. Cat. A: General* **86** (1992), 45.

[183] G.C. Chinchen, P. J. Denny, J. R. Jennings, M. S. Spencer and D. A. Whan, *Appl. Catal A* **30** (1987), 333.

[184] P. B. Rasmussen, M. Kazuta and I. Chorkendorff, *Surf. Sci.* **318** (1994), 267.

[185] J. Weigel, R. Köppel, A. Baiker and A. Wokaun, *Langmuir* **12(22)** (1996), 5319.

[186] M. Kilo, J. Weigel, A. Wokaun, R. A. Köppel and A. Baiker, *J. Mol. Catal. A Chem.* **126(2-3)** (1997), 169.

[187] J. Wambach, A. Baiker and A. Wokaun, *Phys. Chem. Chem. Phys.* **1** (1999), 5071.

[188] S. Bailey, G. F. Froment, J. W. Snoeck and K. C. Waugh, *Catal. Lett.* **30** (1995), 99.

[189] S. Wohlrab, D. Ehrlich, J. Wambach, H. Kuhlenbeck and H.-J. Freund, *Surf. Sci.* **220** (1989), 243.

[190] C. Binet, A. Badri, M. Boutonnet-Kizling and J.-C. Lavalley, *J. Chem. Soc., Faraday Trans.* **90(7)** (1994), 1023

[191] J. Nerlov, S. Sckerl, J. Wambach and I. Chorkendorff, *Appl. Catal. A: General* **191** (2000), 97.

[192] J. H. Larsen and I. Chorkendorff, *Surf. Sci.* **405** (1998), 62.

[193] B. S. Clausen, J. Schiøtz, L. Gråbæk, C. V. Ovesen, K. W. Jacobsen, J. K. Norskov and H. Topsøe, *Top. Catal.* **1** (1994), 367.

[194] H. Topsøe, C. V. Ovesen, B. S. Clausen, N.-Y. Topsøe, P. E. Højlund Nielsen, E. Törnqvist and J. K. Norskov, *Dynamics of Surfaces and Reaction Kinetics in Heterogeneous Catalysis*, G. F. Froment and K. C. Waugh, Elsevier, Amsterdam, 1997.

[195] N.-Y. Topsøe and H. Topsøe, *J. Mol. Catal. A: Chem.* **141** (1999), 95.

[196] T. H. Fleisch and R. L. Mieville, *J. Catal.* **90** (1984), 165.

[197] B. S. Clausen, G. Steffensen, B. Fabius, J. Villadsen, R. Feidenhans'l and H. Topsøe, *J. Catal.* **132** (1991), 524.

[198] K. Waugh, *Catal. Today* **15** (1992), 51.

[199] M. E. Bridge, C. M. Comrie and R. M. Lambert, *Surf. Sci.* **67** (1977), 393

[200] F. Falo, I. Cano and M.Salmerón, *Surf. Sci.* **143** (1984), 303.

[201] M. T. Paffett, C. T. Campbell, T. N. Naylor and S. Srinivasan, *Surf. Sci.* **154** (1985), 284.

[202] U. Schneider, G. R. Castro and K. Wandelt, *Surf. Sci.* **287/288** (1993), 146.

[203] A. Ruban, B. Hammer, P. Stoltze, H. L. Skriver and J. K. Nørskov, *J. Mol. Catal. A* **115** (1997), 421.

[204] B. Hammer and J. K. Nørskov, *Surf. Sci.* **343(3)** (1995), 211.

[205] B. Hammer, Y. Morikawa and J. K. Nørskov, *Phys. Rev. Lett.* **76** (1996), 2141.

[206] J. B. Hansen, *Handbook of Heterogeneoul Catalysis*, G. Ertl, H. Knözinger and J. Weitkamp, VCH, Weinheim, 1997.

[207] G. H. Graaf, P. J. J. M. Sijtsema, E. J. Stamhuis, G. E. H. Joosten, *Chem. Eng. Sci.* **41** (1986), 2883.

[208] R. A. Köppel, A. Baiker and A. Wokaun, *Appl. Catal. A: General* **84** (1992), 77.